

# **AFM-Assisted Nanofabrication using Self-Assembled Monolayers**

Chang-Hyun Jang

Dissertation submitted to the faculty of the  
Virginia Polytechnic Institute and State University  
in partial fulfillment of the requirements for the degree of

Doctor of Philosophy  
In  
Chemistry

William A. Ducker, Chairman

Mark R. Anderson

Alan R. Esker

John R. Morris

Brian M. Tissue

January 13, 2004  
Blacksburg, Virginia

Keywords: Atomic Force Microscopy, Nanofabrication, Self-Assembled Monolayer,  
Lithography, Acetylcholinesterase

Copyright 2004, Chang-Hyun Jang

# **AFM-Assisted Nanofabrication using Self-Assembled Monolayers**

Chang-Hyun Jang

## **Abstract**

This study describes the covalent and the electrostatic attachment of molecules, nano-particles, and proteins to patterned self-assembled monolayers. A scanning probe nanografting technique was employed to produce patterns of various sizes, down to 10 nm. Thus, we are able to demonstrate a degree of surface patterning which is an order of magnitude smaller than that used in the semiconductor industry.

One efficient strategy for creating chemically specific nanostructures is to use the extraordinary catalytic properties of enzymes. However, as the dimension of a catalyst patch is reduced down to nanometer scale, it is difficult to detect the very low concentration of product. This study resolves the problem by developing a new strategy: the surface trapping of a product generated by a nanometer-scale patch of surface-bound enzyme.

An array of proteins finds use when the array contains a number of different proteins. Toward this end, a new and convenient method for immobilizing enzymes is developed, which will allow the preparation of thin films containing several different catalytically-active enzymes on the nanoscale.

The disadvantage of scanning probe nanografting technique is that the AFM tip loses resolution through wear during the patterning procedure. This study examines the possibility of developing a new AFM lithographic method to avoid wear: the use of enzymes covalently attached to a tip as a site-specific catalyst.

## **Dedication**

To my parents, Iksang Jang and Jungja Kim, and my wife, Suyoun Seo:

Thank you all for the love and understanding in this long journey

## Acknowledgement

I would like to express my sincere thanks and appreciation to my advisor, Dr. William A. Ducker, for his guidance, support, and friendship. I clearly remember a conversation with Dr. Ducker in his office where he said, "Chang, everything is possible. We just did not find a solution yet." His encouragement and advice made me overcome the difficulties through my graduate program. He allowed me the freedom to pursue new research areas and techniques while managing to guide and direct me.

Sincere appreciation goes out to the members of my advisory committee, Dr. Mark R. Anderson, Dr. Alan R. Esker, Dr. John R. Morris, Dr. Brian M. Tissue, and Dr. Richey M. Davis. I am especially grateful for the guidance given to me by Dr. Michael A. Calter and Dr. Paul R. Carlier during my research. If it were not for their advice and understanding, I could have never completed this program. I would also like to acknowledge Dr. Harold M. McNair for his encouragement and help.

I would like to thank the group members: Aysen Tulpar, Spencer Clark, William Lokar, Min Mao, Clayton McKee, Weslyn Ward, Robert Cain, Jun-Fu Liu, and Vivek Subramanian. Their collaboration and friendship were invaluable. I would also like to thank all of the graduate students and Post-Docs who have been of great assistance to me during my graduate career. In particular, Francisco Cavadas, Qin Lin, Jianjun Deng, Woojin Lee, Hyong-Jun Kim, and Sheila Gradwell for their help and assistance.

I am extremely grateful to Pastor C. Daniel Kim, Pastor H. David Chung, and the members of Korean Baptist Church of Blacksburg for their love in Jesus Christ. A special round of thanks goes out to all of the members of Korean Student Association for their friendship.

I would like to extend my sincerest gratitude to my parents and brothers. Their great love and prayers always give motivation and courage. My wife, Suyoun Seo, and my children, Youngwoo and Youngki, deserve the most recognition by far. I could have never completed my degree were it not for your love, understanding, and patience. You always remind me of what is most important in life. Last, but not least, I would like to thank God for his grace and love throughout my life.

# Table of Contents

Chapter 1. Introduction -----	1
Chapter 2. Lithographic Techniques -----	7
2.1 Optical and Electron Beam Lithography -----	7
2.1.1 Photolithography -----	7
2.1.2 Laser Ablation Lithography -----	9
2.1.3 Low-Energy Electron Beam Lithography -----	9
2.2 Fabrication of Gold-Thiol SAMs -----	10
2.2.1 Introduction -----	10
2.2.2 Preparation and Characterization of SAMs -----	12
2.2.3 Microcontact Printing -----	14
2.2.4 Optical Patterning of SAMs -----	16
2.3 AFM-assisted Nanolithography -----	17
2.3.1 Introduction -----	17
2.3.2 Tip-assisted Hydrolysis -----	17
2.3.3 Tip-directed Displacement -----	19
2.3.4 Nanografting -----	21
2.3.5 Dip-pen Nanolithography -----	23
2.3.6 Nanofabrication of SAMs with Tunneling Electrons -----	25
2.3.7 Nanometer-scale Protein Patterning -----	26
2.4 Preparation of Uniformly Flat Gold Surfaces -----	29
2.4.1 Evaporation of Gold onto Smooth Substrates -----	29
2.4.2 Template Stripping -----	29
2.4.3 Melting and Freezing of Bulk Gold Samples -----	30
2.4.4 Comparison of Techniques -----	31
2.5 Conclusions -----	32

Chapter 3. Atomic Force Microscopy -----	35
3.1 Introduction -----	35
3.2 Scanning Probe Technology -----	37
3.2.1 Fundamentals -----	37
3.2.2 Basic SPM Components -----	37
3.3 AFM Imaging Modes -----	41
3.3.1 Contact Mode -----	41
3.3.2 Lateral Force Microscopy -----	43
3.3.3 Tapping Mode -----	45
3.3.4 Force Curve Measurements -----	46
3.4 Summary -----	47
Chapter 4. Nanoscale Patterned Protein and Particle Covalent Attachment on Surfaces -----	51
4.1 Introduction -----	51
4.2 Experimental Section -----	54
4.3 Results and Discussion -----	59
4.3.1 Self-assembled Monolayers -----	59
4.3.2 Nanopatterning -----	59
4.3.3 Covalent Modification of a Nanografted Pattern -----	61
4.3.4 Fabrication of a Protein Nanopattern -----	62
4.3.5 Covalent Attachment of Gold Nanoparticles -----	64
4.3.6 Nanofabrication of Polyelectrolyte Multilayers -----	65
4.4 Conclusions -----	68
Chapter 5. Immobilized Enzymes as Catalytically-Active Tools for Nanofabrication --	72
5.1 Introduction -----	72
5.2 Acetylcholine and Acetylcholinesterase -----	74
5.3 Experimental Section -----	76
5.4 Results and Discussion -----	77

5.4.1	Surface Trapping of a Product Generated by Surface-bound Enzyme	77
5.4.2	Control Experiments	81
5.4.3	Contrast Mechanism of Thiocholine	84
5.5	Conclusions	87
Chapter 6. Strategy for the Sequential Patterning of Proteins: Catalytically-Active Multiprotein Nanofabrication		89
6.1	Introduction	89
6.2	Experimental Section	91
6.3	Results and Discussion	94
6.3.1	Possible Reaction of NaIO <sub>4</sub> with Enzymes	94
6.3.2	Preparation of Films Containing Two Different Protein Patches	96
6.3.3	Test of AChE Activity	99
6.4	Conclusions	101
Chapter 7. Chemically Specific Nanolithography using Tip-Bound Enzyme		103
7.1	Introduction	103
7.2	Experimental Section	106
7.3	Results and Discussion	107
7.3.1	Enzyme Catalysts for Lithography	107
7.3.2	Organic Catalysts for Lithography	115
7.4	Conclusions	118
Chapter 8. Summary and Future Work		120
Appendix: Nanoscript Program for Producing 9-dot Pattern in Figure 4.5A		124

## List of Illustrations

Figure 2.1 Photolithography procedures -----	8
Figure 2.2 Structure of a self-assembled monolayer of thiols on gold -----	11
Figure 2.3 Overlayer structure of an n-alkanethiol on Au(111) -----	13
Figure 2.4 Patterning of covalently grafted, hyperbranched poly(acrylic acid) and poly(tert-butyl acrylate) organic thin films using the microcontact printing method -----	15
Figure 2.5 UV patterning of SAMs -----	17
Figure 2.6 AFM images of a pattern produced by tip-assisted hydrolysis -----	18
Figure 2.7 Schematic diagram of the tip-directed displacement mechanism -----	19
Figure 2.8 AFM images of patterns produced by tip-directed displacement -----	20
Figure 2.9 Schematic diagram of the nanografting procedure -----	22
Figure 2.10 AFM image of a nanografted pattern -----	23
Figure 2.11 Schematic representation of DPN -----	24
Figure 2.12 Schematic diagram of STM-induced lithography -----	25
Figure 2.13 Nanoscale protein patterning by DPN -----	28
Figure 2.14 Schematic representation of the annealing method -----	29
Figure 2.15 Schematic representation of the template stripping method -----	30
Figure 2.16 Schematic representation of the gold wire flaming method -----	31
Figure 3.1 Components of a scanning probe instrument -----	37
Figure 3.2 Beam-deflection set-up for the detection of interacting force in an AFM--	38
Figure 3.3 Typical AFM cantilever/tip -----	40
Figure 3.4 Tip convolution occurred by the side contact of tip to the specimen -----	42
Figure 3.5 The image of a steep-wall feature affected by the cone angle of the tip --	43
Figure 3.6 Scan angle selection for frictional imaging -----	44
Figure 3.7 A typical force-versus-distance curve -----	47
Figure 4.1 The homemade sample holder -----	56
Figure 4.2 Schematic representation of nanofabrication of polyelectrolyte multilayers -----	58

Figure 4.3	AFM image of a SAM made from C <sub>12</sub> SH -----	59
Figure 4.4	Topographic AFM image in ethanol of the pattern with 4-aminothiophenol molecules in the matrix of octanethiol monolayer -----	60
Figure 4.5	Covalent modification of patterned surface -----	61
Figure 4.6	Immobilization of insulin on a patterned surface -----	63
Figure 4.7	Immobilization of lipase on a patterned surface -----	64
Figure 4.8	Amino-functionalized gold particle attachment to surface -----	65
Figure 4.9	Tapping-mode AFM images with cross-sections showing the formation of PEM on a patterned carboxylate patch -----	67
Figure 5.1	A schematic of the procedure used to trap the catalysis product -----	73
Figure 5.2	The interaction of acetylcholinesterase with acetylcholine -----	75
Figure 5.3	Tapping mode AFM images in ethanol of the carboxylic acid patch, enzyme, and trap -----	79
Figure 5.4	Tapping mode AFM image in ethanol of the enzyme and trap after the addition of ATCh -----	80
Figure 5.5	AFM images in ethanol of control experiments when the enzyme was not present -----	81
Figure 5.6	AFM images in ethanol of control experiments -----	82
Figure 5.7	Tapping mode AFM image in water of an enzyme patch and a trap after exposure to a 9 mM solution of acetylcholine for 2 h at 31°C -----	83
Figure 5.8	The adsorption of thiocholine on gold measured by surface plasmon resonance -----	84
Figure 5.9	The counterion effect on the contrast change of a quaternary ammonium pattern -----	86
Figure 6.1	Schematic of immobilization of a series of enzymes -----	90
Figure 6.2	Gas chromatography data of the activity of the two-component nitrogenase system in buffer solution in the absence and then in the presence of periodate solution -----	95
Figure 6.3	AFM images in water of an aldehyde pattern from the oxidation of a patterned diol -----	97

Figure 6.4	Tapping-mode AFM images in water showing the formation of two-protein nanopatterns using the diol immobilization strategy -----	98
Figure 6.5	AFM images in water of the proteins and the product trap -----	100
Figure 7.1	Candida cylindracea lipase -----	104
Figure 7.2	Interaction forces between the AFM tip and the different surface functional groups -----	105
Figure 7.3	Two-probe AFM for write-read -----	106
Figure 7.4	Force curve before and after the hydrolysis of an ester SAM -----	108
Figure 7.5	Single spot hydrolysis using a lipase tip -----	110
Figure 7.6	Force-seperation curve for single spot hydrolysis -----	111
Figure 7.7	Attachment of AChE to an AFM -----	113
Figure 7.8	Tethering of an AChE and choline substrate for the enzyme-tip lithography -----	114
Figure 7.9	IRAS spectra of monolayers -----	116
Figure 8.1	Membrane-enclosed electrode -----	122

## List of Schemes

Scheme 5.1 Reaction of acetylcholine -----	74
Scheme 6.1 Oxidative cleavage of 1,2-diols by periodate -----	91
Scheme 6.2 Synthesis of HS(CH <sub>2</sub> ) <sub>11</sub> (OCH <sub>2</sub> CH <sub>2</sub> ) <sub>6</sub> O(CH <sub>2</sub> ) <sub>11</sub> CH(OH)CH <sub>2</sub> OH) -----	92
Scheme 6.3 Reaction of the nitrogenase system -----	94
Scheme 7.1 Esterification of a surface hydroxyl group with a pyridine catalyst -----	115
Scheme 7.2 Esterifications of a surface hydroxyl group -----	117

# Chapter 1. Introduction

On December 29, 1959, Richard Feynman gave a lecture entitled “There is plenty of room at the bottom” to the American Physical Society meeting at the California Institute of Technology. *“Up to now we have been content to dig in the ground to find minerals, ... ultimately – in the great future – we can arrange the atoms the way we want; the very atoms, all the way down! ...”* Although at first his bold vision had been considered a bit eccentric, this vision was realized by IBM scientists. The invention of Scanning Tunneling Microscope (STM)<sup>1</sup> and Atomic Force Microscope (AFM)<sup>2</sup> first enabled the visualization of atoms and molecules, and then the manipulation of individual atoms.

When Eric Drexler dared to publish his vision that nanotechnology will dramatically change the world in the 1980s,<sup>3</sup> most of the people considered his idea to be impossible. But the idea of nanotechnology now has great appeal to the mainstream scientific and engineering communities, not only as a scientific challenge but also for practical reasons. Although it will take time for all of us to accept the feasibility of his grand vision, the nanotechnology “gold rush” is now underway.

There have been a number of driving forces facilitating the revolution of nanoscience and nanotechnology. The primary factors advancing this field are:

1. The desire for faster and smaller-scale electronic devices, biochips, and sensors has created a demand for fabrication of small objects. Gordon Moore, co-founder of Intel, predicted that the data density would double approximately every 18 months. However, scientists predicted that Moore’s law would break down when the dimension of electronic components was reduced below 100 nanometers. Semiconductor line widths are now around 100 nanometers. Currently most computer chips are made by shining ultraviolet light through a template and onto a silicon wafer coated with a surface film called a resist. However, photolithography can only make chip features that are limited by the diffraction limit of the wavelength of light used to illuminate the mask. The limit for current technology means we need new technologies.

2. Although scientists have studied the fundamental mechanisms occurring in biological systems for a long time, in many cases, we still do not know how and why they work. However, with the technological advancements people now want to use or mimic these fundamental activities or mechanisms of biological systems. Biochemists are already trying to construct an active nanomachine of living cells, which are chiefly made of protein.<sup>4</sup>

3. The invention of Scanning Probe Microscope (SPM)<sup>1</sup> enabled us to observe and manipulate materials with atomic scale. It is now used in a wide range of areas. Chip manufacturers use AFMs to examine wafers to make sure that they are defect free. AFM is also a key tool for researchers in the fields of bioscience, life science and materials science. In addition, AFM is now used as a tool for the fabrication of nanometer scale features. The use of AFM for fabrication is the focus of this thesis.

4. When the size of an object approaches atomic dimensions, the wave function of the electrons becomes significantly confined compared to bulk materials. This confinement leads to different chemical properties. Thus, in addition to simply creating smaller objects with the same properties, nanotechnology is capable of delivering materials with new properties. It is hoped that these new materials will allow the development of new products.

## **Development of SPM**

The first type of SPM was the Scanning Tunneling Microscope (STM).<sup>1</sup> It was invented in 1981 by Gerd Binning and Heinrich Rohrer, and they were awarded the Nobel Prize for Physics. The first use of STM was atomic-scale imaging of crystalline materials by recording the variation in tunneling current between a fine sharpened tip and the sample as the tip passes over the atomically corrugated surface. However, the restriction to conductive samples limited the choice of materials investigated. The need for imaging insulating surfaces was satisfied by Gerd Binnig and coworkers when they invented the Atomic Force Microscope (AFM) in 1986.<sup>2</sup> In the AFM, the van der Waals forces acting between the tip and surface provides the contrast mechanism instead of the tunneling current. AFM is now also used for measuring the force between two surfaces.<sup>5</sup>

The use of AFM in nano-scale fabrication of surfaces has accelerated since Gang-yu Liu developed Nanografting techniques in 1997. In Nanografting, an AFM tip is used to create a pattern in an organic self-assembled monolayer (SAM) formed on a gold surface.<sup>6</sup> A force is applied to a selected area of the film to remove the adsorbed thiol molecules. A different thiol is adsorbed to the exposed gold to form a nanometer-scale feature on the surface.

Gold-thiol SAMs provide us with a promising platform to construct chemically specific nanosturctures. These SAMs form a thin, uniform, and chemically stable monolayer. By introducing proper terminal functional groups we can modify the surface properties. A patterned SAM can be used as a template to pattern proteins and other biomaterials.

In 1999, Chad A. Mirkin developed a different scanning probe fabrication method called Dip-Pen Nanolithography (DPN).<sup>7</sup> With this methodology, an AFM tip is coated with a thin film of thiol molecules. When the tip is placed close to the surface in an atmosphere containing a high concentration of water vapor, a minute drop of water condenses between the tip and the surface, and the thiol molecules migrate from the tip to the surface through the water meniscus as the tip moves across the surface. They have extended the use of DPN to silicon and semiconductor surfaces by choosing a suitable inking molecule with the meniscus ink-transport medium.

The primary advantage of AFM lithography is the small scale of fabrication. This method can easily make the structures with dimensions of about 20 nanometers. It can also monitor the fabrication of the pattern, which is useful for any multi-step fabrication procedure. Another important advantage with this instrument is that it is possible to get the information about more than physical dimensions of a surface. For example, a tapping mode imaging method enables us to detect the local hardness, the elasticity, and the electrostatic properties of a surface.<sup>8</sup> It also allows us to observe soft materials, such as polymer and protein, without damaging the surface. The development of various techniques to chemically modify an AFM tip has made this instrument more powerful. We can simultaneously look at the topography and the chemical properties of a surface. With these useful characteristics, AFM shows us tremendous promise in many areas such as precise modification of circuit design and elaborate construction of protein structures.

The secondary advantage of the AFM is that nm-scale fabrication can be achieved for the modest price of about \$100K.

However, there are two important technological issues that should be overcome. First, the writing speed of the AFM lithography systems is too slow for mass production because of the serial patterning process. Typical writing speed for a single tip is about 2  $\mu\text{m/sec}$ . Researchers are making a huge effort to overcome this drawback. The aim is to produce an array of  $n$  tips and to write with all  $n$  tips simultaneously, thereby increasing the speed by a factor of  $n$ . It has been reported that anisotropic wet etching can make arrays of thousands of cantilevers.<sup>9</sup> The second obstacle to be overcome is the friction-induced wear of the SPM tip during fabrication. One potential remedy is the use of nanotube probes. These tips are very robust and because of the cylindrical geometry, they do not increase in diameter during wear. Such probes will enable us to write extremely thin patterns of several nanometers width without noticeable wear. In spite of speed and wear problems, the use of SPM families in nanoscience has been increased continuously. The growing number of publications is good evidence for the widespread use of these techniques.

By now, we have just taken a few steps toward the grand vision of the nano-world. Nanotechnology is still in its infancy, because only simple structures can be created with current technologies. It is hoped that rather than working with bulk materials, we will be able to work with individual atoms and molecules. By learning about an individual molecule's properties, we can put them together in well-defined ways to produce new materials or to build more complex structures with atomically precise control. The hope is that nanoscience and nanotechnology will make possible in the near future an unprecedented technological capability to develop novel materials and advanced material processes at the molecular and possibly atomic scale, which will greatly benefit our life.

In this thesis, I use an AFM to perform chemically specific nanofabrication of molecules, nano-particles, and proteins in a self-assembled monolayer. A scanning probe nanografting technique is employed to produce template patterns of various sizes, down to 10 nm.

I focus on the nanometer scale fabrication of enzymes on surfaces. By now, several groups<sup>10,11</sup> have immobilized nanometer-scale patches of proteins on a surface and confirmed them through the attachment of antibodies that recognize the primary sequence. However, the catalytic activity in these patches has not been demonstrated. This feature is an essential step if the catalytic activity is to be used in hybrid enzyme-semiconductor devices. As the first report on this subject, we demonstrate the catalytic activity of surface-bound enzyme by developing a new strategy: the surface trapping of a product generated by a nanometer-scale patch of surface-bound enzyme.

This study also includes a new and convenient method for immobilizing enzymes that will allow the preparation of thin films containing several different catalytically active enzymes.

## References

- (1) The inventors Scanning Probe Microscopy are Heinrich Rohrer and Gerd K. Binnig. Patent for Scanning Tunneling Microscope was issued Aug. 10, 1982.
- (2) Binnig G.; Quate C. F.; Gerber C. *Phys. Rev. Lett.* **1986**, *56*, 930.
- (3) Drexler, K. E. *Engines of Creation: The Coming Era of Nanotechnology*; New York: Anchor Press/Doubleday, 1986.
- (4) Benenson, Y.; Paz-Elizur, T.; Adar, R.; Keinan, E.; Livneh, Z.; Shapiro, E. *Nature* **2001**, *414*, 430.
- (5) Ducker, W. A.; Senden, T. J.; Pashley, R. M. *Nature*, **1991**, *353*, 239.
- (6) Xu, S.; Liu, G.-Y. *Langmuir* **1997**, *13*, 127.
- (7) Piner, R. D.; Zhu, J.; Xu, F; Hong, S.; Mirkin, C. A. *Science*, **1999**, *283*, 661.
- (8) James, P. J.; Antognozzi, M.; Tamayo, J.; McMaster, T. J.; Newton, J. M.; Miles, M. J. *Langmuir*, **2001**, *17*(2), 349.
- (9) Physics News 511, November 8, 2000.
- (10) Wadu-Mesthrige, K.; Xu, S.; Amro, N. A.; Liu, G.-Y. *Langmuir*, **1999**, *15*, 8580.
- (11) Kenseth, J. R.; Harnisch, J. A.; Jones, V. W.; Porter, M. D. *Langmuir*, **2001**, *17*, 4105.

## Chapter 2. Lithographic Techniques

### 2.1 Optical and Electron Beam Lithography

Conventional lithographic techniques such as microcontact printing,<sup>1-4</sup> photolithography,<sup>5,6</sup> micromachining,<sup>4</sup> and microwriting<sup>2,4,7</sup> can produce micrometer- or submicrometer-sized patterns. The desire for faster and smaller-scale devices has continuously stimulated the development of lithography on ever-smaller scales. Smaller devices offer the promise of low cost, higher speed, and greater convenience. Recently, it has been suggested that the chipmaker Intel will turn to extreme-ultraviolet lithography (EUV) or perhaps direct-write (maskless) electron-beam lithography at decade's end.

Extreme Ultraviolet Lithography (EUV) can produce nanometer-scale circuit patterns on chip surfaces. The main difference between EUV and current photolithography is the wavelength of the light used to create the circuit features. EUV will allow chipmakers to make smaller circuits because of the smaller wavelengths of light.

Electron beam lithography (EBL) is a technique for creating extremely fine patterns for integrated circuits. The electron beam has a wavelength so small that diffraction no longer defines the lithographic resolution. However, EBL requires alternation of environments between vacuum and ambient conditions<sup>8</sup> because electron beam exposures are conducted in a high vacuum and deposition occurs in a solution. This feature makes the procedure slower and more expensive.

#### 2.1.1 Photolithography

Photolithography is the process of transferring features on a mask to the surface of a silicon wafer. Photo patterning is a convenient method for the fabrication of sub micro-scale patterns. The shortcoming of this method is the requirement for multiple photolithographic steps. The steps include wafer cleaning, barrier layer formation, photoresist application, soft baking, mask alignment, exposure and development, and hard baking.

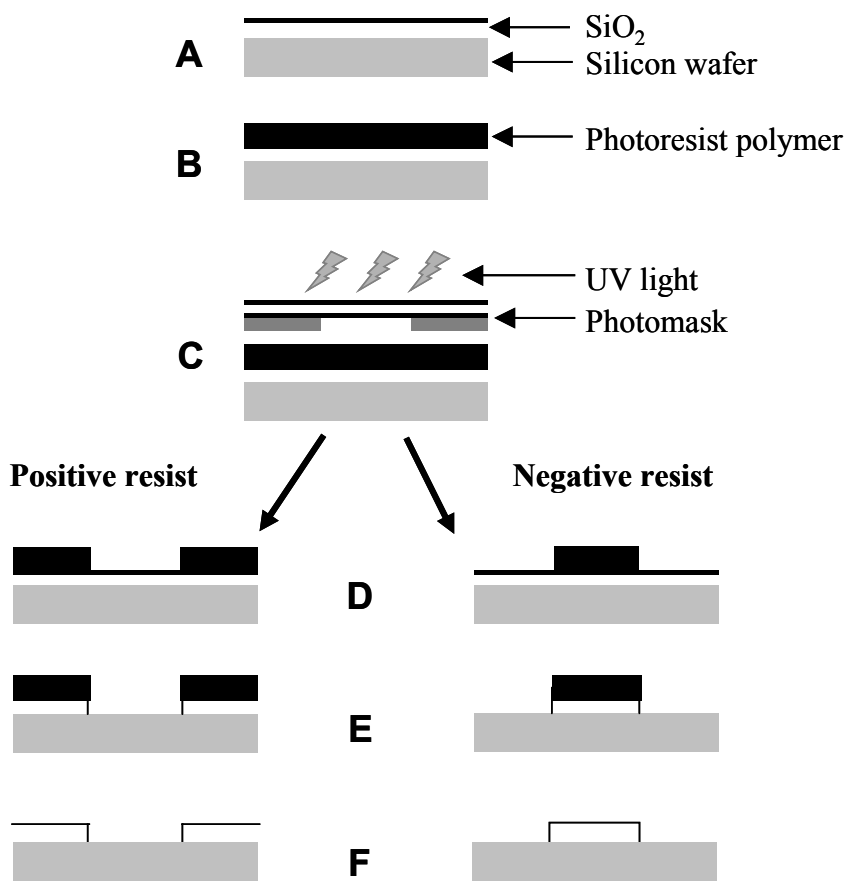


**Figure 2.1** Photolithography procedures

Figure 2.1A shows a thin film of silicon dioxide on a silicon wafer substrate. The aim of this procedure is the selective removal of silicon dioxide to produce a patterned feature on the silicon wafer (F). The wafer is first coated with a photoresist polymer that is sensitive to ultraviolet light (B). A mask is aligned with the wafer, so that the pattern can be transferred onto the wafer surface. Mask alignment is one of the most important steps in photolithography. A mask or photomask is typically a glass plate with a patterned emulsion of metal film on one side. The photoresist is then exposed through the pattern on the mask with a high intensity ultraviolet light (C). There are two types of photoresist (positive and negative). When the light hits the positive resist, it causes a chemical

change that enables the resist to be removed with a solvent. This step transfers a positive image of the mask to the resist layer. The opposite occurs with negative resist materials. The exposed oxide is then removed by using a chemical (E). Finally the resist is removed leaving the patterned oxide (F).

### **2.1.2 Laser Ablation Lithography**

Laser ablation of a polymer was first reported in 1982. Since this process has the advantages of fewer processing steps and fewer design limitations, laser ablation can be used as an alternative or complementary technique to conventional photolithography. Thin-metal films can be patterned directly by laser ablation without the need for the multi-step processes involved in photolithography (mask preparation, resist spinning, exposure, developing, etching, and resist removal). A high intensity pulsed laser vaporizes a small area on the surface of a target. The ablated materials deposit on a substrate under controlled conditions of temperature and pressure, forming a thin film. If the substrate has a uniform crystal lattice structure, the film may be induced to grow on top of it as a crystal with a preferred orientation. Microfabrication by laser ablation of thin films is readily accomplished with commercially available microscope adaptations.<sup>8</sup>

Wei et al.<sup>9</sup> investigated the ablation properties of various polymers at low and high fluences. Fluence signifies the intensity of the laser. High fluence produces high ablation rates in small areas, e.g., drilling or cutting. At low fluence, the ablation rate depends on the structural parameters of the polymer. The low fluence range is important for lithographic applications. In this study, low fluences were defined as  $10\text{-}400 \text{ mJcm}^{-2}$ . Fluence and/or pulse number can control the depth of channels.

### **2.1.3 Low-Energy Electron Beam Lithography**

Electron beam lithography differs from conventional UV lithography in that it is maskless and the dose may be varied throughout the pattern. Electron beam lithography can produce high-resolution nanometer sized patterns. The electron beam has wavelength so small that diffraction no longer defines the lithographic resolution, and therefore the

mask is not required. Electron beam exposures are usually conducted in a scanning electron microscope.

Electron beam lithography can also be applied to organic compounds. Harnett, Satyalakshmi, and Graighead<sup>10</sup> developed patterned SAMs by electron beam lithography and fabricated biomolecules on the selected area. By attaching fluorescent polystyrene spheres to mercaptohexadecanoic acid-cysteamine templates, they could observe the pattern with a fluorescence microscope.

In order to apply this technique to SAMs, low energy, sub-2 kV, electron beams should be used. Because low voltage electrons deposit energy efficiently on the top surface of a material, it is possible to expose the thin monolayer without expanding excess energy in the substrate. Applying an electron beam to a SAM creates the templates. Samples are backfilled by immersing in dilute solutions of reactive filler molecules immediately after development.

## 2.2 Fabrication of Gold-Thiol SAMs

### 2.2.1 Introduction

The fabrication of SAMs has attracted tremendous attention due to their capability to promote or resist the adhesion of specific substances at the molecular level.<sup>1,7,11</sup> Since the first publication of Nuzzo and Allara<sup>12</sup> in this field, SAMs of organic molecules on gold have evolved as a platform to modify the physicochemical properties of solid surfaces because of their promising structural properties (thin and organized) and superior stability due to the strong attractive force between gold and sulfur. The possible areas of their technological applications include lithographic patterning, biomaterials fabrication, corrosion resistance, adhesion promotion/resistance, and microelectronic fabrication.

Self-assembled monolayers are highly ordered 2-dimemsional arrays of molecules, which form spontaneously by chemisorption of functionalized molecules to the surface. By now, various materials have been investigated as an adsorbate and a substrate. The most thoroughly examined SAMs are those generated by the adsorption of

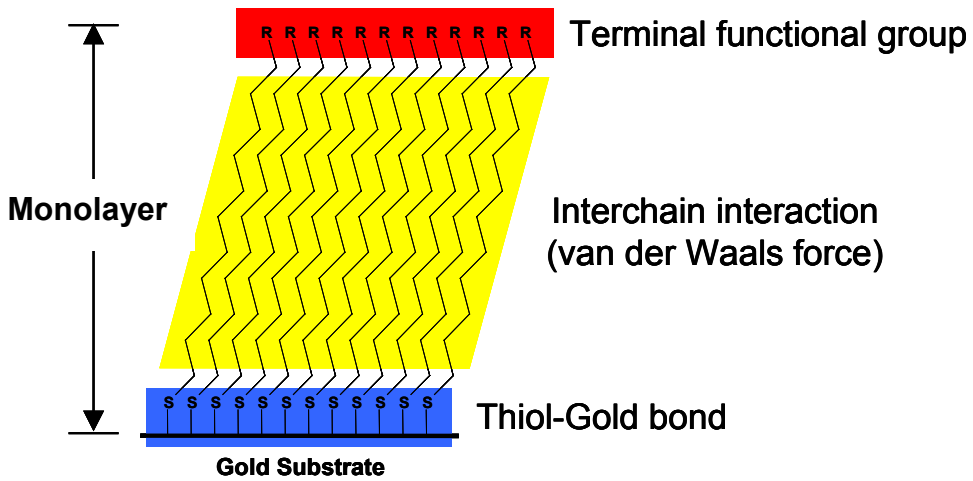


**Figure 2.2** Structure of a self-assembled monolayer of thiols on gold

alkanethiols on gold. Gold surfaces are ideal substrates for the formation of organic monolayers. They are very suitable for many biological and electrochemical systems due to their chemical inertness and high conductivity. Although gold is unreactive to many species, gold does bind strongly to sulfur compounds, especially thiols. This selectivity drives the organization of the adsorbing thiols on gold.

After adsorption to the surface, the adsorbed molecules reorganize themselves and form a crystal structure through the van der Waals interactions between aliphatic chains. When a gold substrate is immersed into a solution of thiol molecules, a fairly good monolayer forms in about 30 min,<sup>13</sup> which contains close-packed domains separated by ditches and pits. These defects are gold areas covered by weakly adsorbed species and are slowly healed over time periods of 24-72 h depending on the structure of adsorbate molecules. The introduction of different terminal functional groups, by using different SAM-forming molecules or by conducting a surface reaction on a SAM, can create a variety of surface properties.

## 2.2.2 Preparation and Characterization of SAMs

### Preparation

A SAM is prepared by placing a fresh gold substrate into a deoxygenated 1-2 mM solution of the selected thiolated molecule for at least 24 hours. Before placing the substrate into the solution, the substrate is usually cleaned with piranha solution (concentrated sulfuric acid:30%-H<sub>2</sub>O<sub>2</sub> = 3:1 in volume) and rinsed thoroughly with purified water and dried under pure N<sub>2</sub> gas. After completing the reaction, the surface is rinsed and sonicated to remove any physisorbed layers.<sup>14</sup>

### Structure

The properties of SAMs have been extensively studied by numerous methods. Colorado, Villazana, and Lee prepared SAMs by the adsorption of aliphatic dithiocarboxylic acids (ADTCAs), CH<sub>3</sub>(CH<sub>2</sub>)<sub>n</sub>CS<sub>2</sub>H, onto the gold substrates, where *n* = 8-17.<sup>14</sup> They compared these films to those generated from their *n*-alkanethiol analogues, CH<sub>3</sub>(CH<sub>2</sub>)<sub>m</sub>SH, where *m* = 9-18. These SAMs were characterized by optical ellipsometry, contact angle goniometry, and polarization modulation infrared reflection spectroscopy, and compared with normal alkanethiol SAMs.

The structure of SAMs on gold substrates depends on two major factors: the thiol-gold interactions and the interchain interactions. Normal alkanethiols, having a single thiol group per molecule, are known to bind to the 3-fold hollow to maximize the sulfur-gold binding and the chains tilt to maximize the interchain interactions (Figure 2.3).<sup>15</sup> Molecular modeling studies have shown that the distance between the centers of the two nearest sulfur atoms in normal alkanethiol SAMs is 5.0 Å. However, the intermolecular distance in ADTCA SAMs is 2.87 Å, indicating a different attachment of ADTCAs to the gold substrate. Colorado et al. reported that the ellipsometric thickness of both SAMs is proportional to the alkyl chain length and indistinguishable for the same chain length.<sup>14</sup> However, considering the longer interchain distance of ADTCAs (2×2.87 = 5.74 Å) compared to 5.0 Å for normal alkanethiols, the alkyl chains on ADTCAs SAM may be more tilted, thus reducing the thickness.

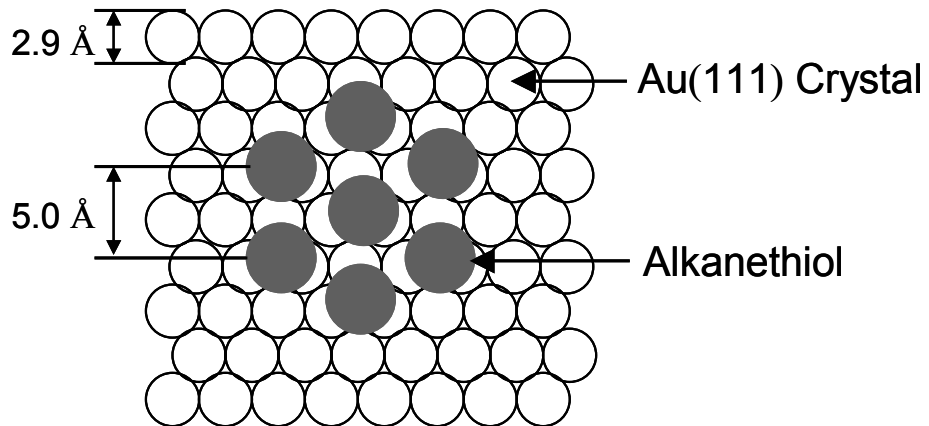


**Figure 2.3** Overlayer structure of an n-alkanethiol on Au(111)<sup>15</sup>

### Thickness

The thickness of a SAM can be determined by several different methods. The traditional methods are ellipsometry<sup>16</sup> and angle-resolved X-ray photoelectron spectroscopy.<sup>17,18</sup> There are many reports in which the thickness of SAMs was measured by these two methods. Ton-That, Shard, and Bradley reported a new method to determine the thickness of spin-cast polymer thin film using an AFM and compared it with the XPS data.<sup>19</sup> This method is also applicable to SAMs. For a thin film, which is relatively soft compared to its substrate, the film thickness can be measured by scratching the film with the AFM tip. By carefully controlling the loading force from the tip to the film, it is possible to scratch through the film without damaging the substrate. The film thickness can then be determined by measuring the depth of the ditch in the AFM image. In their study, correlation within 15 % between the two methods (AFM and XPS) was observed. Considering the thickness variations at different locations on the cast film, the two techniques usually agree within experimental error. This method is very suitable for measuring the thickness of SAMs since the organic layer of a SAM is relatively soft compared to the gold substrate.

## **Wettability**

Both types of SAMs, ADTCAs and normal, show high contact angles for water regardless of alkyl chain length because of the strong hydrophobicity of terminal alkyl groups. However, the contact angle for hexadecane exhibits a zigzag pattern where the value of the contact angles are higher on films composed of even numbered carbon chain lengths and lower on films composed of odd-numbered carbon chain lengths.<sup>14</sup> The hypothesis of this odd-even effect reflects the increased wettability of methylene vs. methyl groups exposed at the interface. This effect is greater for ADTCA SAMs, which suggests the different structural features of ADTCA SAMs compared with those of normal alkanethiol SAMs.

## **Characterization by PM-IRRAS**

Colorado et al. took the surface IR spectroscopy in order to verify that the differences in wettability for the odd- and even-numbered SAMs are due to the different orientation (methylene vs. methyl groups) at the interfaces of those films.<sup>14</sup> The spectrum shows the higher symmetric stretch peak for the even carbon number and the higher asymmetric stretch peak for the odd carbon number,<sup>15</sup> which support the different orientation of molecules. If the terminal C-H bonds are perpendicular to the surface, the symmetric stretch cancels out. Therefore, according to their results, the three terminal hydrogen atoms for molecules with an even carbon number must face toward the SAM surface.

### **2.2.3 Microcontact Printing**

Microcontact printing<sup>4-6, 20-24</sup> is a convenient, nonphotographic technique and has become widely used today for generating patterned features of SAMs on both planar and nonplanar surfaces. Soft stamps are coated with a thiol solution. When the stamp is pressed against a solid, solution from the raised (patterned) section contacts with the surface and reacts to form a patterned SAM. The stamp material should be rigid enough to support a topographic microstructure at its surface, porous enough to incorporate a sufficient amount of active solution, and soft enough to enable a smooth contact with the solid surface onto which printing is desired. Elastomeric stamps are usually made from

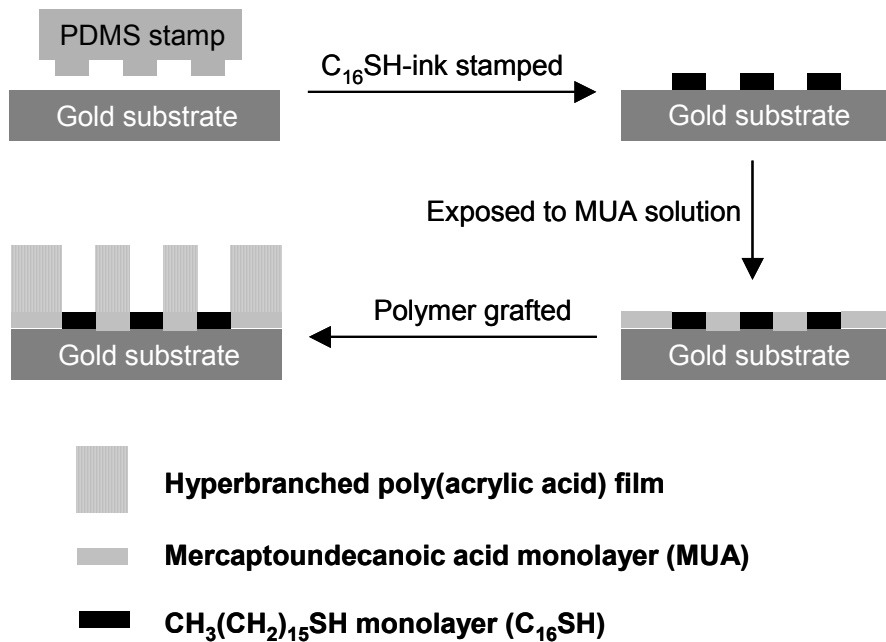


**Figure 2.4** Patterning of covalently grafted, hyperbranched poly(acrylic acid) and poly(tert-butyl acrylate) organic thin films using the microcontact printing method.

poly(dimethylsiloxane) and fabricated by casting a prepolymer against a master which has been patterned using micromachining or photolithography. A stamp wetted with an inking solution, usually a ~2 mM ethanolic solution of thiols, is brought into contact with the surface of gold for 5-10 s, so that the thiol can transfer to the gold. Excess thiol is rinsed off with ethanol then the gold substrate is dried with nitrogen gas. If these islands of thiols are left for more than a few minutes, then the thiols will spread onto the vacant areas of the gold. To fix the pattern, the gold is dipped into a solution of a different thiol (the filling solution). Additional complexity can be incorporated into the film by selectively reacting one of thiols on the patterned surface.

Lackowski, Ghosh, and Crooks<sup>24</sup> covalently grafted hyperbranched polymers on the selected region of microcontact printed SAMs. Figure 2.4 shows the method used to pattern the substrates with poly(acrylic acid) and poly(tert-butyl acrylate). Hexadecanethiol was applied to the PDMS stamp and then the Au substrates were

patterned by manual application of the stamp to the surface for 30 s. HOOC(CH<sub>2</sub>)<sub>15</sub>SH was used as the filling compound. Subsequently, hyperbranched polymers were grafted on the carboxylic acid terminal groups of patterned SAM. Their study revealed the absence of polymer growth in the hexadecanethiol-patterned region and a high degree of geometric uniformity in the 3-PTBA regions.

He et al.<sup>25</sup> reported the patterning of nanoparticles on the patterned surface. They prepared a patterned SAM terminated with –CH<sub>3</sub> and –NH<sub>2</sub> groups using microcontact printing. By reduction of AuCl<sub>4</sub><sup>-</sup> with trisodium citrate, negatively charged Au nanoparticles were made and attached to the –NH<sub>2</sub> terminated pattern by attractive electrostatic forces.

#### 2.2.4 Optical Patterning of SAMs

Deep UV ( $\lambda < 250\text{nm}$ ) contact aligners or projection exposure systems for high-resolution patterning of SAM films are commercially available. The patterned monolayers are used as templates for subsequent selective chemical reactions.<sup>26</sup> The disadvantage of this method is the requirement for multiple photolithographic steps. It is mainly due to the multiple mask alignments and could cause the loss of biological activity. Therefore, this method is not suitable for biological applications, which are important for our current research.

Lee and Clark<sup>27</sup> prepared octadecyltriethoxysilane SAMs from toluene solution onto glass microscope slides with butylamine catalyst. The SAM was covered with chromium-on-fused silica lithographic mask and illuminated by a 200 W mercury arc lamp (Figure 2.5). The UV illumination removes the aliphatic tails from the unmasked area. They observed the patterned SAM using an AFM frictional imaging technique. Frictional effects are very useful in the study of photo patterned SAMs because the tip-surface interactions and friction in the exposed regions can be made very different from those of the unexposed regions.

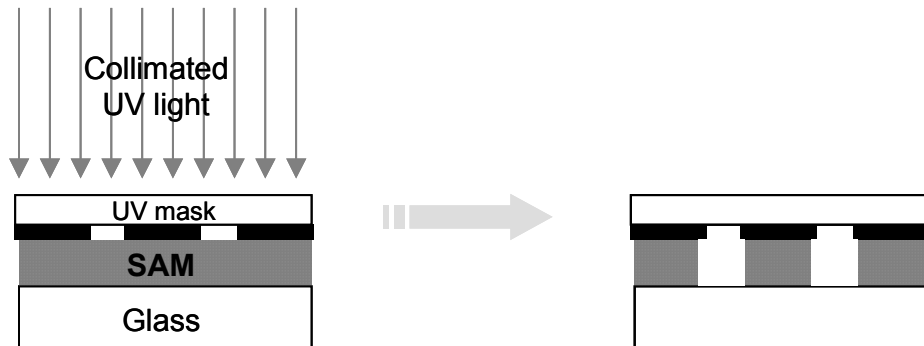


**Figure 2.5** UV patterning of a SAM. The UV illumination removes the aliphatic tails from the unmasked area.

## 2.3 AFM-assisted Nanolithography

### 2.3.1 Introduction

AFM-based lithography is a promising method for high-resolution fabrication. An AFM is a near-field microscope used to map a surface by scanning a sharp tip and measuring the spatial variation in the interaction between the tip and surface. The sharpness of the tip and accurate positioning allow the AFM to make a pattern on a nanometer-scale.<sup>28-31</sup> Various AFM and STM-based nanofabrication methods have been reported. Representative methods are tip-catalyzed surface reactions, nanografting, and dip-pen nanolithography. STM-based lithography includes tip-assisted electrochemical etching and field-induced desorption.<sup>32</sup> In this study, I use nanografting to produce patterns on a SAM.

### 2.3.2 Tip-assisted Hydrolysis.

Wang et al.<sup>31</sup> reported on the use of a scanning force microscope for the tip-assisted base hydrolysis of an ester-terminated alkanethiol monolayer on Au(111). They reported that the contact imaging (scanning of the surface) accelerates the base catalyzed

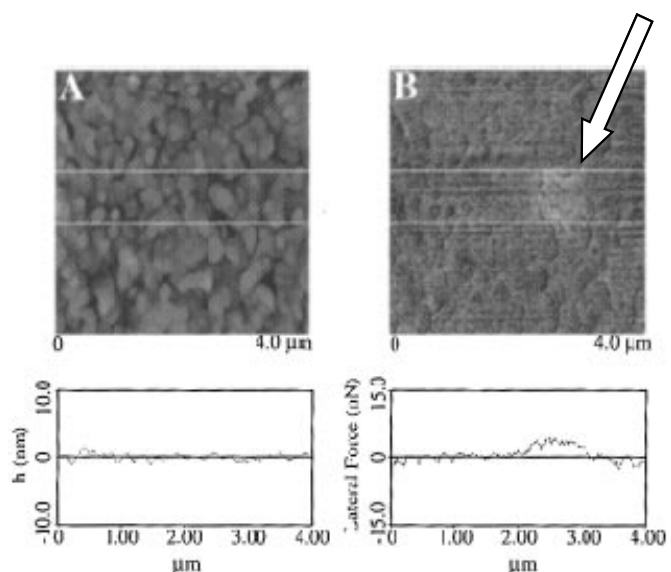


**Figure 2.6** In situ topographic (A) and friction (B) images and cross sections of a DSU monolayer chemisorbed at Au(111) after immersion for 1hr in an alkaline (10 mM KOH) aqueous solution.

Wang, J.; Kenseth, J. R.; Jones, V. W.; Green, J. B.; McDermott, M. T.; Porter, M. D. *J. Am. Chem. Soc.* **1997**, *119*, 12796. Copyright [1997] American Chemical Society.

hydrolysis of a dithiobis(succinimido undecanoate) (DSU) monolayer in the scanned area relative to the surrounding unimaged area.

The SAMs of DSU on Au(111) were prepared. Figure 2.6 shows the topographic and friction images ( $4.0\mu\text{m} \times 4.0\mu\text{m}$ ), and a cross section of a DSU monolayer, after a  $1.0\mu\text{m} \times 1.0\mu\text{m}$  area in the SAM was continually scanned in an alkaline (10 mM KOH) aqueous solution. A high friction area, brighter square, was observed in the friction mode image. Wang et al. rationalize this result as follows: The tip feels a higher friction energy with the carboxylate-terminated surface than the ester-terminated surface, so this high friction (lighter) square may be evidence for the hydrolysis of the ester molecules on the surface.<sup>31</sup> They claim that the AFM tip induces localized disorder in the outer portion of the monolayer, which enhances access of hydroxide ions to the acyl carbon of DSU. The enhanced access to the reaction site accelerates the hydrolysis.

### 2.3.3 Tip-directed Displacement

Assuming a homogeneous force distribution across a tip radius of  $\sim 10$  nm, the normal pressure exerted by a tip during imaging is about 10 MPa. When the loading force is increased on the tip, the thiol molecules in the scanned area are displaced because the Au-S bond is the weakest one at the interface.<sup>33</sup> The RS-Au bond dissociation energy is  $\sim 40$  kcal/mol.<sup>34</sup> The desorption procedure also depends on the solvent. Better solvent allows the desorbed molecules to diffuse away more easily.

The procedure of tip-directed displacement is illustrated in Figure 2.7. First, the surface is characterized under a low imaging force. The second step is zooming in the target area and displacing the molecules by increasing the applied force. Finally, a larger area is scanned to characterize the lithography. By immersing the fabricated SAMs into a solution with a different kind of thiol, the displaced area can be filled with the desired molecules. There is only a narrow range of force over which the tip can selectively

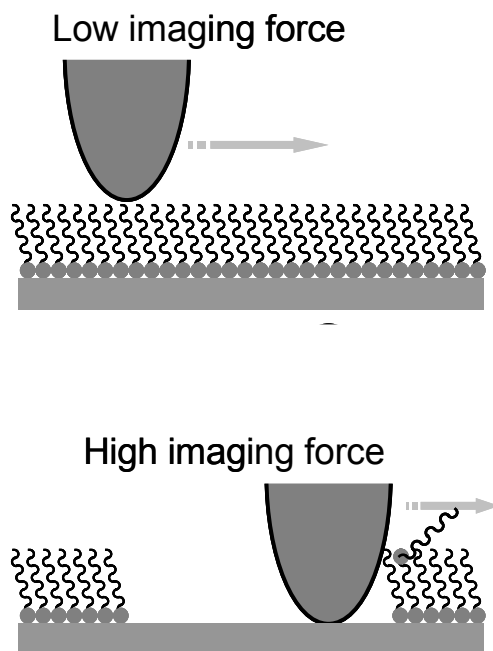


**Figure 2.7** Schematic diagram of the tip-direct displacement mechanism

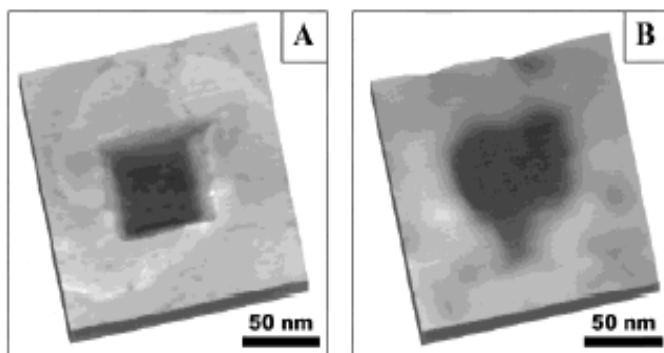


**Figure 2.8**  $160 \times 160 \text{ nm}^2$  topographic images of (A)  $\text{C}_{18}\text{S}-\text{Au}(111)$  and (B) OTS-mica with the thiols shaved away from the central  $50 \times 50 \text{ nm}^2$  square.

Liu, G. Y.; Xu, S.; Qian Y. *Acc. Chem. Res.* **2000**, 33, 457. Copyright [2000] American Chemical Society.

desorb the thiol. Too much loading force on the tip during the displacement process will cause plastic deformation of the underlying gold substrate. If the force is too low, adsorbed molecules will not be displaced. Therefore, the appropriate force for desorption should be determined by monitoring the changes in surface structure with a gradual increase in applied load. Because the threshold force depends on the local structure of the SAM, the geometry of the AFM tip, and the fabrication environment, it must be determined *in situ* for each experiment. If the displaced molecules are not sufficiently soluble in the solvent, a sharp pattern cannot be acquired because the thiol may redeposit. Figure 2.8A shows a topographic image of the square pattern produced in a  $\text{C}_{18}\text{S}-\text{Au}(111)$  SAM.

Siloxane layers on mica substrates can also be patterned using this method. A few covalent bonds exist between the siloxane molecules and the mica substrate due to the low density of hydroxyl groups on the mica surface. The siloxane SAMs are prepared by reacting the adsorbate and the substrate at  $120^\circ\text{C}$  for 2 hrs, which produces the cross-linking of the chains through the Si-O network. Due to the low reactivity of displaced molecules with the substrate, the displacement reaction is irreversible in a broad range of solvents. Figure 2.8B shows a hole formed in an octadecyltriethoxysilane(OTS)-mica SAM by the tip displacement method.

### 2.3.4 Nanografting

Tip-directed displacement is performed in a pure solvent so that desorbed thiol is dissolved away from the interface. If tip-directed displacement is performed in a solution of a different thiol, then the solvent can deliver a new thiol as well as remove the old thiol. The newly adsorbed thiol forms a pattern surrounded by the original one. Therefore, the advantage of this method over the previous one is its ability to complete the fabrication without a post-filling step.

The process of nanografting includes three steps (Figure 2.9B).<sup>35</sup> The first step is to characterize the SAM surface and select the area for fabrication. The second step is fabricating the desired pattern with a force greater than the displacement threshold. The final step is to characterize the pattern using the same tip with a reduced imaging force.

It is well known that the deposition of a high quality thiol film onto a macroscopic gold surface requires about 24 h. In contrast, a high quality nanografted pattern can be created in seconds. This implies that adsorption is accelerated under the condition of nanografting. Liu et al. attribute this acceleration to the spatial confinement of the thiol.<sup>33</sup> During nanografting, the AFM tip displaces adsorbed thiols within the matrix. Therefore, surrounding thiols and the tip spatially confine the newly exposed gold surface. This spatial confinement contributes to the acceleration of the substitution reaction and an improvement of monolayer quality in the substituted area. The accelerated kinetics and the resulting scar-free layer are illustrated in Figure 2.9. SPM and diffraction studies reveal that unconstrained self-assembly occurs in two main steps. Molecules initially attach to gold with their axis parallel to the surface, forming a “lying-down” phase as a reaction intermediate. To reach the final product, the thiol must “stand up” which requires activation energy to desorb the alkyl chain. During nanografting, a bare gold surface is exposed following the movement of the tip. The exposed gold surface is spatially confined by the tip and surrounding thiols. Due to the spatial confinement, the adsorption skips a lying down configuration. Thus, direct adsorption in the “standing up” configuration can proceed. The overall activation energy for the spatially confined self-assembly is probably lower than that in the unconstrained self-assembly process.<sup>33</sup>

This method can produce a great variety of patterns. A variety of shapes can be drawn, of different heights and with different functional groups. The broad choice of

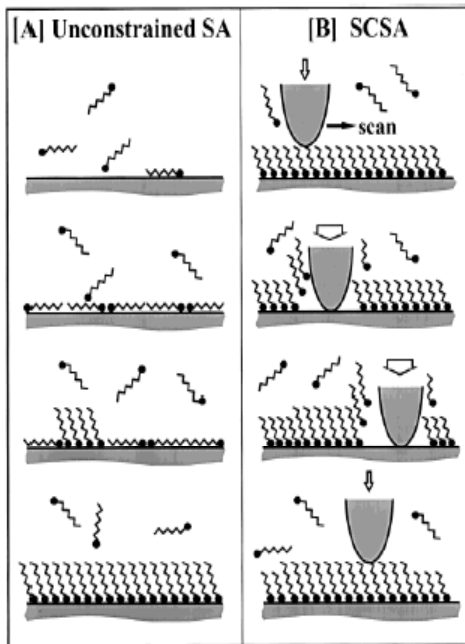


**Figure 2.9** Schematic diagram showing the reaction pathway for the (A) unconstrained and (B) spatially constrained self-assembly reaction

Liu, G. Y.; Xu, S.; Qian Y. *Acc. Chem. Res.* **2000**, 33, 457. Copyright [2000] American Chemical Society.

surface functional groups gives the opportunity to facilitate further reactions. It is also possible to produce multiple patterns with different functional groups by successive fabrication steps in different filling solutions.

Figure 2.10 shows a topographic image of a multiple material pattern. The spatial precision measured for both nanografting experiments is 2 nm. The corresponding cross-sectional line shows that the surfaces of the C<sub>22</sub>S and C<sub>18</sub>S islands are 1.17 ± 0.03 nm and 0.85 ± 0.05 nm higher than the C<sub>10</sub>S matrix monolayer, respectively. The vertical origin in the cursor profile represents the gold surface, the position of which is determined by displacing the adsorbed thiol layer.

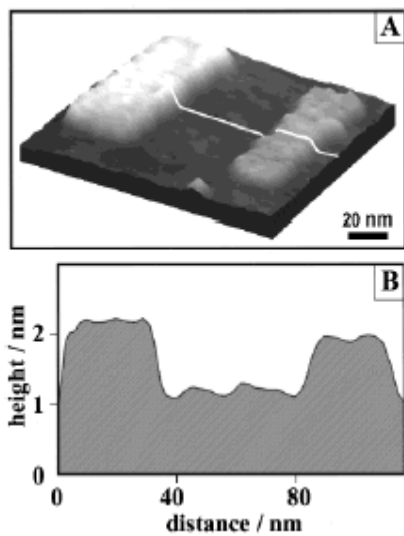


**Figure 2.10** (A) Topographic image of a  $\text{C}_{10}\text{S}$  matrix with a  $25 \times 60 \text{ nm}^2$   $\text{C}_{22}\text{S}$  and  $20 \times 60 \text{ nm}^2$   $\text{C}_{18}\text{S}$  nanoisland. (B) Corresponding cursor profile.  
Xu, S.; Miller, S.; Laibinis, P. E.; Liu, G. U. *Langmuir* **1999**, *15*, 7244. Copyright [1999] American Chemical Society.

### 2.3.5 Dip-pen Nanolithography

Dip-pen Nanolithography (DPN)<sup>36-38</sup> uses an AFM tip to deliver molecules to a surface through a solvent meniscus, which naturally forms in the ambient atmosphere. In this technique, an AFM tip is coated with a thin film of thiol molecules. When the tip is placed close to the surface in an atmosphere containing a high concentration of water vapor, a minute drop of water condenses between the tip and surface, and the thiol molecules migrate from the tip to the surface through the water meniscus. The tip is then scanned across the surface to deliver the thiols where desired. The chemisorption of ink molecules to the substrate is the driving force for the transportation of the ink from the AFM tip through the water to the substrate. Due to the high reactivity of thiol functional groups with gold, a compact monolayer can be formed as the ink molecules migrate onto the substrate following a scanning track (Figure 2.11).

The success of DPN depends on two main factors: a narrow spatial deposition of patterning molecules, and self-assembly of the functionalized ink molecules to form a compact monolayer. The transport rate and the linewidth of the pattern depend on the size of the meniscus, which can be controlled by adjusting the relative humidity. The tip-substrate contact time and thus the scan speed also influence DPN resolution. Faster scan speeds can produce narrower lines, however, too much speed results in a failure of effective transportation of the ink molecules.

Piner et al.<sup>36</sup> prepared the dot patterns by DPN to demonstrate the diffusion properties of the ink molecules. The tip was coated with 1-octadecanethiols or 16-mercaptophexadecanoic acids and brought into contact with the gold substrate for a set period of time. The size of dot pattern depends on the contact time and the diffusion properties of ink molecules on the substrate. The uniform shape of the dots reflects an even flow of molecules in all directions from the tip to the surface. An array of 25 dots, 0.46  $\mu\text{m}$  in diameter, spaced 0.54  $\mu\text{m}$  apart was generated by holding a tip in contact with the surface for 20 s for each dot and moving to the next position. A grid consisting of eight intersecting lines 2  $\mu\text{m}$  in length and 100 nm wide was generated by scanning the tip across the gold surface at a 4- $\mu\text{m}/\text{s}$  scan speed with a 1-nN force for 1.5 min to form each line.

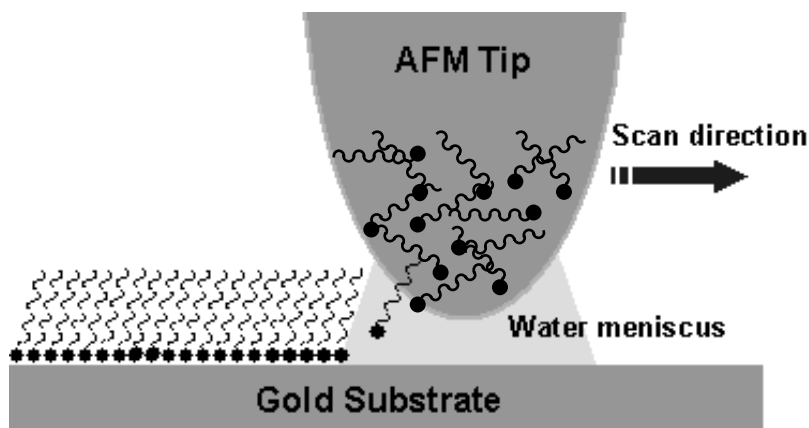


**Figure 2.11** Schematic representation of DPN

### 2.3.6 Nanofabrication of SAMs with Tunneling Electrons

In STM-based lithography, tunneling electrons are used to achieve nanofabrication of SAMs. As illustrated in Figure 2.12, SAMs are first imaged under a very low tunneling current, and then fabrication locations are chosen. Unlike in AFM, STM tips are not in contact with the surface during imaging. Under ultrahigh vacuum, the tunneling current is slowly increased while the bias voltage is maintained. As the tunneling current is increased beyond a certain threshold, the displacement of adsorbate molecules occurs. The resulting patterns can then be imaged at a reduced current.

STM-induced lithographic fabrication of patterns in SAM surfaces is a complex process controlled by numerous parameters. Patterning is critically dependent on the tip-substrate bias and total Coulomb dose. The fabrication current is the key parameter in maintaining a local tip-surface interaction. At a fixed bias voltage, the tunneling current in STM increases exponentially with decreasing tip-surface distance. Currents that are too high cause the STM tips to attach to the surface, resulting in non-local fabrication such as

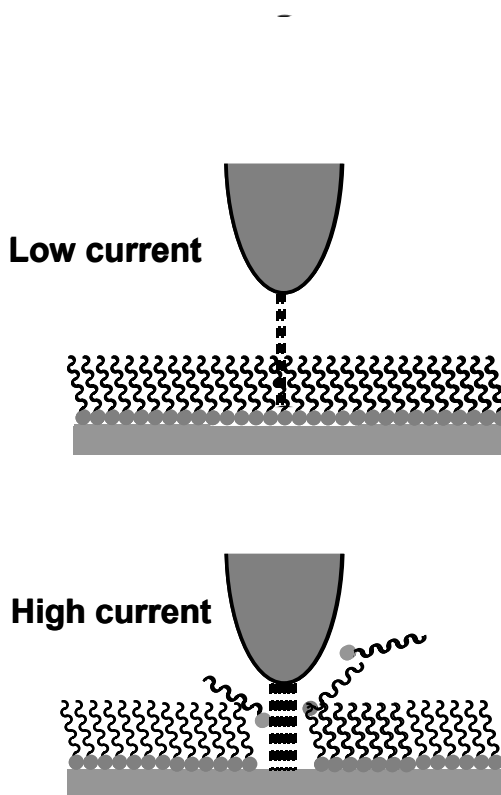


**Figure 2.12** Schematic diagram of STM-induced lithography

the formation of deep pits or irregularly shaped clusters. On the other hand, if the current is too low, molecules cannot be displaced. To determine the threshold current, the imaging conditions for SAMs should be optimized first. This process is done by keeping the voltage constant, while gradually increasing the current by moving the tip toward the surface. A large increase in current is observed when the current reaches the fabrication threshold. The increase is attributed to the displacement of the surface molecules under the tip.

### 2.3.7 Nanometer-sized Protein Patterning

The attachment of biomolecules, in particular proteins, onto solid substrates is a fundamental step in the development of advanced biosensors, bioreactors, affinity chromatographic separation materials, and many diagnostic techniques. In order to investigate the biomolecular structure and function with AFM, a strong attachment of the biomolecule to a substrate is often required.

SAMs provide ideal model systems for the study of the interactions of proteins and cells. With AFM lithography, interfaces can be produced, whose physical and chemical properties can be fabricated at the molecular level at the terminal position of the alkanethiols. They are stable enough to be used in model studies of the adsorption of proteins and the adhesion of cells to surfaces.

Protein patterning on SAMs is produced through two main steps. First, producing a patterned self-assembled monolayer, which contains spatially separated components terminated with protein resistive and adhesive groups, respectively. Second, selectively adsorbing proteins onto the patterned substrate. The quality of the protein nanostructures depends on the special precision of SAM nanopatterns and on the selectivity of protein adsorption.

Wadu-Mesthrige et al.<sup>28</sup> produced nanometer-sized patterns of SAMs using an AFM-based lithography technique and also characterized the patterns *in situ* using AFM. The patterning and imaging of SAMs were conducted in an aqueous medium containing 1 mM HS(CH<sub>2</sub>)<sub>2</sub>COOH within a matrix CH<sub>3</sub>(CH<sub>2</sub>)<sub>9</sub>S/Au(111) SAM. After washing the patterned SAM with deionized water, 10 µg/mL lysozyme (LYZ) solution was injected into the cell. At neutral pH, LYZ exhibits net positive charges while ~10 % of the

carboxylate termini have negative charge. Therefore, the selective adsorption of LYZ is driven onto the HOOC-terminated areas by electrostatic attraction. It is known that proteins adsorb on the hydrophobic surfaces, including methyl-terminated SAMs. But LYZ did not adsorb onto alkanethiol SAMs under their conditions. A large portion of proteins retains their activity after adsorption. The electrostatic immobilization process of proteins is reversible. By changing the pH and washing out with surfactant solution, adsorbed proteins can be removed and substituted by other proteins.

While electrostatic immobilization is pH dependent, a more stable protein pattern can be achieved by the formation of covalent bonds. Nanopatterns of immunoglobulin G and LYZ were produced within aldehyde-terminated areas through the formation of imine bonds. Proteins adsorb on both aldehyde- and methyl terminated areas. However, by washing with surfactant solution, the adsorbed proteins in the methyl-terminated areas by hydrophobic interaction can be completely removed. 50% of IgG molecules within nanopatterns retain their bioactivity. These studies provide a useful guide for the exploration of chemical and biochemical reactions, and the development of biosensors and biochips.

Recently, Jinho Hyun et al.<sup>39</sup> demonstrated the stepwise fabrication of protein nano patterns using DPN (Figure 2.13). First, they produced a pattern with a SAM of 16-mercaptophexadecanoic acid (MHA) using DPN on a gold substrate and the pattern was resolved by lateral force microscopy (A). The surrounding gold background of the surface was then incubated with 11-mercaptopundecyltri(ethylene glycol) (EG<sub>3</sub>-SH) solution to create a protein-resistant SAM in the unpatterned region. Because of the longer chain length of ethylene glycol as compared with the patterning molecule, the height image of the patterned regions shows negative contrast (E). The terminal COOH groups in the patterned SAM were converted to activated N-hydroxysuccinimidyl ester,<sup>40</sup> followed by reaction with biotin-NH<sub>2</sub>, which results in covalent binding of biotin to the patterned region. An AFM image after the covalent attachment of biotin shows a 0.8 nm height difference between the patterned area and the background (B, E). The patterned surface was then immersed into a solution of fluorescently labeled streptavidin. Figure C and E shows that streptavidin preferentially adsorbed on the patterned region. The streptavidin-patterned surface was immersed again into a solution of conjugated biotin-

bovin serum albumin in order to demonstrate the ability to immobilize other biomolecules on the patterned streptavidin. Figure D and E shows the height increase of the patterned feature compared to the streptavidin pattern.

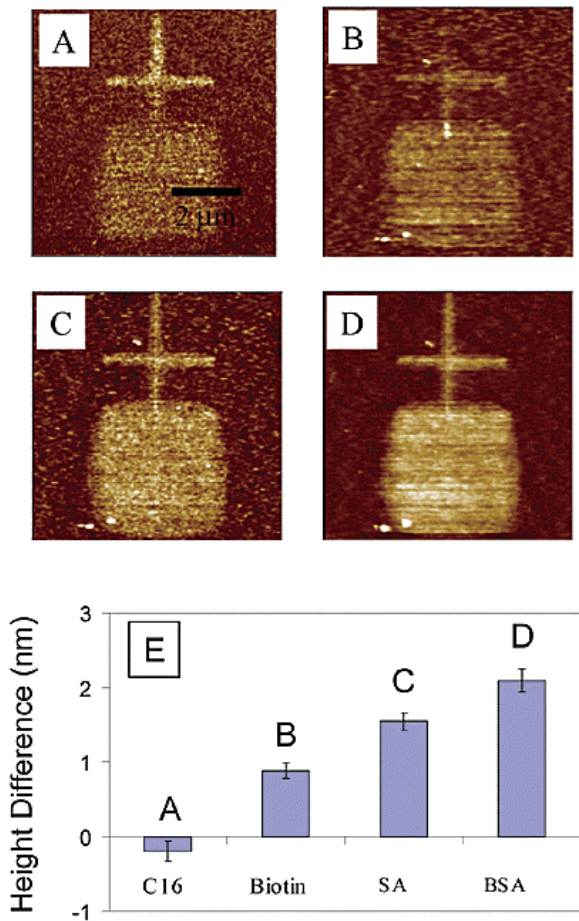


**Figure 2.13** (A) Lateral force image of an MHA SAM on gold patterned by DPN. (B) Height image (Tapping Mode) of biotin-amine coupled to the MHA SAM after backfilling the background in (A) with an EG<sub>3</sub>-SH SAM and activation of the terminal COOH groups of the MHA SAM. (C) Height image (Tapping Mode) of the same surface after incubation of the biotin pattern in (B) with streptavidin. (D) Height image (Tapping Mode) of the surface after incubation of the streptavidin pattern in (C) with biotinylated BSA. (E) Height difference between the pattern and the background referenced to the background EG<sub>3</sub>-SH SAM in (B) (labels A-D refer to images A-D). Hyun, J.; Ahn, S. J.; Lee, W. K.; Chilkoti, A.; Zauscher, S. *Nano Lett.* **2002**, 2(11), 1203. Copyright [2002] American Chemical Society.

## 2.4 Preparation of Uniformly Flat Gold Surfaces

AFM lithographic techniques produce features that are very small: about 20-1000 nm in width and about 0.1-5 nm in height. In order to view these structures, it is essential to have a very smooth and uniform starting substrate. Ideally, the substrate should have a roughness of < 0.5 nm over an area of about 10  $\mu\text{m}$ . In this section, I describe methods for preparing such substrates.

### 2.4.1 Evaporation of Gold onto Smooth Substrates

The most traditional and simple way is the annealing method (Figure 2.14).<sup>41</sup> Gold can be evaporated onto mica or silicon to produce thin films. However, gold does not wet these substrates and the gold forms discrete islands of about a few 100 nm in size that are not suitable for AFM experiments. The wetting problem can be overcome by the deposition of a thin “adhesion layer” of titanium or chromium before deposition of gold. The gold then forms a continuous film but the film is not smooth. A smoother film can be obtained by heating the film in a hydrogen/oxygen flame or in an oven. This annealing process produces samples with flat Au(111) terraces as large as  $300 \times 300 \text{ nm}^2$ . However, in many cases, these terraces are too small for complex pattern formation.

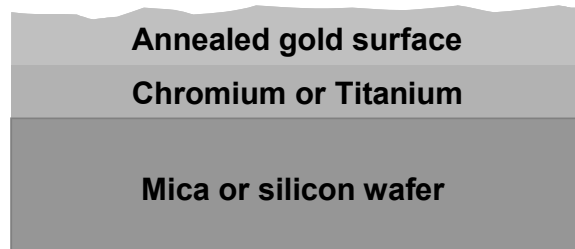


**Figure 2.14** Annealing method produces a flat Au(111) terraces as large as  $300 \times 300 \text{ nm}^2$

### 2.4.2 Template Stripping

The second method is template stripping.<sup>42</sup> A thin gold layer is evaporated onto a fresh mica sheet, and another substrate is glued to the gold surface. After curing of the

glue, the glued substrate, together with the gold, is stripped from the mica. The exposed gold surface is a replica of mica surface. Many people use silicon wafers instead of mica because it is easier to cleave silica than mica from the gold surface. Using this method, flat gold terraces as large as a few  $\mu\text{m}^2$  can be acquired. The advantages of this technique are the production of larger flat area and the practically unlimited storage time because the surfaces can be kept unstripped.

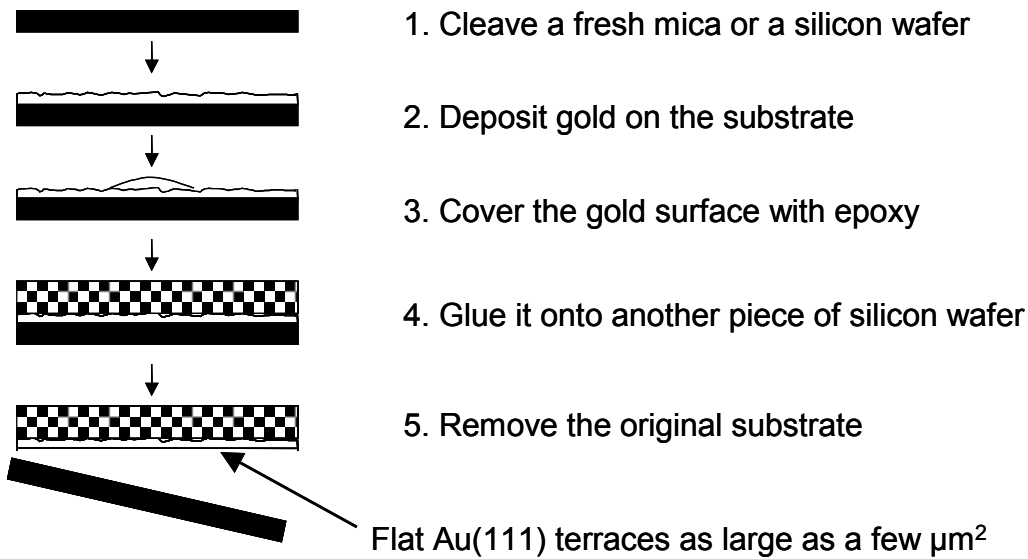


**Figure 2.15** The template stripping method produces a flat gold terrace as large as a few  $\mu\text{m}^2$

#### 2.4.3 Melting and Freezing of Bulk Gold Samples

If nm- or larger-sized pieces of gold are melted then frozen, the frozen surface contains large (several  $\mu\text{m}^2$ ) regions of crystalline (111) terraces of atomically smooth gold. This method is usually applied to gold wire.<sup>43</sup> A piece of pure gold wire is cleaned with piranha solution and rinsed with ultra-pure water. The wire is then placed in a hydrogen/oxygen flame and allowed to melt until a droplet is formed. The radius of the

droplet is ~ 2 times bigger than the wire. The droplet is further annealed for a short time in a cooler part of the flame. The resulting gold surfaces are composed of two distinct regions: large flat (111) terraces (several  $\mu\text{m}^2$ ) separated by atomic steps and a rough V-shaped region.

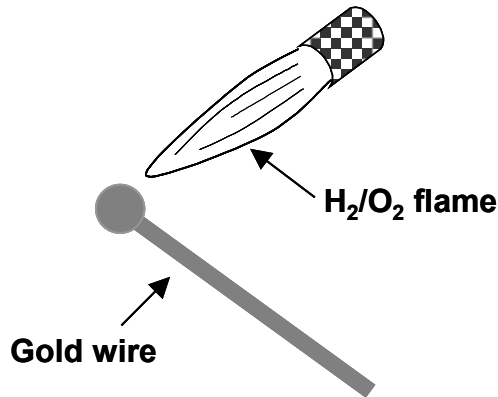


**Figure 2.16** Gold wire flaming method produces large flat Au(111) terraces (several  $\mu\text{m}^2$ ) and ripples

#### 2.4.4 Comparison of Techniques

Template stripping is a useful method when a large flat area is required. However, the surface made by template stripping is less smooth than the one obtained by annealing. Another problem with this technique is that cleavage is not always successful. When very large flat areas are not required, the annealing method is recommended because of its ease of manufacture. The shortcoming of the annealing method is that it gives small flat areas. Gold wire flaming is a good method but does not appear to be popular. All three methods were examined in this study. We ultimately used the gold wire flaming method for our study because it provides large and ultra-flat gold surfaces, and it is also relatively easy to prepare samples.

## 2.5 Conclusion

In undergraduate chemistry, we learned that gold is inert toward virtually all chemicals except for the most aggressive oxidants. One important exception is the reactivity with thiol. This great selectivity allows researchers to attach a variety of functional groups to gold via thiols: Gold surfaces are covered rapidly by monolayers of thiolate units when exposed to either thiol-containing solutions or to thiol vapors. The diversity and the ease of fabrication of SAMs with the inertness of gold provide an excellent interface between electronics and complex structures.

AFM- or STM-induced lithographic fabrication of patterns in SAMs is a complex process controlled by numerous parameters that can be manipulated by varying experimental conditions such as the scan rate, tunneling current, applying force, and number of patterning scans to obtain desired patterns of nanoscale dimension. The beauty of AFM lithography over conventional methods is extremely small and precise modification of surfaces. However, the limitation is relatively low fabrication speeds because the fabrication steps are serial instead of parallel in nature. Therefore, at present, AFM-assisted lithography is used as a research tool in laboratories instead of as a manufacturing tool for high throughput applications. One solution for the speed limitation is to use multiple AFM probes to write in series. Quate's group is fabricating multiple AFM probes on a single chip, and demonstrated independent lithography with 1000 probes in parallel.<sup>44</sup> Another solution is to use AFM lithography to produce a master that rapidly stamps out multiple copies like microcontact printing.

Although not yet practical for high throughput applications and manufacturing, AFM lithography studies provide fundamental information on tip-surface interactions, structures, and properties on a nanoscopic level. The precisely engineered nanostructures allow the exploration of chemical and biochemical reactions under spatially well-defined and controlled environment. These studies serve as a useful guide in the development of nanoelectronic devices, biosensors, and biochips.

## References

- (1) Bishop, A.; Nuzzo, R. G. *Curr. Opin. Colloid Interface Sci.* **1996**, *1*, 127.
- (2) Abbott, N. L.; Kumar, A.; Whitesides, G. M. *Chem. Mater.* **1994**, *6*, 596.
- (3) Tiberio, R. C.; Craighead, H. G.; Lercel, M.; Lau, T.; Sheen, C. W.; Allara, D.L. *Appl. Phys. Lett.* **1993**, *62*, 476.
- (4) Xia, Y.; Whitesides, G. M. *J. Am. Chem. Soc.* **1995**, *117*, 3274.
- (5) Huang, J. Y.; Dahlgren, D. A.; Hemminger, J. C. *Langmuir* **1994**, *10*, 626.
- (6) Talov, M. J.; Burgess, D. R. F.; Gillen, G. *J. Am. Chem. Soc.* **1993**, *115*, 5305.
- (7) Kumar, A.; Abbott, N. L.; Kim, E.; Biebuyck, H. A.; Whitesides, G. M. *Acc. Chem. Res.* **1995**, *28*, 219.
- (8) Tender, L. M.; Worley, R. L.; Fan, H.; Lopez, G. P. *Langmuir* **1996**, *12*, 5515.
- (9) Wei, J.; Hoogen, N.; Lippert, T.; Nuyken, O.; Wokaun, A. *J. Phy. Chem. B* **2001**, *105* (6), 1267.
- (10) Harnett, C. K.; Satyalakshmi, K. M.; Graighead, H. G. *Langmuir* **2001**, *17*, 178.
- (11) Bumm, L. A.; Arnolds, J. J.; Cygan, M. T.; Dunbar, T. D.; Brugge, T. P.; Jones, L.; Allara, D. L.; Tour, J. M.; Weiss, P. S. *Science* **1996**, *271*, 1705.
- (12) Nuzzo R. G.; Allara D.L. *J. Am. Chem. Soc.* **1983**, *105*(13), 4481.
- (13) Xu, S.; Laibinis, P. E.; Liu, G. Y. *J. Am. Chem. Soc.* **1998**, *120*, 9356.
- (14) Zhang, Z.; Hou, S.; Zhu, Z.; Liu, Z. *Langmuir* **2000**, *16*(2), 537.
- (15) Colorado, R.; Villazana, R. J.; Lee, T. R. *Langmuir* **1998**, *14* (22), 6337.
- (16) Karpovich, D. S.; Blanchard G. J. *Langmuir* **1997**, *13*, 4031.
- (17) Kondo, T.; Yanagida, M.; Shimazu, K.; Uosaki, K. *Langmuir* **1998**, *14*, 5656.
- (18) Yamamoto, H.; Butera, R. A.; Gu, Y.; Waldeck, D. H. *Langmuir* **1999**, *15*, 8640.
- (19) Ton-That C.; Shard, A. G.; Bradley, R. H. *Langmuir* **2000**, *16*, 2281.
- (20) Zhou, Y.; Fan, H.; Fong, T.; Lopez, G. P. *Langmuir* **1998**, *14*, 660.
- (21) Vaeth, K. M.; Jackman, R. J.; Black, A. J.; Whitesides, G. M.; Jensen, K. F. *Langmuir* **2000**, *16*, 8495.
- (22) Fery, T. P.; Herminghaus, S.; Kriele, A.; Lorenz, H.; Kotthaus, J. P. *Langmuir* **1999**, *15* (7), 2398.

- (23) Libioulle, L.; Bietsch, A.; Schmid, H.; Michel, B.; Delamarche, E. *Langmuir* **1999**, *15* (2), 300.
- (24) Lackowski, W. M.; Ghosh, P.; Crooks, R. M. *J. Am. Chem. Soc.* **1999**, *121* (6), 1419.
- (25) He, H. X.; Zhang, H.; LI, Q. G.; Zhu, T.; Li, S. F. Y.; Liu, Z. F. *Langmuir* **2000**, *16*, 3846.
- (26) Dulcey, C. S.; Georger, J. H.; Chen, M.S.; McElvany, S. W.; O'Ferrall, E.; Benezra, V. I.; Calvert, J. M. *Langmuir* **1996**, *12*, 1638.
- (27) Lee, B. W.; Clark, N. A. *Langmuir* **1998**, *14* (19), 5114.
- (28) Wadu-Mesthrige, K.; Xu, S.; Amro, N. A.; Liu, G. *Langmuir* **1999**, *15*, 8580.
- (29) Amro, N. A.; Xu, S.; Liu, G. *Langmuir* **2000**, *16*, 3006.
- (30) Jonathan K.; Schoer and Richard M.; Crooks. *Langmuir* **1997**, *13*, 2323.
- (31) Wang, J.; Kenseth, J. R.; Jones, V. W.; Green, J. B.; McDermott, M. T.; Porter, M. D. *J. Am. Chem. Soc.* **1997**, *119*, 12796.
- (32) Ross, C. B.; Sun, L.; Ceooks, R. L. *Langmuir* **1993**, *9*, 632.
- (33) Liu, G. Y.; Xu, S.; Qian Y. *Acc. Chem. Res.* **2000**, *33*, 457.
- (34) Schessler, H. M.; Karpovich, D. S.; Blanchard, G. J. *J. Am. Chem. Sco.* **1996**, *118*, 9645.
- (35) Xu, S.; Miller, S.; Laibinis, P. E.; Liu, G. Y. *Langmuir* **1999**, *15*, 7244.
- (36) Piner, R. D.; Zhu, J.; Xu, F; Hong, S.; Mirkin, C. A. *Science*, **1999**, *283*, 661.
- (37) Hong, S.; Zhu, J.; Mirkin, C. A. *Science*, **1999**, *286*, 523-525.
- (38) Hong, S.; Mirkin, C. A. *Science*, **2000**, *288*, 1808-1811.
- (39) Hyun, J.; Ahn, S. J.; Lee, W. K.; Chilkoti, A.; Zauscher, S. *Nano Lett.* **2002**, *2*(11), 1203.
- (40) Lahiri, J.; Isaacs, L.; Tien, J.; Whitesides, G. M. *Anal. Chem.* **1999**, *71*, 777.
- (41) Liedberg, B.; Tengvall, P. *Langmuir* **1995**, *11*, 3821.
- (42) Stamou, D.; Gourdon, D.; Liley, M.; Burnham, N. A.; Kulik, A.; Vogel, H.; Duschl, C. *Langmuir* **1997**, *13*, 2425.
- (43) Li, L.; Yu, Q.; Jiang, S. *J. Phys. Chem. B* **1999**, *103*, 8290.
- (44) Physics News 511, November 8, 2000.

## **Chapter 3. Atomic Force Microscopy**

### **3.1 Introduction**

Scanning Probe Microscopy (SPM) is a revolutionary set of techniques, which enables researchers to obtain three-dimensional images of surfaces at the nm to atomic scale. Conventional microscopy (optical and electron microscopy) is far-field microscopy. In far-field microscopy, the characteristics of the sample are discovered by placing a detector a long way ( $\gg \lambda$ ) from the sample. Far-field microscopy is thus diffraction limited. In near-field microscopy, the detector is placed very near the sample ( $\ll \lambda$ ) so that the detection is not diffraction limited. The very high lateral resolution of near-field microscopy arises from the very small lateral extent of the detector – information is only gathered from a very small part of the sample. The basic elements of a near-field microscope are:

1. Part of the detector (the tip) is close to the sample to enable near field detection.
2. A very small tip to obtain high resolution.
3. A very precise and accurate 3-dimentional translation stage to position the detector.
4. A computer to control the position and to record the output from the detector.

The first type of SPM to be developed was the Scanning Tunneling Microscope (STM). It was developed by Binnig and Rohrer working at IBM in Switzerland in 1981. In STM, an extremely fine conducting probe is held close to the sample. A tunneling current generated between the surface and the tip produces an electrical signal while the tip slowly scans across the surface at a distance of only about an atom's diameter. The tip is raised and lowered in order to keep the signal constant and maintain the distance. Recording the vertical movement of the tip produces a computer-generated contour map of the surface.

The second type of SPM was Atomic Force Microscopy. It was developed by Binnig and Quate in 1986.<sup>1</sup> Although the ability of STM to obtain an atomic-scale image is clearly outstanding, there is a severe limitation: both the tip and the surface must be good conductors. The invention of AFM satisfied the need for imaging an insulating surface. In AFM, the sum of long-range attractive interactions and short-range repulsive interactions between the probe and the sample surface provides the contrast mechanism instead of a tunneling current. The probe tip is brought into continuous or intermittent contact with the surface by a piezoelectric scanner. A constant force between the tip and the sample is maintained while the tip is raster scanned across the surface. Then the system produces a three-dimensional surface image by mapping scanner movements in z direction relative to the x-y scan direction. AFM enables not only imaging the surface in atomic resolution but also measurements of the force between the tip and the surface at the nanonewton scale. The force between the tip and surface is measured by tracking the deflection of the cantilever.<sup>2</sup>

Another representative type of SPM is Scanning Near-field Optical Microscopy (SNOM). It was developed by Betzig, Trautman, and Harris at the AT&T Bell laboratories in 1991.<sup>3</sup> In SNOM, Light passes through a sub-wavelength diameter aperture and illuminates a sample that is placed at a distance much smaller than the wavelength of the light. The changes in light intensity or the polarization of the light are usually used to obtain contrast.

Although the features and the characteristics of each method are different, a common instrumental principle rules whole families of SPM, the measurements of which are performed with a sharp probe scanning over the surface at very short distances. As the tip can be modified in many different ways, the number of techniques is continuously growing. Of the many SPMs, AFM is currently the most widely used variant. It is the focus of this chapter.

## 3.2 Scanning Probe Technology

### 3.2.1 Fundamentals

Near-field operation means that the probe has to maintain a very small separation from the surface during the scanning. In order to obtain high spatial resolution, the probe has to be maintained in the near-field regime and lateral position has to be precisely controlled.

The development of the piezoelectric actuator made positioning possible with atomic and even sub-atomic accuracy.<sup>4</sup> A piezoelectric material undergoes a change in geometry when an electric field is applied to it. If a sample is attached to one end of the piezoelectric scanner, the sample moves when the piezoelectrode changes shape. The direction and the amount of motion depend on the type and the shape of piezoelectric material and the field strength.

### 3.2.2 Basic SPM Components

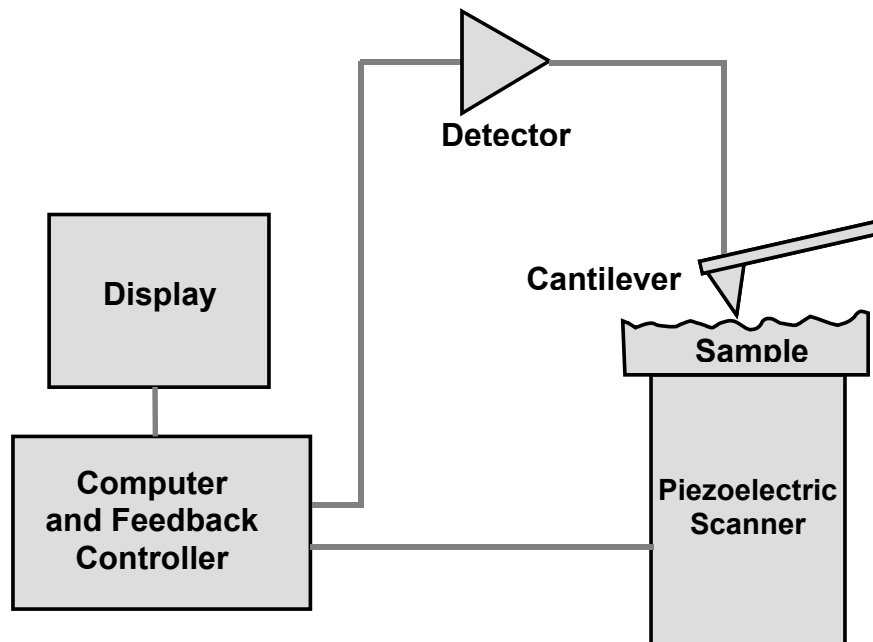


**Figure 3.1** Components of a scanning probe instrument

**Detector :** In order to detect local forces and maintain a narrow spacing, the sharp probe has to be linked to a force sensor which detects the force between the probe and the surface. By assuming that constant force means constant separation between two surfaces, it provides a correction signal to the piezoelectric scanner to keep the spacing constant. A light beam deflection system is widely used for SPM. In this system, a laser beam is directed onto the back of the cantilever. A segmented photodiode measures the deflection of a cantilever spring by detecting the reflected laser beam. The light signal detected is then converted into forces according to Hook's law:

$$\Delta z = \Delta F/c \quad (1)$$

where  $\Delta z$  is the deflection of cantilever,  $\Delta F$  is the acting force and  $c$  is the spring constant. A position-sensitive photodiode detector, segmented into four quadrants, detects the spatial variation of the reflected laser beam. The relative displacement of a reflected laser beam is then converted into the cantilever deflection ( $\Delta z$ ).

If the reflected laser beam moves between the upper and the lower part of the segmented detector as the tip scans over the surface, the relative displacement of the laser beam can be represented as:

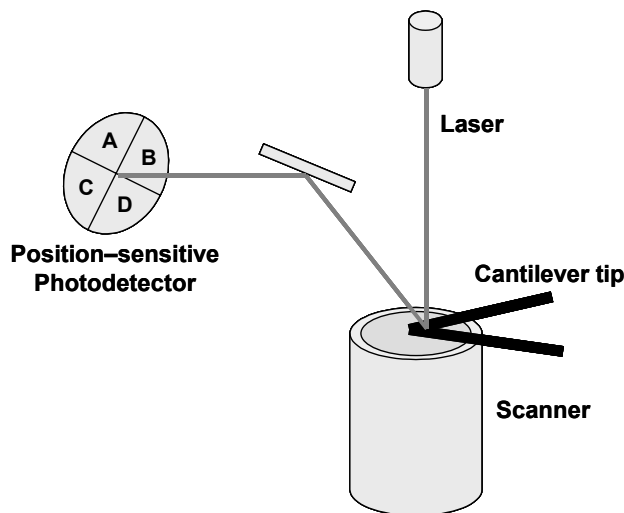


**Figure 3.2** Beam-deflection set-up for the detection of interacting force in an AFM.

$$\Delta I_{vertical} = (\Delta I_A + \Delta I_B) - (\Delta I_C + \Delta I_D) \quad (2)$$

where  $\Delta I_i$  is the change in intensity on segment  $i = A$  through  $D$ . For small deflections, the deflection of the cantilever ( $\Delta z$ ) is related to  $\Delta I_{vertical}$  by

$$\Delta I_{vertical} = \Delta z d/l \quad (3)$$

where  $d$  is the length of the light path subsequent to reflection and  $l$  is the length of the cantilever. If the cantilever is scanned across a sample surface with mechanical contact, the frictional force causes the twisting of cantilever as well as the vertical deflection. Then the twisting of the cantilever results in a horizontal displacement of the laser beam on the photodetector surface:

$$\Delta I_{horizontal} = (\Delta I_A + \Delta I_C) - (\Delta I_B + \Delta I_D) \quad (4)$$

In standard imaging, a triangular cantilever is normally used to minimize the torsion effect. Recently, it has been shown that this is not true. The torsional stiffness is actually greater for rectangular beams. However, this torsion effect can be used for mapping frictional forces between the probe and sample surfaces in Lateral Force Microscopy (LFM).

**Probe :** A variety of commercial cantilever-tips are available. The following parameters are important in tip selection.

1. Material
2. Spring constant
3. Sharpness

Silicon nitride ( $Si_3N_4$ ) is hard and tough (tough means it does not fracture), so it is ideal for imaging.  $Si_3N_4$  is not reflective so  $Si_3N_4$  cantilever must be gold coated. Because of the different thermal expansion co-efficient between silicon nitride and gold, these cantilevers bend when the temperature changes. Silicon is sometimes used as an alternative because it is reflective and can be used without a gold coating. Anisotropic

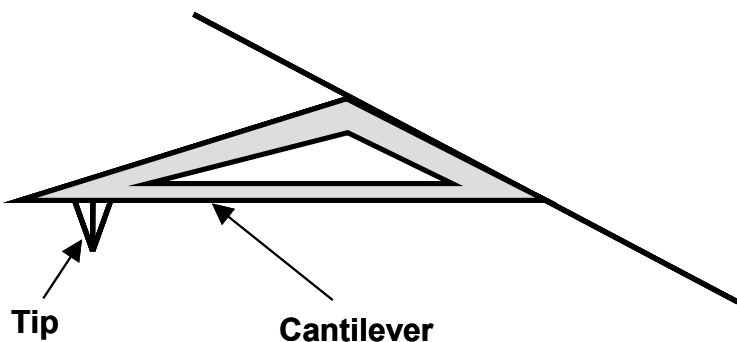


**Figure 3.3** Typical AFM cantilever/tip

etching of silicon can also be used to make sharper tips than for silicon nitride. The best tip may have a radius of curvature of around 5 nm. However, silicon is more brittle than silicon nitride.

Each cantilever has its own spring constant usually less than the inter-atomic bond strength (about 1 Newton/m). One can achieve the topographic image of a surface by sliding the cantilever/tip across the surface and monitoring the cantilever deflection. Most contact mode AFM uses a silicon nitride tip. This tip is more flexible than a silicon tip, which makes it easier to use and less brittle. Because a silicon tip is very stiff, more caution is required while setting up the tip and the sample. Due to the continuing growth of SPM technology, new kinds of probes are constantly developed. A wide range of chemically functionalized tips is commercially available today.

**Electronics and Control System :** The electronics units provide the interface between the scanning system and the computer. It supplies voltages to the scanner to position the tip in the correct place and synchronize the signal from the position-sensing units. It includes the feedback control system for maintaining a constant spacing between the tip and sample surface.

The feedback loop is designed to keep the force between the tip and sample at a constant value. The feedback loop compares the actual force to a “set-point” force. If the

two are not identical, a signal is sent to the z-component of the piezoelectric scanner to move the tip closer to or further away from the sample. Thus, the feedback loop causes a constant force as desired by the user. In tapping mode AFM, the feedback loop is used to maintain constant RMS amplitude of vibration. By the control of a suitable feedback-loop system, a probe can scan along the x and y directions upon continuously varying the z direction, so that the interaction is kept constant. A three-dimensional image of the surface can be constructed by plotting the z driving voltage of the piezoelectric actuator as a function of x-y coordinates.

**Vibration Isolation :** AFM images are very sensitive to vibration. If vibration from the environment causes a tip-sample displacement then this will appear as noise in the AFM image. Vibration isolation must be used to keep tip-sample vibration below about 1 Å. The AFM must be made small and rigid in order to have a high resonance frequency. Low frequency vibrations are removed by connecting the AFM to the surroundings by a mechanical low-pass filter. One effective system consists of a large mass (~10 kg) suspended from elastic bungee cords with a resonant frequency of less than 1 Hz. This set-up isolates the AFM from building vibrations. The AFM can also be isolated from airborne acoustic vibrations by placement within an enclosure.

### 3.3 AFM Imaging Modes

#### 3.3.1 Contact-Mode

Contact mode is the most common operation method of AFM. As the name suggests, the tip stays within a few Angstroms of the sample during imaging. While raster-scanning across the surface, the cantilever exhibits a locally varying deflection, which represents the corrugation of the sample surface. Because the deflection of the cantilever is directly proportional to the force between the two surfaces, the cantilever deflection represented by the laser spot intensity for quadrants, (A+B)-(C+D), can be regarded as the vertical force signal. The feedback loop constantly measures the local tip-sample interaction by recording the deflection of the tip and sends the correction signal to

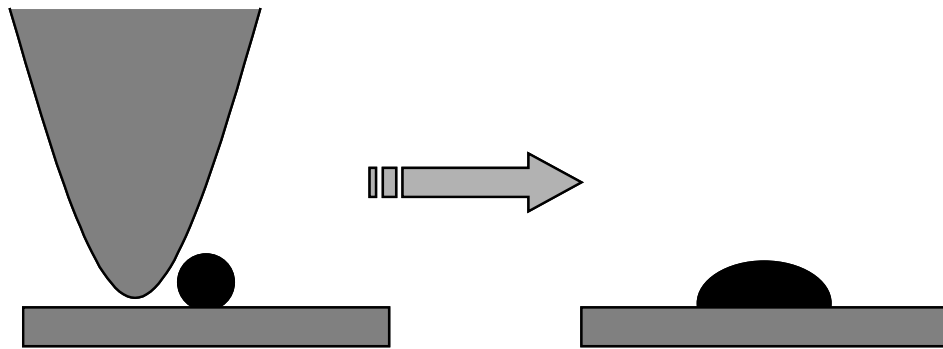


**Figure 3.4** Tip convolution occurred by the side contact of tip to the specimen

the scanner to keep the cantilever deflection constant. Therefore, the sample-tip spacing is increased if the local force exerted on the tip becomes higher than the set-point value and it is decreased if the force falls below the set point. Three-dimensional height image of the surface is then constructed by plotting the vertical movements of the piezoelectric scanner versus horizontal coordinates. Color mapping is widely used for displaying local height differences, for example black for the lowest features and white for the highest features.

One of the most important factors for obtaining true atomic resolution with an AFM is the sharpness of the tip. The need for a sharp tip is well explained in terms of tip convolution. The main influences of the tip on an image are

- Broadening
- Compression
- Aspect ratio

Tip broadening arises when the radius of curvature of the probe is greater than or comparable to the size of the object being imaged. As the probe scans over the object, the side of the probe contacts the specimen before the apex does, which results in the broadening of the object in the image (Figure 3.4). This phenomenon is called tip convolution.

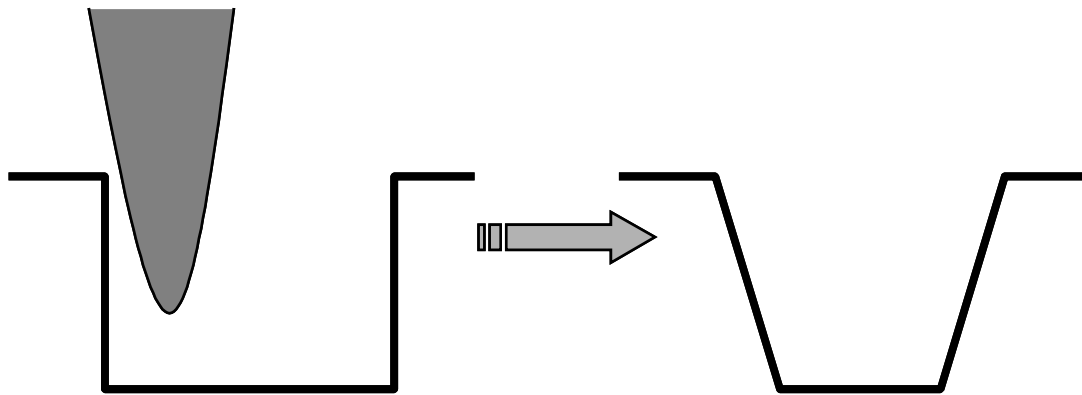


**Figure 3.5** The image of a steep-wall feature affected by the cone angle of the tip

Compression occurs when the probe scans over some soft biological polymers such as DNA. Even though the force between the tip and sample may only be nN, the pressure onto the sample surface can be MPa.

The aspect ratio (cone angle) of the tip affects on the image when observing a steep sloped feature (Figure 3.5).

### 3.3.2 Lateral Force Microscopy

Friction is a well-known phenomenon occurring when two surfaces in contact are in relative motion. A frictional force  $F_f$  is related to the contact area between the two bodies. Since all surfaces are rough in microscopic scale, the actual contact area is the sum of relatively few exposed sites establishing a mechanical contact between the two bodies. Therefore, the total frictional force  $F_f$  is proportional to the actual contact area  $A$ .

$$F_f \propto A \quad (5)$$

When a loading force  $F_l$  is increased, the number of microcontact sites and thus the total contact area is increased.

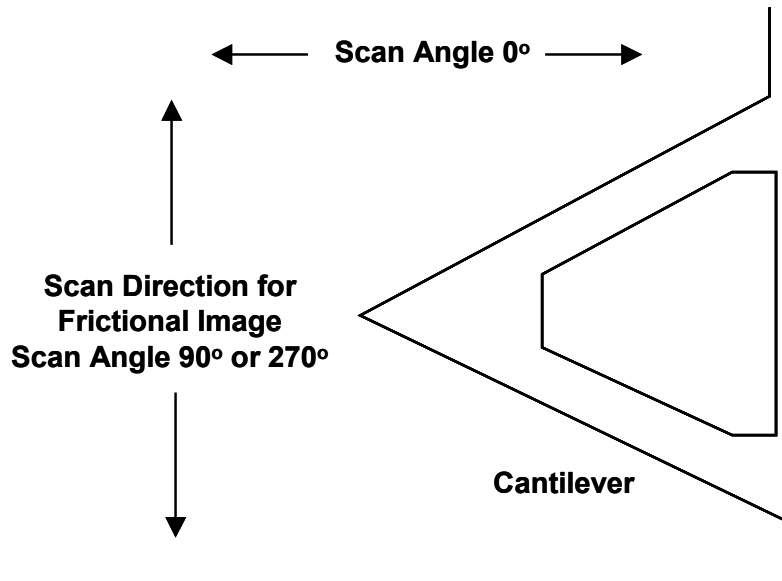


**Figure 3.6** Scan angle selection for frictional imaging

$$A \propto F_l \quad (6)$$

The combination of Eqs. (5) and (6) leads to Amontons' well-known law

$$F_f = \mu F_l \quad (7)$$

where  $\mu$  is the frictional coefficient. Eq (7) implies that the frictional force is independent of the interfacial area between two contacting bodies.  $\mu$  is a characteristic phenomenological quantity of the involved materials.

AFM is a very suitable tool for studying friction at a nanometer scale. In contact mode AFM, it is possible to measure the torsional motion of the cantilever during the scanning. The torsion of the cantilever depends on the lateral force or friction acting on the scanning probe. This interaction in turn depends on chemical properties of surface as well as topography. Even if a surface exhibits only minor topographical variations but

pronounced variations in chemical composition, AFM friction mode can still map the variation in the material properties at the surface. Lateral Force Microscopy is a special application of contact mode AFM that is extremely suitable for studying both of the microscopic foundations of friction and the local variations in chemical composition. The cantilever probe is most susceptible to the frictional effect when the scan direction is perpendicular to the major axis of the cantilever as shown in figure 3.6. Therefore, the scan angle must be set to  $90^\circ$  or  $270^\circ$  to get a high quality frictional image.

### 3.3.3 Tapping-Mode

The biggest disadvantage of contact mode imaging is that lateral motion of the tip in contact with the sample produces friction and wear of both of the tip and the sample. Wear of the tip causes a loss of resolution and wear of the sample obviously changes the sample. Sample alteration is particularly acute for soft or weakly bound samples such as biological or polymer surfaces.

Tapping mode imaging overcomes these limitations by alternately placing the tip on the surface and lifting the tip off the surface during scanning. If the rate of oscillation is high relative to the frequency of scanning, then the tip effectively does not slide in contact with the sample.<sup>5,6</sup> When tapping mode imaging is implemented in ambient air, the cantilever is oscillated at or near its resonant frequency using a piezoelectric crystal and positioned above the surface, so that it only taps the surface for a very small fraction of its oscillation period. As the oscillating cantilever begins to intermittently contact the surface, the cantilever oscillation is reduced and the phase is changed due to energy loss caused by the tip contacting the surface. The magnitude of amplitude damping and the amount of phase change depend on the surface chemical compositions as well as the physical properties of the surface. Thus, the reduction in oscillation amplitude can be used to observe the contrast between regions of varying mechanical or chemical composition of the sample surface.

A feedback loop maintains the cantilever oscillation amplitude during an imaging. Under ambient conditions, amplitudes as large as  $10 - 100$  nm are frequently used for cantilevers with resonant frequency of  $100$  kHz or more. When the probe passes over a bump in a surface, the cantilever has less room for oscillation, so the amplitude

decreases. On the other hand, when the probe meets a depression, the cantilever has more room for oscillation and the amplitude increases. The oscillation amplitude is measured by the detector and the signal is sent to the controller electronics. Then the feedback loop adjusts the probe sample spacing by moving the scanner up and down to maintain constant amplitude and the force on the sample surface. Under liquid immersion, the amplitude is set much smaller because of damping by the fluid. Operation of tapping mode in a fluid provides the same advantages of tapping mode in air, with the additional ability to image samples under native liquid conditions, which is enormously advantageous for the observation of various bio-samples.

Recently, there has been considerable interest in phase imaging,<sup>7,8</sup> which works by monitoring the phase differences between the driving oscillation of the cantilever and the actual cantilever oscillation during imaging. In phase imaging, the phase lag of the cantilever oscillation relative to the driving signal is simultaneously monitored. The phase lag is very sensitive to the variations in material properties of the surface such as elastic, electrostatic, magnetic, and thermal properties. Therefore, it provides us more than topographical information: variation in composition, adhesion, viscoelasticity and others.

### 3.3.4 Force Curve Measurements

In addition to topographic measurements, the AFM can also record the amount of force felt by the tip as a function of the separation between the tip and sample. A force curve (force-versus-distance curve) can be constructed by monitoring deflection of the cantilever as a function of the distance normal to the sample surface plane.

Force measurements are more interesting in liquids. In liquids, the electrostatic interactions between the dissolved ions and other charged groups play an important role in determining the forces sensed by an AFM cantilever.<sup>2,9,10</sup> One can control many details of the probe-surface force interaction by changing the properties of liquid. The electrostatic tip-sample forces strongly depend on pH and salt concentration. It is often possible to adjust the pH or salt concentration such that repulsive electrostatic forces effectively negate the attractive Van der Waals forces.

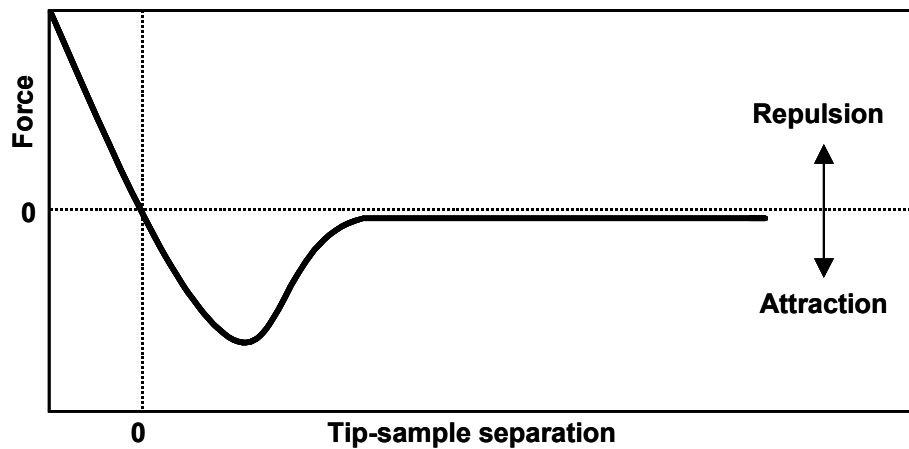


**Figure 3.7** Typical variation of the interacting force between a tip and a sample surface as a function of their relative distance

### 3.4 Summary

The development of scanning probe microscopy has enabled us to observe features with unprecedented resolution and without the need for complex sample preparation. STM produced the first image with atomic resolution and AFM broadened the capability to insulating surfaces. AFM tapping mode operation has an advantage over contact mode in that it minimizes damage to a specimen. It also provides a tool for investigating forces between the surfaces, such as van der Waals forces, electrostatic forces, magnetostatic forces. A useful aspect in the application of AFM is that it can be operated in various environments such as in aqueous solution, which allows imaging of enzymes in their native configuration.

Apart from being a nondestructive method, AFM is also a tool for modifying and functionalizing samples on a nanometer scale. A huge advantage of this application is that fabrication and subsequent imaging can be carried out with the same instrument by just changing parameters of operation. This advantage provides a useful basis for developing new approaches in nanoscience and nanotechnology.

## **Chronology of SPM developments**

<b>Year</b>	<b>Developments</b>
1981	Binnig and Rohrer at IBM-Zurich invented STM
1982	Binnig demonstrated atomic resolution on Si(7x7) with STM
1984	Near-field Optical Microscope invented
1985	Binnig, Gerber, and Quate developed the AFM
1986	Binnig and Rohrer received the Nobel Prize in physics for the invention of STM
1987	Albrecht at Stanford demonstrated atomic resolution with AFM Noncontact AFM introduced MFM invented
1988	Digital Instruments produces the first commercial AFM
1991	Ducker and Senden directly measured the colloidal forces with AFM Microfabricated AFM probes introduced
1992	Piezolevers introduced Shear-force detection type SNOM introduced
1993	Tapping Mode introduced
1994	Tapping Mode in fluids introduced
1997	Liu's group developed the Nanografting technique
1999	Mirkin's group developed Dip-pen nanolithography

## References

- (1) Binnig, G., Quate, C. F., and Gerber, C. *Phys. Rev. Lett.* **1986**, *56*, 930.
- (2) Ducker W. A., Senden T. J., and Pashley R. M. *Nature* **1991**, *353*, 239.
- (3) Betzig, E.; Trautman, J.; Harris, T. *Science* **1991**, *251*, 1468.
- (4) Akamine, S.; Albrecht, T. R.; Zdeblick, M. J.; and Quate, C. F. *Sensors and Actuators A* **1990**, *23*, 964.
- (5) Brandsch, R.; Bar, G.; Whangbo, M.-H. *Langmuir* **1997**, *13*(24), 6349.
- (6) Radmacher, M.; Tillmann, R. W.; Fritz, M.; Gaub, H. E. *Science* **1992**, *257*, 1900.
- (7) Sanders, G. H. W.; Davies, M. C.; Roberts, C. J.; Tendler, S. J. B.; Williams, P. M. *Langmuir* **1999**, *15*(17), 5433.
- (8) Knoll, A.; Magerle, R.; Krausch, G. *Macromolecules* **2001**, *34*(12), 4159.
- (9) Ducker, W. A.; Senden, T. J.; Pashley, R. M. *Langmuir* **1992**, *8*, 1831.
- (10) Lokar, W. J.; Ducker, W. A. *Langmuir* **2002**, *18*(8), 3167.
- (11) Chen, C. J. *Appl. Phys. Lett.* **1992**, *60*, 132.
- (12) Giessibl, F. J. *Science* **1995**, *267*, 68.
- (13) Gould, S. A. C., Burke, K., and Hansma, P. K. *Phys. Rev. B* **1989**, *40*, 5363.
- (14) Güthner, P. J. *Vac. Sci. Technol. B* **1996**, *14*, 2428.
- (15) Landman, U., Luedtke, W. D., Burnham, N. A., and Colton, R. J. *Science* **1990**, *248*, 454.
- (16) Antognozzi, M., Szczelkun M. D., Round A. N., and Miles M. J. *Single Mol.* **2002**, *3*, 105.
- (17) Meyer, G., and Amer, N. M. *Appl. Phys. Lett.* **1990**, *56*, 2100.
- (18) Rugar D., Mamin H. J., and Guethner P. *Appl. Phys. Lett.* **1989**, *55*, 2588.
- (19) Zhong, W., and Tománek, D. *Phys. Rev. Lett.* **1990**, *64*, 3054.
- (20) Wiesendanger, R. *Proc. Natl. Acad. Sci.* **1997**, *94*, 12749.
- (21) Stevens, R. M., Frederich, N. A., Smith, B. L., Morse, D. E., Stucky, G. D., and Hansma, P. K., *Nanotechnology* **2000**, *11*, 1.
- (22) Stark, R. W., Drobek, T., Heckl, and W. M. *Appl. Phys. Lett.* **1999**, *74*, 3296.
- (23) Rogers, B., York, D., Whisman, N., Jones, M., Murray, K., and Adams, J. D. *Rev. Sci. Instrum.* **2002**, *73*, 3242.

- (24) Liu, G. Y., Xu, S., and Qian, Y. *Acc. Chem. Res.* **2000**, *33*, 457.
- (25) Wang, J., Kenseth, J. R., Jones, V. W., Green, J. B., McDermott, M. T., and Porter, M. D. *J. Am. Chem. Soc.* **1997**, *119*, 12796.
- (26) Xu, S., Miller, S., Laibinis, P. E., and Liu, G. Y. *Langmuir* **1999**, *15*, 7244.
- (27) Hong, S., Zhu, J., and Mirkin, C. A. *Science* **1999**, *286*, 523.
- (28) Hong, S. and Mirkin, C. A. *Science* **2000**, *288*, 1808.
- (29) Ivanisevic, A. and Mirkin, C. A. *J. Am. Chem. Soc.* **2001**, *123*, 7887.

## **Chapter 4. Nanoscale Patterned Protein and Particle Covalent Attachment on Surfaces**

### **4.1 Introduction**

There is currently significant scientific interest in the nanofabrication of self-assembled monolayers (SAMs) as a means for the creation of well-defined two- and three-dimensional structures with specific chemical functionality. In particular, scanning probe microscope (SPM) based lithography shows significant promise for the fabrication of surfaces at nanometer length scales.<sup>1-5</sup> It is hoped that these patterns will provide for the fabrication of optical and electronic devices, locally biologically active systems and highly ordered colloidal networks with previously unattainable dimensions. To this end, the next significant hurdle is to use these patterns for the direct control of the spatial distribution, density, and orientation of micro- and nano-scale objects.

The immobilization of proteins on surfaces has significant meaning in a variety of applications ranging from fundamental studies in biology to the development of various biochips.<sup>6,7</sup> For the latter case, miniaturization of protein arrays is required for use in multi-immunoassay,<sup>29</sup> protein screening,<sup>30,31</sup> and related applications.<sup>32,33</sup> SAMs have been broadly investigated as biocompatible interfaces for the integration of nanoscale devices.<sup>8</sup> Among these, Oligo(ethylene glycols)-modified surfaces have shown particular promise as bioresistive films.<sup>9-11</sup> The electrostatic immobilization of proteins on a patterned SAM has been studied in combination with SPM lithographic techniques.<sup>4,12</sup> However, the physical interactions are reversible and the proteins can desorb during subsequent fabrication steps. Hence, methods to produce covalently attached protein patterns are required in many cases.

The covalent attachment of proteins onto SAMs can be obtained through the formation of amide, disulfide, or imine bonds. Frey and Corn have reported the immobilization of poly(L-lysine) onto an 11-mercaptoundecanoic acid SAM by forming an activated intermediate ester between the terminal carboxylate group and N-hydroxysulfosuccinimide.<sup>13</sup> Wadu-Mesthrige et al. immobilized lysozyme on an

aldehyde-terminated pattern by forming imine bonds between terminal aldehyde and amine groups on a protein surface.<sup>12</sup>

Colloidal particles are potentially an extremely versatile material for the fabrication of functional two and three-dimensional microstructures. Accordingly, there has been significant interest in understanding the process of particle attachment and in demonstrating the concepts involved. A number of groups have demonstrated the non-patterned (or uniform) electrostatic attachment of particles to surfaces.<sup>14-16</sup> In this chapter, I investigate the production of patterned particle attachment. A wide range of techniques have been used to create the patterned surfaces while an equally broad range of surface forces have been used to attach the particles to those patterned regions.

Kokkoli and Zukoski<sup>17</sup> investigated how surface heterogeneity alters surface forces; a property fundamental to the miniaturization of particle patterning. They demonstrated that hydrophobic and hydrophilic interactions are not additive, and the net interaction between a particle and a patterned surface depends on the relative size of the hydrophobic and hydrophilic sites. Sato et al.<sup>18</sup> and Sastry et al.<sup>19</sup> demonstrated the use of electrostatic forces to preferentially attach particles to patterned surfaces. They showed that either the combination of positively charged particles with a negatively charged pattern, or negatively charged particles with a positively charged pattern in an uncharged surface, could be used to preferentially attach particles in the patterned regions. Aizenberg et al.<sup>20</sup> combined the use of electrostatic forces to initially attach particles to a patterned surface, with a second drying stage. Interestingly, they found that there was an additional ordering of the structure upon drying which they attributed to lateral capillary interactions. He et al.<sup>21</sup> investigated the use of both electrostatic and covalent forces to attach particles to surfaces. The chemical attachment of Au nanoparticles was achieved at -SH terminated locations on the surface. Finally, Masuda et al.<sup>22</sup> attached SiO<sub>2</sub> spheres modified to have terminal -COOH groups to a patterned surface. The surface had a pattern drawn with terminal -OH groups in a background SAM of terminal phenyl groups. They found that the spheres preferentially, although not exclusively, attached to the patterned region. While the initial attachment was most likely driven by electrostatics, they suggest that ester bonds form between the spheres and the silanol surface.

Since Schmitt et al. demonstrated the basic principle in 1992,<sup>35</sup> that a uniform polyelectrolyte multilayer (PEM) can be formed by sequentially adsorbing alternating charged polyelectrolytes on a hydrophilic substrate. Subsequently, this process has been extensively studied.<sup>36-40</sup> Due to the versatility of the multilayers with respect to the usability of various materials as building blocks, PEMs have attracted huge interest in practical applications as well as in fundamental physical studies. The PEM procedure provides us a nice and easy route to make a uniform reversal of the surface charge and to deposit reproducible quantities of material on the surface. It would be very beneficial if this technique can be combined with current nanotechnology. However, no one has reported the application of PEM techniques to nanofabrication on a surface yet.

This chapter is focused on demonstrating the following: (1) the control of selective chemical reactions on a patterned SAM with nanometer scale, (2) the ability to produce covalently attached protein nanopatterns with virtually no adsorption to the surrounding regions, (3) the chemical bonding of nano-particles at specific points and in small arrays on a surface, and (4) the nanometer scale fabrication of PEM.

The nanografting technique developed by Xu et al.<sup>2,3</sup> was used to produce carboxylic acid-terminated patterns of the desired size and functionality on an atomically flat gold surface. We were then able to produce insulin and lipase nanopatterns on a carboxylic acid patch through amide bonds by producing activated intermediate esters on terminal carboxylate groups with N-hydroxysuccinimide (NHS). The proteins were then immobilized on the surface through amide bonds by displacement reaction with NHS esters. The covalent attachment of proteins on a patterned SAM was verified by observing the preservation of the pattern through a series of washing processes with surfactant solution and organic solvent.

An NHS protocol was also employed for the covalent attachment of nano-particles at specific points on a surface. Amino functionalized gold nanoparticles were immobilized on a localized pattern containing terminating carboxylate groups through a displacement reaction with NHS esters. Atomic force microscopy (AFM) images confirmed that particles were attached to the surface at the specific points of the drawn pattern.

The possibility of applying PEM techniques to nanometer scale fabrication of the surface was examined. A standard PEM procedure was employed for the construction of multilayers on specifically patterned sites with carboxylate groups using poly(allylamine hydrochloride) and poly[1-[4-(3-carboxy-4-hydroxyphenylazo)benzenesulfonamido]-1,2-ethanediyl, sodium salt]. The localized multilayer formation was then observed by tapping-mode AFM imaging and the layer thickness measured from the height image was compared with the ellipsometry data.

## 4.2 Experimental Section

### 4.2.1 Materials

The tri(ethylene glycol)-terminated thiol ( $\text{HS}(\text{CH}_2)_{11}(\text{OCH}_2\text{CH}_2)_3\text{OH}$ ) and the carboxylic acid-terminated thiol ( $\text{HS}(\text{CH}_2)_{11}(\text{OCH}_2\text{CH}_2)_6\text{OCH}_2\text{CO}_2\text{H}$ ) were synthesized in Professor Michael Calter's laboratory in the Department of Chemistry at the University of Rochester. Other materials and chemicals were used as received. 1-Dodecanethiol, 1-octadecanethiol, 4-aminothiophenol, 11-mercaptoundecanoic acid, 16-mercaptophexadecanoic acid, 11-mercapto-1-undecanol, poly(allylamine hydrochloride) (PAH,  $M_w \approx 15000$  g/mol), and poly[1-[4-(3-carboxy-4-hydroxyphenylazo)benzenesulfon amido]-1,2-ethanediyl, sodium salt] (PCBS,  $M_w \approx 65000-100000$  g/mol) were purchased from Aldrich. N-Hydroxysuccinimide (NHS), sodium dodecyl sulfate (SDS), 1-ethyl-3-(3-dimethylaminopropyl)carbodiimide (EDC), insulin (human, recombinant, expressed in *E. coli*), and lipase (type VI-S, from porcine pancreas) were purchased from Sigma. Au wire (1.0 mm diameter, 99.9985 %) was obtained from AlfaAesar. Phosphate-buffer saline (PBS: 10 mM phosphate, 138 mM NaCl, and 2.7 mM KCl - pH 7.4) was obtained from RICCA Chemical.

#### 4.2.2 Sample Preparation

##### Au(111) Substrates

Flat gold substrates were prepared by annealing a gold wire in a H<sub>2</sub>/O<sub>2</sub> flame.<sup>23-25</sup> The 1-mm diameter gold wire was cleaned with piranha solution (3:1 v/v ratio of H<sub>2</sub>SO<sub>4</sub>/30 wt. % H<sub>2</sub>O<sub>2</sub>) for 20 min and thoroughly rinsed with pure water. One end of the wire was then placed in a H<sub>2</sub>/O<sub>2</sub> flame and allowed to melt until a 2.0-2.5 mm diameter droplet forms. The droplet was further annealed for several seconds in a cooler region of the flame and was cooled down to room temperature. The resulting gold surface shows large atomically flat <111> crystalline terraces and monatomic steps that are suitable for AFM nanolithography.

##### Monolayers

Monolayers were prepared with 1-dodecanethiol or tri(ethylene glycol)-terminated thiol. Immediately after being annealed in a H<sub>2</sub>/O<sub>2</sub> flame, the gold substrates were immersed in a 2 mM ethanolic solution of selected thiol molecules for 24 hours. The substrates were then placed into pure ethanol for several hours to remove the physisorbed layer and were ultimately dried in a N<sub>2</sub> stream.

#### 4.2.3 Atomic Force Microscopy

All imaging and patterning were carried out in a desired solution with a NanoScope IIIa AFM (Digital Instruments, Santa Barbara, CA). 85 μm long, 18 μm wide, V-shaped Si<sub>3</sub>N<sub>4</sub> cantilever (Park Scientific Instruments) with a force constant of 0.5 N·m<sup>-1</sup> and a radius of <20 nm were used for both imaging and patterning. Prior to use, cantilevers were exposed to an UV lamp for 10-15 minutes to remove organic contaminants. SAM samples were mounted inside a fluid cell with a homemade sample holder (Figure 4.1). This fluid cell was fabricated to hold the gold balls that were used as the support for the SAMs. A conventional fluid cell is too shallow (<1 mm) to hold the gold ball (r = 1 mm). My cell has a recessed bath (Figure 4.1B) to fit the ball and a cylindrical hole (Figure 4.1D) to hold the gold wire. The wire is press-fitted into the hole,

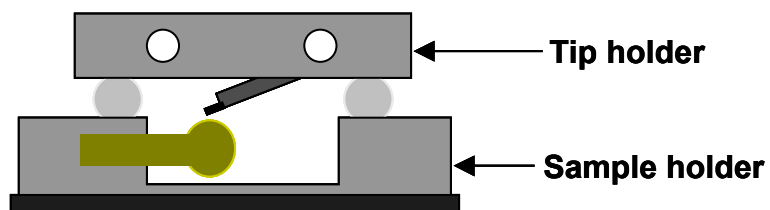
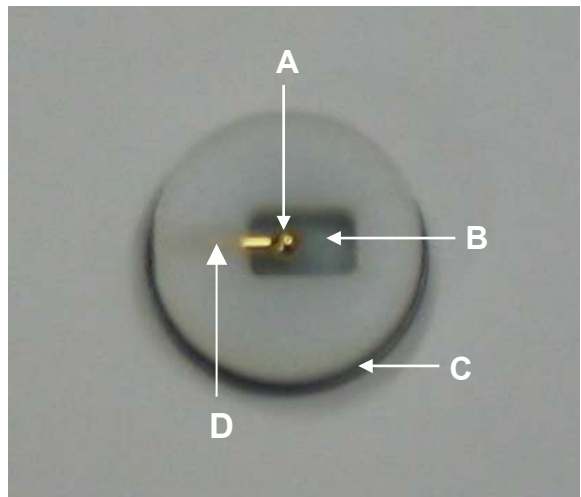


**Figure 4.1** The homemade sample holder. The bottom of this sample holder is attached to the AFM piezoelectric scanner and the top presses against a silicon O-ring to seal against the tip-holder. (A) Gold ball. (B) Liquid pool. Solution is delivered from the tip holder. (C) A metal plate for securing the sample holder to the magnetic stage of AFM scanner. (D) Hole for holding gold wire.

which allows the ball to be rotated in one dimension. This enabled me to select a suitable area of the surface for AFM studies. The sample holder was fabricated from Teflon in order to minimize contamination from the cell. The scanner was operated by a NanoScope IIIa SPM controller (Digital Instruments). To minimize the mechanical and thermal drift, the AFM probe and the sample were equilibrated in a solution for 2-3 hours before imaging or the fabrication procedure.

#### **4.2.4 Nanopatterning**

Xu et al.'s <sup>2,3</sup> nanografting technique was used to produce patterns of the desired size, shape, and functionality. The basic principles of nanografting lithography are illustrated in section 2.3.4. The scanner movements for each patterning process were programmed using Nanoscript software (Digital Instruments).

#### **4.2.5 Immobilization of Protein**

For the selective immobilization of proteins, the template patterns were produced with the hexa(ethylene glycol)-carboxylic acid ((EG)<sub>6</sub>CO<sub>2</sub>H)-terminated thiol on the tri(ethylene glycol) ((EO)<sub>3</sub>OH)-terminated thiol SAM. An aqueous mixture of 0.20 M EDC and 0.05 M NHS was prepared. The patterned SAM surface was activated by injecting PBS into the AFM fluid cell. The surface carboxylic acid groups were then transformed into NHS esters by injecting EDC-NHS solution and equilibrating for 7 min. The surface was washed with PBS solution for 3 min and the aqueous solution of protein was injected over the surface for 7 min. The protein was then immobilized on the pattern through amide bonds formed by the displacement reaction with the NHS ester. The surface was washed again with PBS solution and pH 8.6 buffer to deactivate the excess NHS. The surface was thoroughly cleaned with buffer, pure water, and ethanol to remove the physisorbed proteins.

#### **4.2.6 Attachment of Nanoparticles**

A hexa(ethylene glycol)-carboxylic acid ((EG)<sub>6</sub>CO<sub>2</sub>H)-terminated pattern was drawn in a tri(ethylene glycol) ((EO)<sub>3</sub>OH)-terminated SAM. Amino group-functionalized gold nanoparticles (10 nm diameter) were then immobilized on a localized pattern by EDC-NHS protocol.

#### **4.2.7 Nanopatterning of Polyelectrolyte Multilayers**

Polyelectrolytes were dissolved in water in a concentration of 10 mM with respect to the monomer repeat unit. The solution pH values of PAH and PCBS were adjusted to 7.5 and 7.0 respectively. The template patterns were nanografted with the hexa(ethylene glycol)-carboxylic acid ((EG)<sub>6</sub>CO<sub>2</sub>H)-terminated thiol on the tri(ethylene glycol)

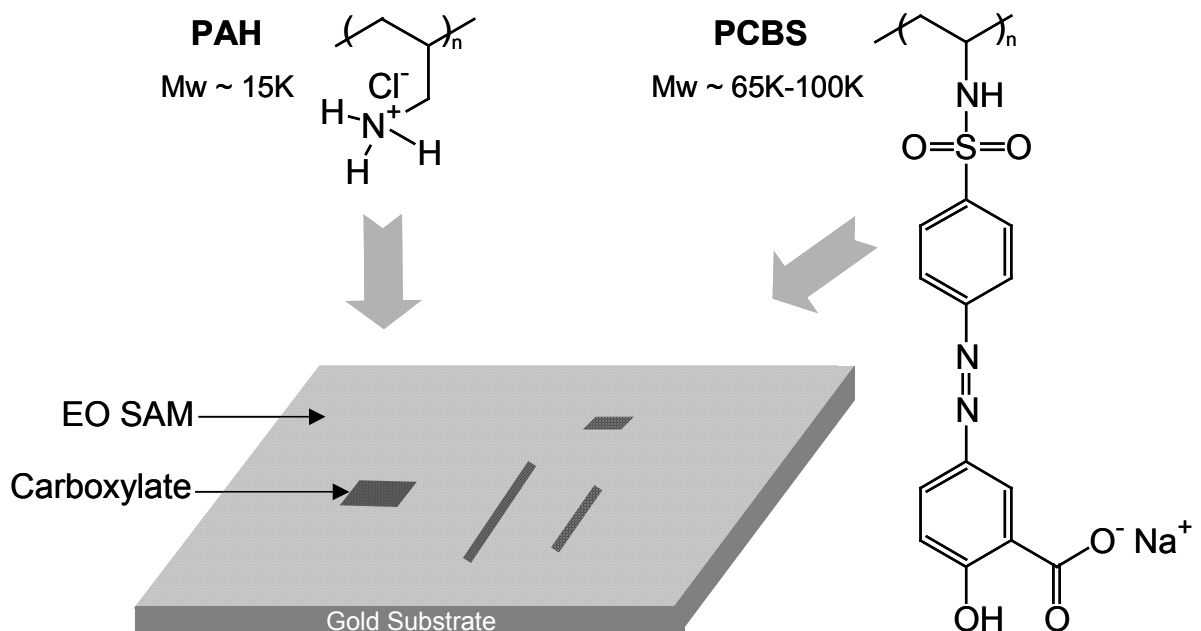


**Figure 4.2** Schematic representation of nanofabrication of polyelectrolyte multilayers

((EO)<sub>3</sub>OH)-terminated thiol SAM. Sequential adsorption of polyelectrolytes was performed by hand dipping the patterned surface into each solution. The deposition time of each layer was 4 min. The surface was rinsed with pure water between alternate exposures to two polymer solutions. A total of two bilayers (PAH-PCBS-PAH-PCBS) were deposited on the surface (Figure 4.2). After careful rinsing with pure water, the surface was set into the AFM. The formation of PEM on the patterned area was investigated using tapping mode imaging.

#### 4.2.8 Data Analysis

The average heights of each pattern with respect to the background were measured using our image analysis program (MATLAB, programmed by Mr. Corey Moore). Those data were used to assess whether the surface reactions occurred selectively on a patterned area.

## 4.3 Results and Discussion

### 4.3.1 Self-assembled Monolayers

Figure 4.3 shows a typical AFM image of a SAM formed on a gold substrate. The typical average roughness of this monolayer appears to be less than 0.5 nm over several  $\mu\text{m}$  ranges. Having a large and smooth surface is very important for the AFM nanofabrication study, which deals with nanometer scale structures in many cases.

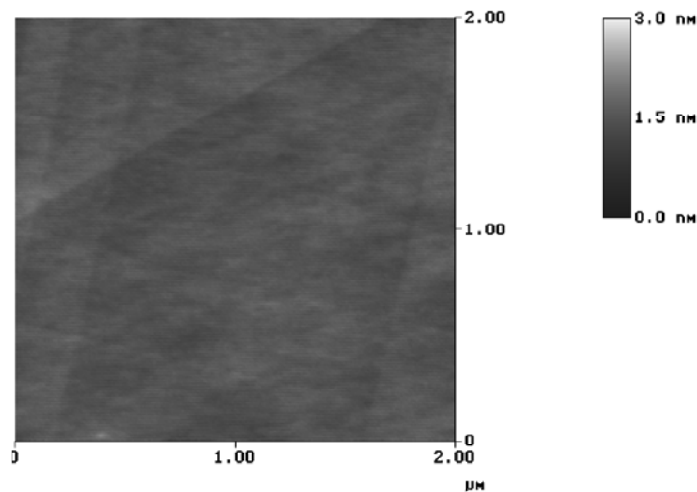


**Figure 4.3** AFM image of the SAM of  $\text{C}_{12}\text{SH}$  onto a freshly prepared  $\text{Au}(111)$  surface from a ethanol solution. The concentration of  $\text{C}_{12}\text{SH}$  was 2 mM.

### 4.3.2 Nanopatterning

Nanografting was performed following the procedure described in section 2.3.4. The approximate loading force was 2 nN. The threshold force for nanografting is a function of the tip radius, the type of the thiol, and the roughness of the gold surface. Therefore, the applied force for nanografting is determined for each individual experiment.

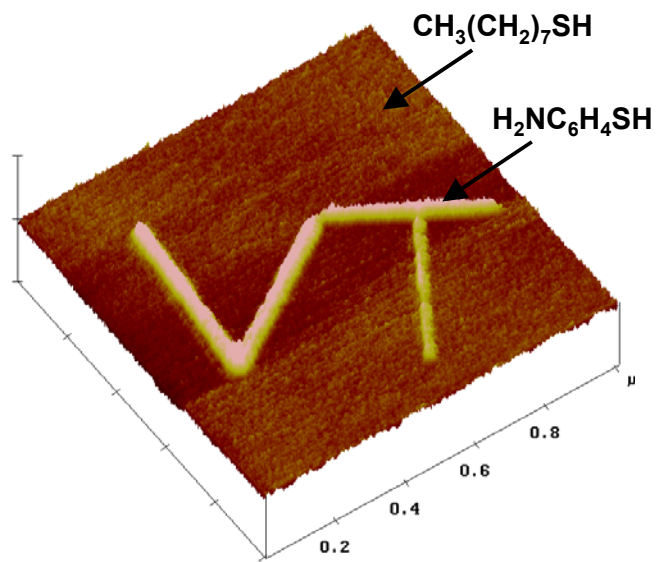


**Figure 4.4**  $1 \times 1 \mu\text{m}^2$  topographic AFM image in ethanol of the pattern with 4-aminothiophenol molecules in the matrix of octanethiol monolayer.

An example of the fabricated pattern with 4-aminothiophenol in a matrix of octanethiol monolayer is shown in Figure 4.4. The patterned molecules produce about 1 nm higher contrast than the surrounding monolayer in a tapping mode AFM image in ethanol. Contrast in tapping mode arises from differences in height, electrostatic force, and elasticity. However, none of those factors can clearly explain this high contrast. The extended van der Waals length of 4-aminothiophenol is shorter than the octanethiol. The terminal amines can be protonated by a protic solvent and produce charge. But, in ethanol, most of the amine groups must be neutral. Even if the surface amines are transformed to quaternary ammonium groups, the long-range electrostatic force of the quaternary ammonium will make the contrast even more negative, because the silicon nitride AFM probe has an opposite (negative) charge on its surface. We do not know what produces this high contrast, even at this stage.

### 4.3.3 Covalent Modification of a Nanografted Pattern

A nanometer-scale VT pattern of 11-mercaptoundecanoic acid in a dodecanethiolate monolayer was first produced using nanografting. The pattern was then modified through a subsequent chemical reaction: pentylamine was covalently attached to the carboxylic acid via amide bonds with a standard N-hydroxysuccinimidyl ester protocol.<sup>9,13</sup> Because the surface reaction increases the chain length, we would expect increased contrast of the pattern in AFM imaging.

Figure 4.5 illustrates the verification of the surface reaction: additional line patterns were produced above and below the VT pattern after the amidation reaction, and the average local heights of each pattern relative to the background were compared. The line pattern above VT was drawn with octadecanethiol, which has approximately the same chain length as the amidation reaction product, so this should have provided approximately the same local height. The bottom three lines were produced with the same carboxylic acid as the initial patterning material in the VT pattern. They act as a control

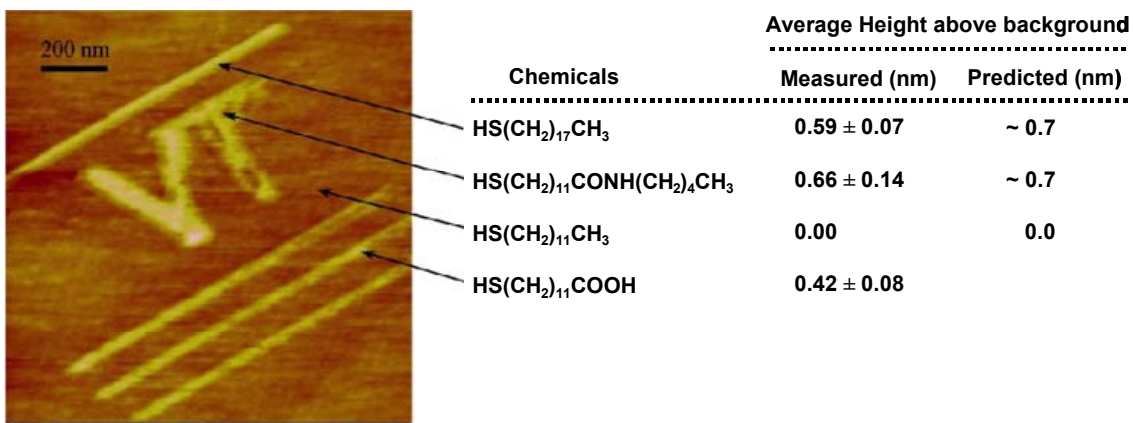


**Figure 4.5** Covalent modification of a patterned surface. 1. VT pattern was nanografted using  $\text{HS}(\text{CH}_2)_{11}\text{COOH}$  in a monolayer of  $\text{HS}(\text{CH}_2)_{11}\text{CH}_3$ . 2. Pentylamine was then covalently attached to the VT patch by displacement reaction with N-hydroxysuccinimidyl ester. 3. After the amidation reaction, additional line patterns were produced above and below the VT pattern using  $\text{HS}(\text{CH}_2)_{17}\text{CH}_3$  and  $\text{HS}(\text{CH}_2)_{11}\text{COOH}$  respectively.  $\text{HS}(\text{CH}_2)_{17}\text{CH}_3$  has the same chain length as the amidation product and  $\text{HS}(\text{CH}_2)_{11}\text{COOH}$  is the initial VT-patterning molecule. The prediction of the height of each pattern was made based on the known thickness of  $\text{HS}(\text{CH}_2)_{11}\text{CH}_3$  SAM (1.7 nm).

for no reaction. Figure 4.5 shows that the average height of the VT pattern is similar to the top line pattern and higher than the bottom three lines. These data show that the chain length of the molecules in VT region increased by the correct amount during the amidation reaction.

Note that the carboxylic acid patterns show higher contrast than the surrounding molecules in the SAM. It is interesting that the carboxylic acid molecules produce such high contrast in AFM images in ethanol despite the chain length of both molecules being almost the same. In this case, the positive contrast may be induced from the long-range electrostatic interaction of the patterned carboxylates with the negatively charged AFM tip. The same high contrast was observed for the charged amine (4-aminothiophenol).

#### 4.3.4 Fabrication of a Protein Nanopattern

The same fabrication method as the covalent modification in the previous section was used for the patterned immobilization of proteins. The images shown in Figures 4.6 and 4.7 present the results, nanopatterns with insulin and lipase. The scanner movements for the fabrication of these patterns was programmed using Nanoscript software (Digital Instruments). The program used for producing the 9-dot pattern is shown in Appendix A.

A monolayer of tri(ethylene glycol)-terminated thiol ( $\text{HS}(\text{CH}_2)_{11}(\text{OCH}_2\text{CH}_2)_3\text{OH}$ ) was first prepared on the gold surface by deposition from ethanol solution for 24 hrs. Ethylene glycol-modified surfaces are known to resist the adsorption of proteins.<sup>26,27</sup> A nine square-pattern (40 nm × 40 nm each, 200 nm of separation between squares) was produced on the surface by nanografting hexa(ethylene glycol)-carboxylic acid-terminated thiol ( $\text{HS}(\text{CH}_2)_{11}(\text{OCH}_2\text{CH}_2)_6\text{OCH}_2\text{CO}_2\text{H}$ ) (Figure 4.6A). The lighter area region is a deposited monolayer of carboxylic acid-terminated thiol and the exterior area is an ethylene glycol monolayer.

The accompanying cross section in Figure 4.6A shows that the carboxylic acid pattern was again higher than expected based solely on the length of the respective molecules; the pattern was more than 2 nm higher than the surrounding molecules, although the actual chain length difference between the two was only about 1.3 nm. Figure 4.6B shows the insulin pattern covalently attached to the carboxylate patch through the formation of activated intermediate esters on terminal carboxylate groups

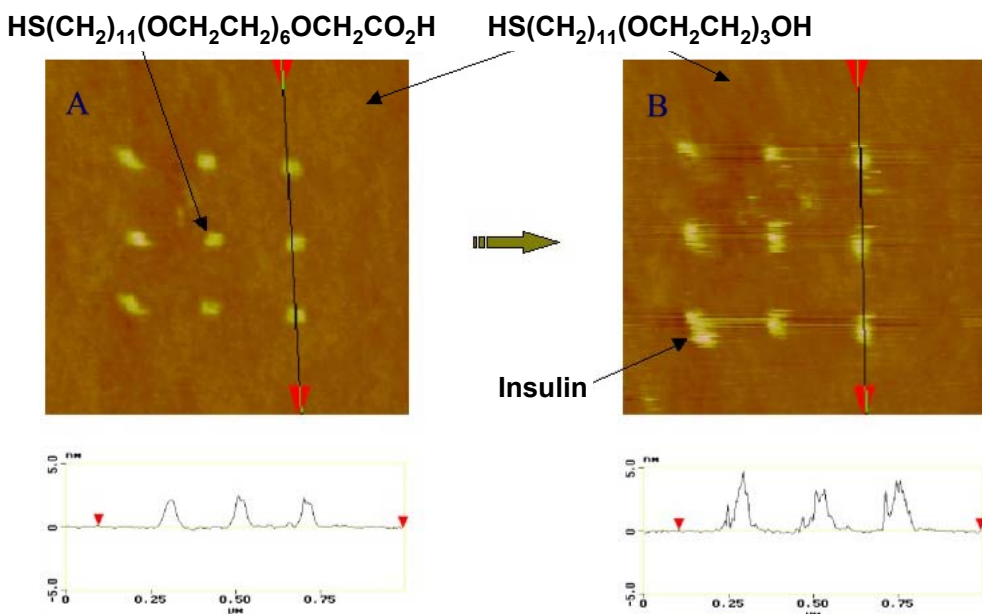


**Figure 4.6** Immobilization of insulin on a patterned surface. (A) AFM image of nine hexa(ethylene glycol)-carboxylic acid-terminated thiol ( $\text{HS}(\text{CH}_2)_{11}(\text{OCH}_2\text{CH}_2)_6\text{OCH}_2\text{CO}_2\text{H}$ ) patches ( $40 \text{ nm} \times 40 \text{ nm}$  each,  $200 \text{ nm}$  of separation) produced in a background of tri(ethylene glycol)-terminated thiol ( $\text{HS}(\text{CH}_2)_{11}(\text{OCH}_2\text{CH}_2)_3\text{OH}$ ). (B) The proteins were immobilized on the pattern via amide bonds by NHS protocol.

with N-hydroxysuccinimide (NHS). The proteins were then immobilized on the surface through amide bonds by a displacement reaction with NHS esters. The surface was thoroughly washed with buffer and then with ethanol to remove unwanted reactants and non-specifically bound enzyme. The accompanying cross section shows that the bound protein layer was 4-5 nm higher than the background molecules (Figure 4.6B). Because the carboxylate thiol is about 1.3 nm longer than the surrounding molecules, the actual height of the protein layer was 2.7-3.7 nm, approximately the monolayer thickness of insulin. The molar mass of insulin is 5.8 kDa and the diameter of the monomer is  $\sim 2.7 \text{ nm}$ <sup>34</sup>.

Figure 4.7 shows the lipase pattern ( $25 \times 25 \text{ nm}$ ,  $50 \text{ nm} \times 50 \text{ nm}$ ) produced by the same method as the insulin pattern. The cross-sectional line shows that the height of the pattern was increased by about 3 nm after immobilizing lipase on it, which is

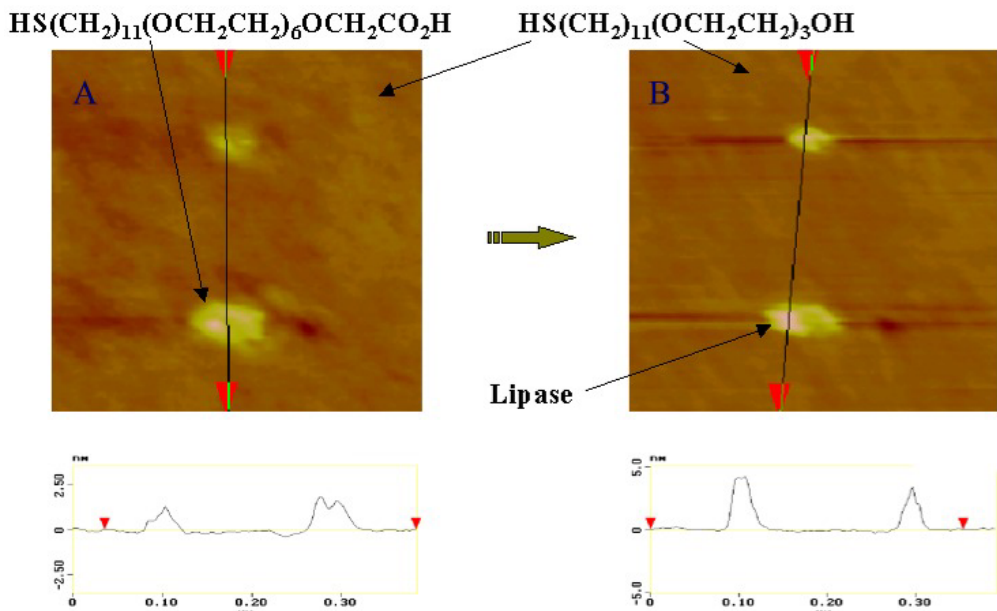


**Figure 4.7** Immobilization of lipase on a patterned surface. (A) AFM image of a hexa(ethylene glycol)-carboxylic acid-terminated thiol ( $\text{HS}(\text{CH}_2)_{11}(\text{OCH}_2\text{CH}_2)_6\text{OCH}_2\text{CO}_2\text{H}$ ) pattern ( $25 \times 25 \text{ nm}$ ,  $50 \text{ nm} \times 50 \text{ nm}$ ) nanografted into a tri(ethylene glycol)-terminated thiol ( $\text{HS}(\text{CH}_2)_{11}(\text{OCH}_2\text{CH}_2)_3\text{OH}$ ) surface. (B) The proteins were immobilized on the pattern through amide bonds by displacement reaction with NHS ester.

approximately the monolayer thickness of lipase. The molar mass of lipase is 52 kDa and the diameter of the monomer is  $\sim 4 \text{ nm}$ .<sup>41</sup>

Because all proteins have amino functional groups on their surface, this procedure can generally be used to create high density protein arrays on a surface, applicable for the development of miniaturized biochip platforms.

#### 4.3.5 Covalent Attachment of Gold Nanoparticles

Ordered arrays of covalently attached Au nanoparticles were formed at the substrate surface. A colloidal solution of amino group-functionalized Au nanoparticles was first prepared. Again, a nine dot-pattern ( $40 \text{ nm} \times 40 \text{ nm}$  each,  $200 \text{ nm}$  of separation) was produced on a tri(ethylene glycol)-terminated thiol ( $\text{HS}(\text{CH}_2)_{11}(\text{OCH}_2\text{CH}_2)_3\text{OH}$ ) surface by deposition of hexa(ethylene glycol)-carboxylic acid-terminated thiol ( $\text{HS}(\text{CH}_2)_{11}(\text{OCH}_2\text{CH}_2)_6\text{OCH}_2\text{CO}_2\text{H}$ ). Figure 4.8A shows that the Au particles selectively

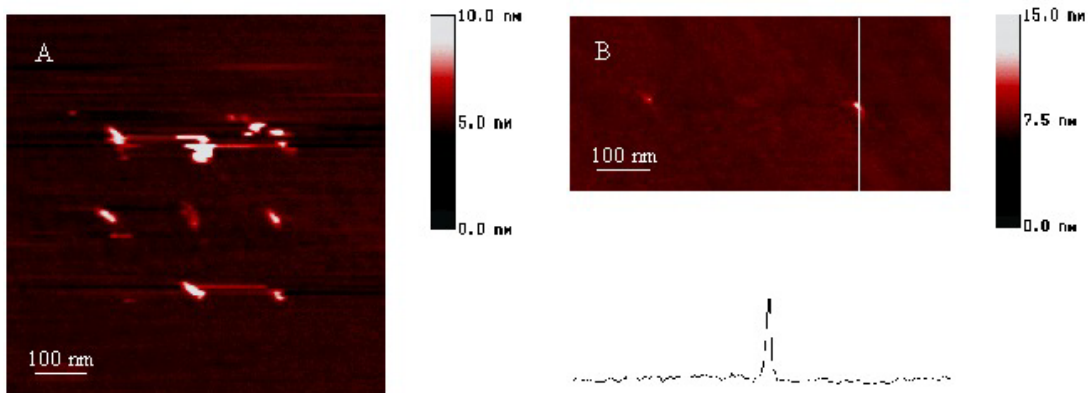


**Figure 4.8** Amino-functionalized gold particle attachment to surface. (A) AFM image of gold particles covalently bonded on the nine dots-pattern (40 nm × 40 nm each, 200 nm of separation) by NHS substitution reaction. The template pattern was produced on a tri(ethylene glycol)-terminated thiol ( $\text{HS}(\text{CH}_2)_{11}(\text{OCH}_2\text{CH}_2)_3\text{OH}$ ) surface by deposition of hexa(ethylene glycol)-carboxylic acid-terminated thiol ( $\text{HS}(\text{CH}_2)_{11}(\text{OCH}_2\text{CH}_2)_6\text{OCH}_2\text{CO}_2\text{H}$ ). (B) A tapping mode image of a three-dot pattern (10 nm × 15 nm each, 200 nm of separation), two of which bear single Au particle on each patch. The middle patch failed to hold a particle.

attached to the carboxylate patch through the NHS substitution procedure. The brighter region shows the particles attached to the carboxylate patch and the exterior area is a monolayer of ethylene glycol. Because the size of the carboxylic acid patch (40 nm) is bigger than the particle size (10 nm), each patch bears more than one gold particle. We also demonstrated the attachment of a single gold sphere (10 nm). A straight-line array of three small squares (10 nm × 15 nm each, 200 nm of separation) was patterned on the substrate. Figure 4.8B shows the tapping mode image of a three-dot pattern, two of which bear single Au particle on each patch. The middle patch either failed to attract and hold a particle, or the particle was removed during subsequent imaging.

#### 4.3.6 Nanofabrication of Polyelectrolyte Multilayers

The PEM procedure has been broadly studied<sup>36-40</sup> to build-up 1-dimensional nanostructures (normal to surface) with unique properties. As an attempt to extend this

technique to the construction of 3-dimensional structures, nanoscale patterning of PEM on a SAM was performed.

Two squares (100 nm × 100 nm and 200 nm × 200 nm) and two line patterns (length: 500 nm and 300 nm, line width: 30 nm) of carboxylic acid-terminated thiol were produced in an ethylene glycol SAM. The brighter region is patterned carboxylate and the rest of the area is a monolayer of ethylene glycol (Figure 4.9A). Two bilayers (PAH-PCBS-PHA-PCBS) of polyelectrolytes were then sequentially adsorbed on the patterned surface. Figure 4.9B shows that the polymers are preferentially adsorbed on the carboxylate patch by the strong electrostatic interactions. A small amount of nonspecifically bound polymers were also observed outside the pattern. However, because they were loosely bound to the surface, they could be removed by gentle scraping of the surface using contact-mode imaging.

The corresponding cursor profile shows that the height of the carboxylate pattern has been increased by about 5.5 nm after the adsorption of polymer. According to ellipsometry data measured by Professor Randy Heflin's group in the Department of Physics at Virginia Tech, the thickness of one bilayer adsorbed on a homogeneous carboxylate surface is 1.5 nm. Therefore, the increment of height for the patterned site is 2.5 nm greater than that would be expected from the ellipsometry data. Two alternative explanations or the combination of both are possible for this observation. First, the top layer is covered by PCBS that has one carboxylate group per each ethylene-repeating unit. The charge density of the top polymer film may be higher than the one of the carboxylate pattern nanografted in the SAM. This higher negative charge density of PCBS causes a stronger repulsion to the negatively charged AFM tip during the tapping-mode imaging, which resulted in the exaggeration of contrast.

Second, an extra amount of polymer for the monolayer formation may have adsorbed on each layer in the PEM. Kovacevic et al.<sup>40</sup> report that an increase of the adsorbed amount occurs in the beginning of the layering procedure. The adsorbed amount then decreases again after several minutes and reaches the equilibrium. The dipping time (4 min) and the subsequent rinsing in this experiment may not be sufficient to achieve the equilibrium state and form a monolayer. Figure 4.9 also shows the increase of patch size

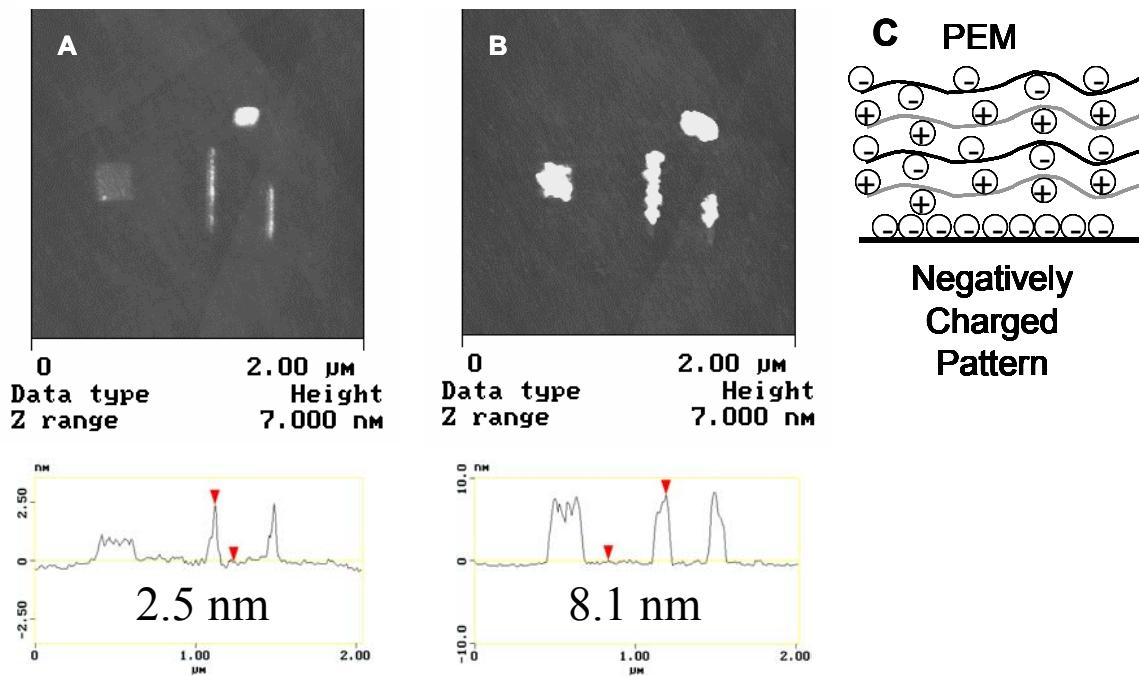


**Figure 4.9** Tapping-mode AFM images with cross-sections showing the formation of PEM on a patterned carboxylate patch. (A) The brighter areas are hexa(ethylene glycol)-carboxylic acid-terminated thiol ( $\text{HS}(\text{CH}_2)_{11}(\text{OCH}_2\text{CH}_2)_6\text{OCH}_2\text{CO}_2\text{H}$ ) pattern nanografted into a tri(ethylene glycol)-terminated thiol ( $\text{HS}(\text{CH}_2)_{11}(\text{OCH}_2\text{CH}_2)_3\text{OH}$ ) surface. (B) The same surface was imaged after the deposition of two bilayers (PAH-PCBS-PHA-PCBS). PEM were preferentially formed on the patterned area. Corresponding cross-sectional lines show the height of each patch. All images have a 7-nm Z-range. (C) Schematic of the polyelectrolyte layers on the nanografted pattern.

after the formation of PEM, which indicates the lateral growth of polymer layers. This lateral growth is more obvious for the line pattern than the square pattern.

Clearly, more experiments are required to understand the adsorption of polyelectrolytes to nanografted pattern. At this stage we have simply demonstrated that the polyelectrolytes will follow the nanografted pattern. This combination of techniques shows great promise because PEM formation is simple, and a variety of materials can be used. For example, the patterned PEM can be used as a specifically positioned nanowire

for the fabrication of nanoelectronics by adsorbing desired conducting polymer on the nanoscale patch.

#### 4.4 Conclusions

This study has examined the nanometer-scale control of electrostatic and chemical adsorption for the patterning of proteins, particles, and polymers on a SAM. I demonstrated that the NHS protocol is a useful method for nanofabrication by applying it to the covalent attachment of molecules, proteins, and nano-particles to patterned self-assembled monolayers. Using this method, I could immobilize enzymes that are catalytically active tools for further fabrication (described in chapter 5). Single particle attachment on each pattern with amino-functionalized gold particles reduced the fabrication scale down to 10 nm. The increased levels of miniaturization demonstrated here are steps toward meeting the demand for the construction of structured nanodevices. PEM has been widely used to create 1-dimensional nanostructures. Here I have shown that they can be used to produce patterns with nanoscale features in 3 dimensions.

## References

- (1) Wang, J. H.; Kenseth, J. R.; Jones, V. W.; Green, J. B. D.; McDermott, M. T.; Porter, M. D. *J. Am. Chem. Soc.* **1997**, *119*, 12796-12799.
- (2) Xu, S.; Liu, G. Y. *Langmuir* **1997**, *13*, 127-129.
- (3) Xu, S.; Miller, S.; Laibinis, P. E.; Liu, G. Y. *Langmuir* **1999**, *15*, 7244-7251.
- (4) Liu, G. Y.; Xu, S.; Qian, Y. L. *Accounts Chem. Res.* **2000**, *33*, 457-466.
- (5) Amro, N. A.; Xu, S.; Liu, G. Y. *Langmuir* **2000**, *16*, 3006-3009.
- (6) Kenseth, J. R. H., J. A.; Jones, V. W.; Porter, M. D. *Langmuir* **2001**, *17*, 4105-4112.
- (7) Mrksich, M. W. G. M. *Trends Biotechnol.* **1995**, *13*, 228.
- (8) Mrksich, M. W. G. M. *Annu. Rev. Biophys. Biomol. Struct.* **1996**, *25*, 55-78.
- (9) Lahiri, J.; Isaacs, L.; Tien, J.; Whitesides, G. M. *Anal. Chem.* **1999**, *71*, 777-790.
- (10) Chapman, R. G. O., E.; Yan, L.; Whitesides, G. M. *Langmuir* **2000**, *16*, 6927-6936.
- (11) Prime, K. L.; Whitesides, G. M. *J. Am. Chem. Soc.* **1993**, *115*, 10714-10721.
- (12) Wadu-Mesthrige, K.; Xu, S.; Amro, N. A.; Liu, G. Y. *Langmuir* **1999**, *15*, 8580-8583.
- (13) Frey, B. L.; Corn, R. M. *Anal. Chem.* **1996**, *68*, 3187-3193.
- (14) Zhu, T.; Zhang, X.; Wang, J.; Fu, X. Y.; Liu, Z. F. *Thin Solid Films* **1998**, *329*, 595-598.
- (15) Wang, J.; Zhu, T.; Song, J. Q.; Liu, Z. F. *Thin Solid Films* **1998**, *329*, 591-594.
- (16) Gole, A.; Sainkar, S. R.; Sastry, M. *Chem. Mat.* **2000**, *12*, 1234-1239.
- (17) Kokkoli, E.; Zukoski, C. F. *Langmuir* **2001**, *17*, 369-376.
- (18) Sato, T.; Hasko, D. G.; Ahmed, H. *J. Vac. Sci. Technol. B* **1997**, *15*, 45-48.

- (19) Sastry, M.; Gole, A.; Sainkar, S. R. *Langmuir* **2000**, *16*, 3553-3556.
- (20) Aizenberg, J.; Braun, P. V.; Wiltzius, P. *Phys. Rev. Lett.* **2000**, *84*, 2997-3000.
- (21) He, H. X.; Zhang, H.; Li, Q. G.; Zhu, T.; Li, S. F. Y.; Liu, Z. F. *Langmuir* **2000**, *16*, 3846-3851.
- (22) Masuda, Y.; Seo, W. S.; Koumoto, K. *Thin Solid Films* **2001**, *382*, 183-189.
- (23) Demir, U.; Shannon, C. *Langmuir* **1994**, *10*, 2794-2799.
- (24) Hayes, W. A.; Shannon, C. *Langmuir* **1998**, *14*, 1099-1102.
- (25) Li, L.; Yu, Q.; Jiang, S. *J. Phys. Chem. B* **1999**, *103*, 8290.
- (26) Pale-Grosdemange, C.; Simon, E. S.; Prime, K. L.; Whitesides, G. M. *J. Am. Chem. Soc.* **1991**, *113*, 12-20.
- (27) Prime, K. L.; Whitesides, G. M. *Science* **1991**, *252*, 1164-1167.
- (28) Jang, C.-H.; Benjamin D. Stevens; Paul R. Carlier; Michael A. Calter; William A. Ducker. *J. Am. Chem. Soc.* **2002**, *124*(41), 12114-12115.
- (29) Joos, T. O.; Schrenk, M.; Hopfl, P.; Kroger, K.; Chowdhury, U.; Stoll, D.; Schorner, D.; Durr, M.; Herick, K.; Rupp, S.; Sohn, K.; Hammerle, H. *Electrophoresis* **2000**, *21*, 2641.
- (30) Lueking, A.; Horn, M.; Eickhoff, H.; Bussow, K.; Lehrach, H.; Walter, G. *Anal. Biochem.* **1999**, *270*, 103.
- (31) MacBeath, G.; Schreiber, S. L. *Science* **2000**, *289*, 1760.
- (32) MacBeath, G.; Koehler, A. N.; Schreiber, S. L. *J. Am. Chem. Soc.* **1999**, *121*, 7967.
- (33) Hergenrother, P. J.; Depew, K. M.; Schreiber, S. L. *J. Am. Chem. Soc.* **2000**, *122*, 7849.
- (34) Smith, L. F. *Am. J. Med.* **1966**, *40*, 662.
- (35) Schmitt, J.; Decher, G.; Hong, J. D. *Thin Solid Films* **1992**, *210/211*, 831.
- (36) Liu, Y.; Claus, R. O. *J. Appl. Phys.*, **1999**, *85*(1), 419.
- (37) Krasemann, L.; Tieke, B. *Langmuir* **2000**, *16*, 287.
- (38) Castelnovo, M.; Joanny, J. -F. *Langmuir* **2000**, *16* 7524.
- (39) Schlenoff, J.; Dubas, S. T. *Macromolecules* **2001**, *34*, 592.

- (40) Kovacevic, D.; Burgh, V.; Keizer, A.; Stuart, M. A. C. *Langmuir* **2002**, *18*, 5607.
- (41) Moreno, J. M.; Sinisterra, J. V. *J. of Molecular Catalysis* **1994**, *93*, 357.

# Chapter 5. Immobilized Enzymes as Catalytically-Active Tools for Nanofabrication

## 5.1 Introduction

The miniaturization of molecular arrays produces many useful effects, some stemming purely from the greater density of information,<sup>1</sup> some arising from new material properties that arise when the dimensions of the components approach the dimensions of the constituent molecules.<sup>2,3</sup> One efficient strategy for creating nanostructures on surfaces is to use surface molecules to template the construction of self-assembled arrays.<sup>4</sup> This strategy takes advantage of the *binding* properties of the template molecules. Another potential strategy is to use the *catalytic* properties of a surface molecule. Such a strategy would benefit from the amplification and chemical specificity inherent in catalysis. In this study, we describe a demonstration of the key step of such a strategy: the surface trapping of a product generated by a nanometer-scale patch of surface-bound enzyme.

When one reduces the dimensions of a catalyst patch, one also decreases the amount of product that can be produced within a given time, and, therefore, one increases the difficulty in analyzing for the product. Even given turnover rates as high as one thousand reactions per second, a patch of one hundred catalytic sites produces only ten billion product molecules per day. If these molecules diffuse into a volume of 100  $\mu\text{L}$ , then there is an analytical difficulty in accurately finding the product in the resulting  $1.5 \times 10^{-10} \text{ M}$  solution. We solve the dilution problem by trapping some of the catalyzed-reaction product at the surface in a second reaction before it can diffuse away. Subsequent reaction of the catalysis product is more than an analytical necessity, it also offers a new route to nanometer-scale fabrication: the enzyme is used for the further fabrication of the thin film. In this way, a set of enzymes catalyzing different reactions could be used to build up additional complexity on a nanometer-scale without human intervention on the nanometer scale.

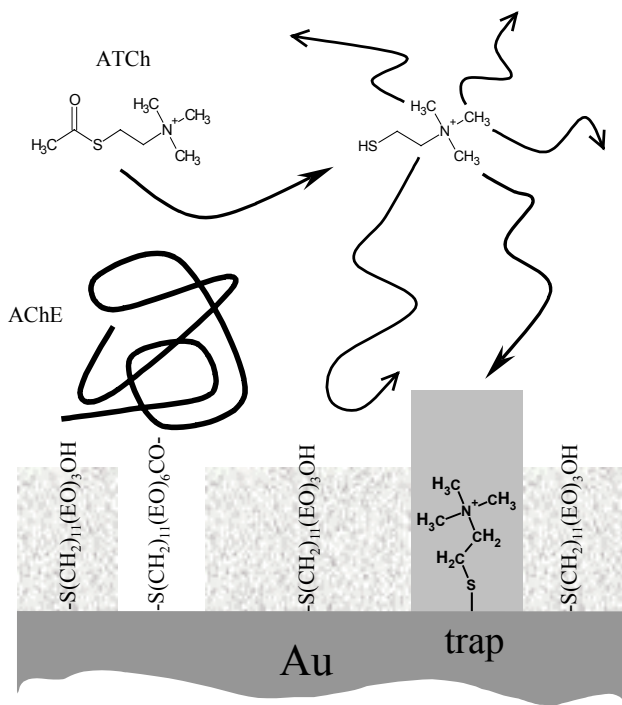
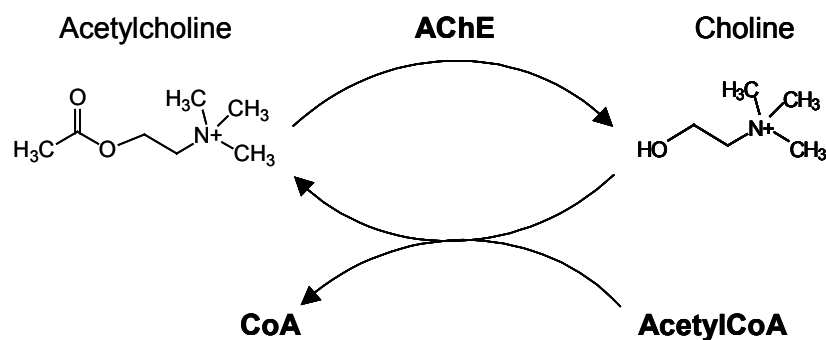


**Figure 5.1** A schematic of the procedure used to trap the catalysis product. A nanometer-sized trap is located near a nanometer-sized enzyme patch, while the remainder of the surface is coated in a film that resists the adsorption of the enzyme, reactant, and product. Some of the product of catalysis is captured in the trap before it can diffuse into bulk solution

We have investigated reactions on gold surfaces. In this case, a simple method for trapping molecules is to create a product that reacts directly with the gold surface. The enzyme acetylcholinesterase (AChE) can be used to cleave acetylthiocholine (ATCh) to produce a free thiol (thiocholine).<sup>5</sup> This free thiol can react with gold to form a stable structure (Figure 1). Thiocholine is a particularly attractive analyte because it produces high contrast for atomic force microscope (AFM) imaging.

## 5.2 Acetylcholine and Acetylcholinesterase

Acetylcholine (ACh) is one of the first neurotransmitters to be discovered, and performs a central role at the neuromuscular junctions and in the brain by activating the synapse and the neural response. AChE is the enzyme that is responsible for the rapid elimination of ACh by efficiently hydrolyzing it into choline and acetic acid within one millisecond after its release from cholinergic synapses. This enzyme hydrolysis affects on many vital functions ranging from precise control of muscle contraction to proper brain action.<sup>6</sup> AChE is one of the fastest enzymes known; the catalytic turn over rate for ACh is about  $1.6 \times 10^4$  reactions/second. It is surprising that this fast rate can be achieved when the active site is known to be accessible only through a deep (2 nm) and narrow catalytic gorge. After degradation by AChE, ACh is reproduced by choline acetyltransferase, which uses acetyl coenzyme A and choline as substrates for the formation of acetylcholine.<sup>6</sup>



Scheme 5.1

### Structure and Function of Acetylcholinesterase

AChE is a glycoprotein that exists in a variety of chemical structures; some of them are hydrophobic, while others are hydrophilic. The hydrophobic species primarily work at the synaptic cleft or the neuromuscular junction to break ACh into acetate and

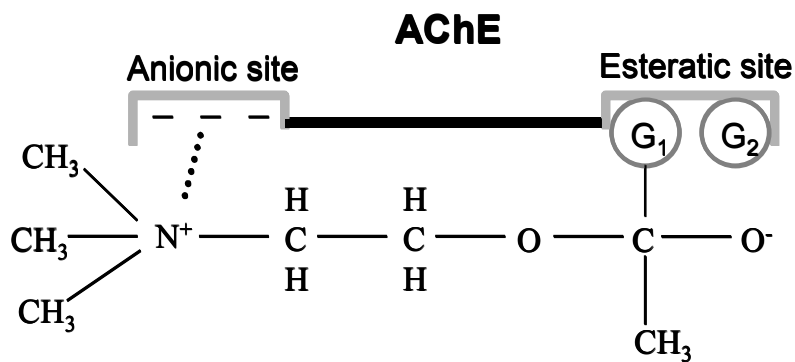


**Figure 5.2** The interaction of acetylcholinesterase with acetylcholine.<sup>12</sup>

choline. The hydrophilic varieties, on the other hand, generally work within the cell to break down excess amounts of intracellular ACh.

With many different chemical structures and quantities, the catalysis mechanisms for all the species of AChE are surprisingly similar. The active site of AChE is made up of two subsites: the anionic site and the esteratic subsite. The anionic site is made up of one or more negatively charged groups that serve to bind a substrate (ACh) to the enzyme. They electrostatically interact with the positively charged quaternary nitrogen of the ACh molecule (Figure 5.2).

The esteratic site is composed of three amino acid residues that are referred to as a catalytic triad (Ser203, His447, and Glu334). The reaction starts from the nucleophilic addition of the Ser203 O to the carbonyl C of acetylcholine. Simultaneous proton transfer from Ser203 to His447 facilitates the reaction. Glu334 is known to be essential in stabilizing the transition state through electrostatic interactions. Through this reaction the ester bond of ACh is broken and, the acetate and the choline are released. Choline is then either temporarily trapped within the junction of the muscular endplate or immediately taken up by the choline uptake system. Acetate, however, is covalently bonded to serine residues within the esteratic subsite and a temporary acetylated form of AChE is formed. A water molecule then reacts with this intermediate and the liberated acetate group

diffuses into the surrounding medium. Finally, an active form of the enzyme remains and is ready to react with a newly released molecule of ACh.

## 5.3 Experimental Section

### 5.3.1 Materials

The tri(ethylene glycol)-terminated thiol ( $\text{HS}(\text{CH}_2)_{11}(\text{OCH}_2\text{CH}_2)_3\text{OH}$ ), the carboxylic acid-terminated thiol ( $\text{HS}(\text{CH}_2)_{11}(\text{OCH}_2\text{CH}_2)_6\text{OCH}_2\text{CO}_2\text{H}$ ) and the quaternary ammonium group-terminated thiol ( $\text{HS}(\text{CH}_2)_{11}\text{N}^+(\text{CH}_3)_3\text{Cl}^-$ ) were synthesized. Other materials and chemicals were used as received. N-Hydroxysuccinimide (NHS), 1-ethyl-3-(3-dimethylaminopropyl)carbodiimide (EDC), AChE (*Electrophorus electricus* Type V-S), ATCh, and acetylcholine(ACh) were purchased from Sigma. 11-mercpto-1-undecanol was purchased from Aldrich. Au wire (1.0 mm diameter, 99.9985 %) was obtained from AlfaAesar. Phosphate-buffer saline (PBS: 10 mM phosphate, 138 mM NaCl, and 2.7 mM KCl) was obtained from RICCA Chemical.

### 5.3.2 Sample Preparation

#### Au(111) Substrates

The surface of a smooth gold ball was used as a substrate. The 1-mm diameter gold wire was cleaned with piranha solution (3:1 v/v ratio of  $\text{H}_2\text{SO}_4$ /3 wt. %  $\text{H}_2\text{O}_2$ ) and thoroughly rinsed with pure water. One end of the wires was then melted and annealed in a  $\text{H}_2/\text{O}_2$  flame. The result was a 2.0-2.5 mm diameter droplet with atomically flat <111> crystalline terraces suitable for AFM nanolithography.

#### Monolayers

Monolayers were prepared with tri(ethylene glycol)-terminated thiol and 11-mercpto-1-undecanol. Gold substrates were immersed in a 2-mM ethanolic solution of the selected chemical for 24 hours immediately after the annealing step. These substrates

were then placed into pure ethanol for several hours to remove the physisorbed layer and was finally dried in a N<sub>2</sub> stream.

### **5.3.3 Atomic Force Microscopy**

AFM experiments were performed as described in section 4.2.3.

### **5.3.4 Patterning of Carboxylic Acid and the Trap**

We created a nanometer-scale pattern and trap sites using the procedures of nanoshaving and nanografting as described in section 2.3.3 and 2.3.4.<sup>7</sup>

### **5.3.5 Immobilization of Protein**

For the selective immobilization of proteins, we used the NHS-EDC protocol that was developed by Whitesides and co-workers.<sup>8</sup> The procedure is described in section 4.2.4.

### **5.3.6 Trapping Hydrolyzed Product**

We create a trap for the reaction product, thiocholine, by using nanoshaving to create a region of exposed gold. We have investigated enzyme reactions on gold surfaces by trapping a product directly onto the exposed gold surface. The patterned enzyme acetylcholinesterase (AChE) cleaves acetylthiocholine (ATCh) to produce a free thiol (thiocholine). This free thiol can adsorb on the exposed gold via a S-Au bond (Figure 5.1). The catalytic activity of AChE for ATCh is known to be comparable to acetylcholine.<sup>9,10</sup>

## **5.4 Results and Discussion**

### **5.4.1 Surface Trapping of a Product Generated by Surface-bound Enzyme**

In this study, we first coated a very smooth gold sphere with a monolayer of HS(CH<sub>2</sub>)<sub>11</sub>(OCH<sub>2</sub>CH<sub>2</sub>)<sub>3</sub>OH<sup>8</sup> (EOthiol) by deposition from ethanol solution for 24 h (Figure 5.3A). The  $\omega$ -ethylene oxide groups are known to resist the adsorption of protein

molecules.<sup>11</sup> We then use nanografting to create a small patch of carboxylate groups on the surface by deposition of an acid-terminated thiol ( $\text{HS}(\text{CH}_2)_{11}(\text{OCH}_2\text{CH}_2)_6\text{OCH}_2\text{CO}_2\text{H}$ ) (Figure 5.3B).<sup>8</sup> Note that the carboxylic acid has a longer oligo(ethylene oxide) segment than the alcohol, so the carboxylic acid should protrude from the surrounding area. AChE (*Electrophorus electricus* Type V-S, Sigma) was covalently attached to the carboxylic acid via an amide bonds with a standard N-hydroxysuccinimidyl ester protocol (Figure 5.3C).<sup>8</sup> The surface was thoroughly washed with phosphate buffer (pH 7), with water, and then with ethanol to remove both unwanted reactants and non-specifically bound enzyme. We used the highest purity of AChE that is commercially available (60% protein, 1000-2000 units AChE/mg protein). The turnover rate of AChE is approximately 16,000 sec<sup>-1</sup> and the molar mass is about 70 kDa per catalytic site,<sup>12</sup> so the proteinaceous material contains 7-15% active AChE. The exterior of the *electrophorus electricus* AChE presents eight lysines that have amino groups available for tethering.<sup>13</sup> The AChEs were randomly attached to the carboxylic acid groups. Therefore, the AChE bound through the amino group located near the catalytic gorge will lose activity because the access of substrate molecules from the bulk is not favorable.

We created a trap for the reaction product, thiocholine, by using nanoshaving to create a region of exposed gold. The result is shown by the AFM image in Figure 5.3D. Note that the enzyme is localized to a small patch. Nanografting can be used to draw much smaller patches, but a large patch was drawn to raise the probability of obtaining active enzyme. A 9-mM aqueous solution of ATCh in phosphate buffer (pH 7) at 33°C was introduced for 2 hours and then the reaction vessel was rinsed with buffer, water, and then ethanol (See Figure 5.3E). The very bright spots in the trap show the adsorption of the thiocholine. The bright patch where the enzyme is attached is also larger and brighter. We attribute this to weakly bound ATCh or thiocholine. This weakly bound material was removed by rinsing with NaBr solution (Figure 5.3F). Possible mechanisms for this salt rinse are replacement of  $\text{ATCh}^+$  or  $\text{thiocholine}^+$  with  $\text{Na}^+$ , or replacement of  $\text{ATChPO}_4^-$  or  $\text{thiocholine PO}_4^-$  with  $\text{Br}^-$ . In other experiments it was removed by gentle scraping of the surface with the AFM tip. Comparing the trap before and after the addition of ATCh, it is clear that most of the trap has been filled.

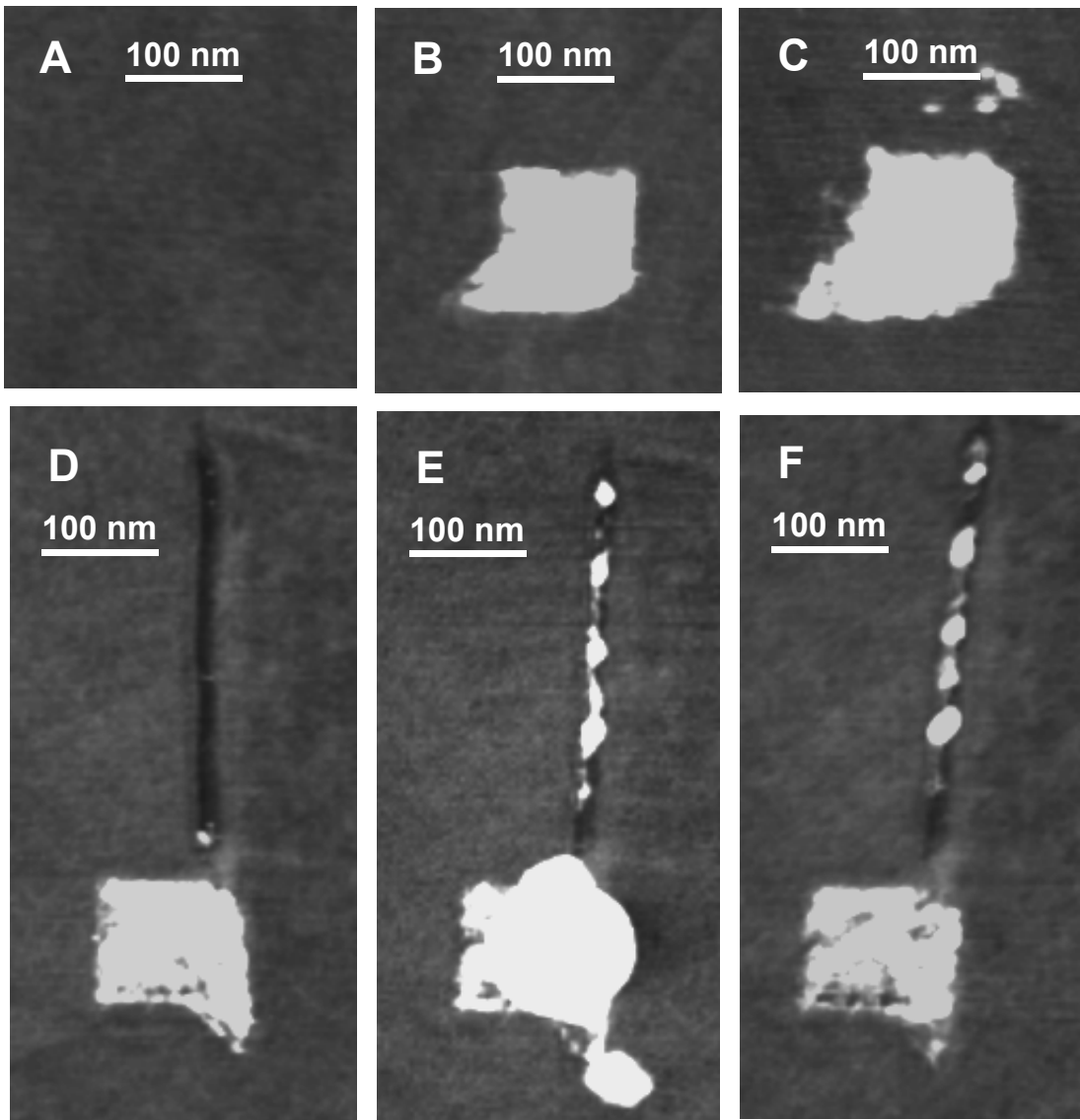


**Figure 5.3** Tapping mode AFM images in ethanol of the carboxylic acid patch, enzyme, and trap. They are on the surface of a smooth gold ball that was produced by melting a 1-mm radius gold wire in a H<sub>2</sub>/O<sub>2</sub> flame. **A.** EOthiol monolayer is self-assembled on the gold substrate. **B.** A carboxylic acid patch (white square) is produced in the EOthiol monolayer. **C.** AChE is covalently attached to the carboxylic acid patch using NHS-EDC procedure. **D.** A thin rectangular region of exposed gold, “the product trap” (dark line), is produced next to the AChE patch using nanoshaving. The product trap is exposed gold. The remaining area is covered in EOthiol. **E.** After addition of ATCh, most of the trap is filled with material (white), which we attribute to adsorption of thiocholine. There is also a large “plume” of material around the enzyme, which is either reactant or product. **F.** The original shape of the enzyme patch is approximately recovered by rinsing with 15-mM NaBr. Image **D**, **E**, and **F** were taken from the 90 degree.

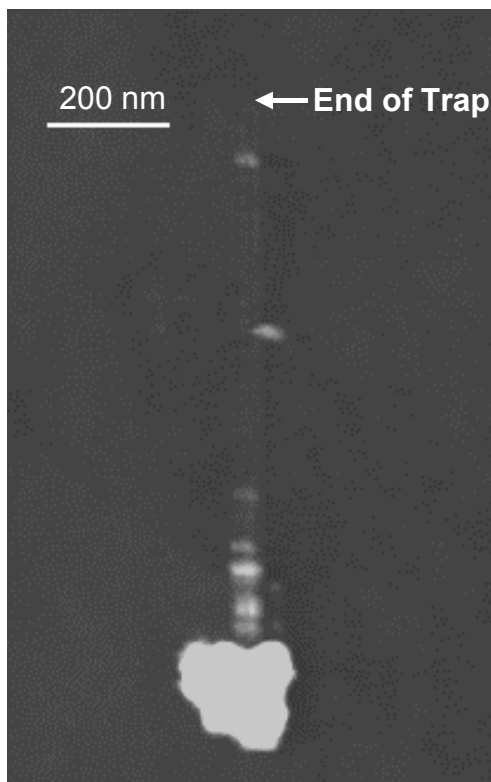


**Figure 5.4** Tapping mode AFM image in ethanol of the enzyme and trap after the addition of ATCh. In this experiment, there are fewer white patches in the trap, and they are concentrated near the enzyme. The proximity of the white patches to the enzyme is consistent with the formation of a product (e.g. thiocholine) that diffuses from the enzyme.

If the immobilized enzymes on the carboxylic acid patch catalyze the formation of thiols, one would expect to see that the gold areas near the enzymes were filled first. To demonstrate this, we produced a longer trap ( $1\text{-}\mu\text{m}$  long) next to an AChE patch and observed the trap filling phenomena within a short amount of time (10 min). As clearly seen in Figure 5.4, there is a particularly dense patch of material near the enzyme. This supports the idea that the filling material comes from the physical location of the enzyme, and thus is consistent with a product that diffuses from the enzyme.

Another important observation is that the thiocholine product adsorbed in the trap is not continuous: distinct lumps are visible in the AFM image. One possible reason for

the discontinuity is the electrostatic interaction between the charged products. Thiocholine has a positive charge on its quaternary ammonium group. When thiocholine is produced by the patterned AChE, it initially fills the trap very near the enzyme patch. Additional thiocholine product diffusing from the enzyme patch will then feel electrostatic repulsion by the first trapped thiocholine. This repulsive interaction will result in the change of diffusion pass and make the second adsorption at some distance, which I attribute to the discontinuous trap filling.

#### 5.4.2 Control Experiments

Two alternate explanations of the observed line-filling need to be addressed before we attribute the AFM observation to enzyme catalysis of ATCh. (1) The remainder of the film consists of thiol molecules. Did the EOthiol simply migrate to fill the hole? Consistent with the original claims from Liu's group,<sup>14</sup> in control experiments in the absence of enzyme and ATCh, a nanoshaved hole in an EOthiol film was stable for at least 16 h (Figure 5.5A). Thus lateral migration of the EOthiol does not fill the hole.

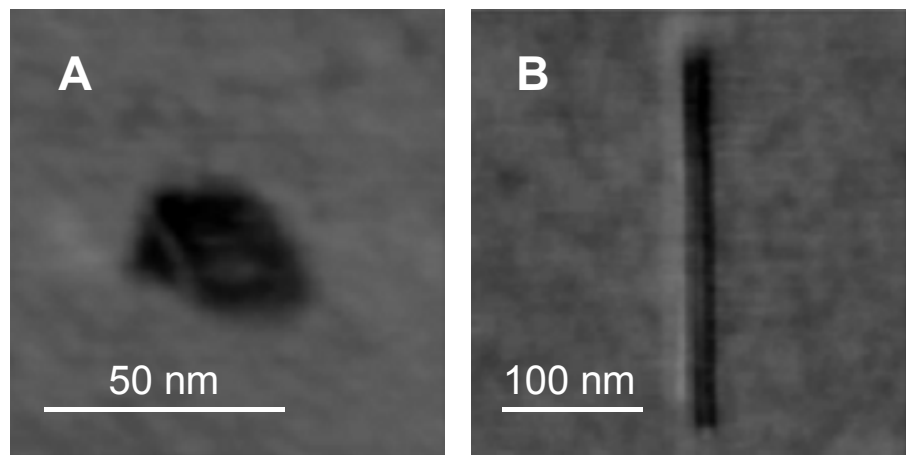


**Figure 5.5** AFM images in ethanol of control experiments when the enzyme was not present. **A.** A small hole was scratched in the EOthiol and left for 16 h in water. The size and shape are stable over this period. (10 nm Z-range) **B.** A line-trap was left in 9-mM phosphate buffer (pH 7) ATCh solution at 33°C for 2 h. ATCh does not fill the trap. (10 nm Z-range)

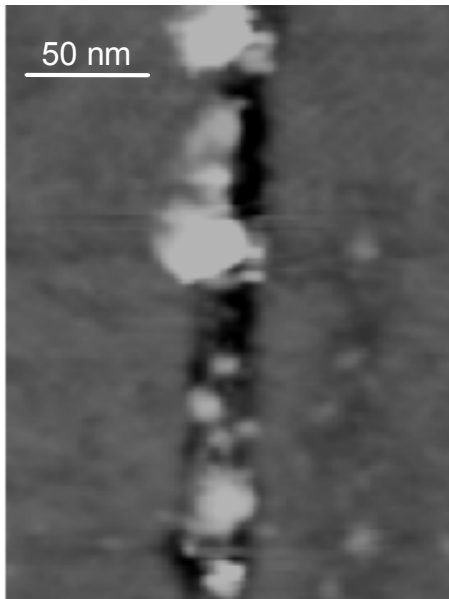


**Figure 5.6** AFM images in ethanol of control experiments when the enzyme was not present. A line-trap was exposed to a solution of ATCh at pH 9 for two hours. At pH 9, the ATCh is hydrolyzed to the free thiol in solution, and then trapped on the surface. (10 nm Z-range)

(2) Does the reactant, ATCh, fill the hole? Figure 5.5B shows that the hole was also stable in the presence of ATCh when the enzyme was absent.

As a further check for the consistency of our hypothesis that the filling material is actually thiocholine, we observed the adsorption of thiocholine that was produced by homogeneous inorganic catalysis in aqueous solution. ATCh is easily hydrolyzed by  $\text{OH}^-$ .<sup>15</sup> Figure 5.6 is an AFM image of a nanoshaved line that was exposed to a 5 mM solution of ATCh at pH 9. The bright spots that appear are very similar to those observed in the presence of enzyme and ATCh.

We have also repeated the entire experiment, but with acetylcholine, which is the native substrate for the AChE, instead of acetylthiocholine. (See Figure 5.7) AChE hydrolyses ACh to give acetic acid and choline that does not have a thiol functional

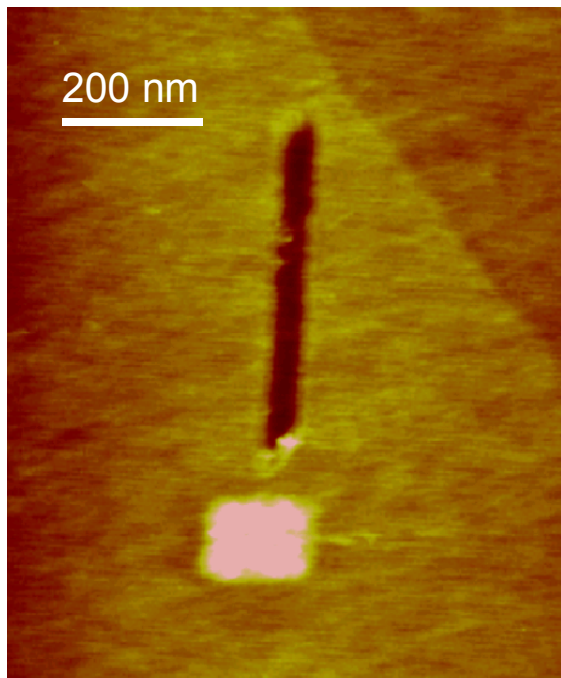


**Figure 5.7** Tapping mode AFM image in water of an enzyme patch and a trap after exposure to a 9 mM solution of acetylcholine (ACh) for 2 h at 31°C. The trap is empty. ACh is the natural substrate for AChE. It hydrolyses to give acetic acid and choline. The empty trap is a control showing that the bright patches observed in the trap in Figure 2 are not (a) enzyme or other components washed into the trap by salt, or (b) acetic acid. (10 nm Z-range)

group. Experiment shows, as expected, that the trap is empty. This is a control that none of the other components in the system (enzyme, buffer, acetic acid (product)) fill the trap.

We have performed a macroscopic experiment to enhance confidence that the thiol does adsorb and that the enzyme is active. I used surface plasmon resonance (SPR), to determine that thiocholine binds to gold surfaces. (See figure 5.8). A solution of thiocholine was prepared by hydrolyzing ATCh at pH 10. A fresh gold surface was then exposed to a solution of thiocholine and the adsorption of thiocholine to gold was measured by SPR. There was a large jump in the adsorption signal after the addition of thiol solution. The signal decreased when I subsequently injected water. I interpret this as

the desorption of physisorbed thiol. However, there was a large difference between the initial and final signal. I attribute this gap to the chemisorption of thiocholine to gold surface.

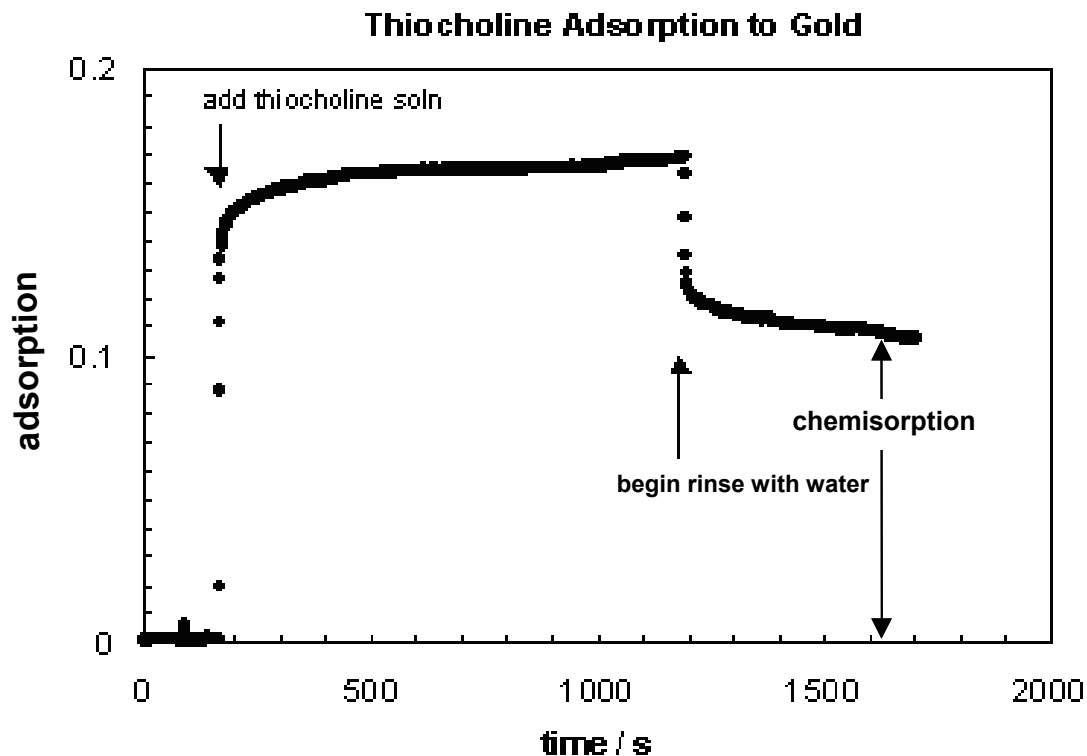


**Figure 5.8** The adsorption of thiocholine on gold measured by surface plasmon resonance (SPR). A fresh gold surface was exposed to a solution of thiocholine (created by hydrolysis of ATCh at pH 10 prior to injection into the SPR cell). There is a large adsorption, of which about 2/3 remains after rinsing with water.

#### 5.4.3 Contrast Mechanism of Thiocholine

Surface-trapped thiocholine molecules produce high contrast in an AFM image (Figure 5.3). When imaged by tapping mode in ethanol solution, the thiocholine molecules are about 3.9 nm higher than the surrounding EOthiol, even though the extended van der Waals length of the EOthiol is about 1.7 nm longer than the thiocholine.

Contrast in tapping mode arises from differences in height, force, and elasticity.<sup>16</sup> However, none of these factors can clearly explain such a high contrast of thiocholine product adsorbed in the trap. I observed similar high contrast for carboxylate groups imaged under the same conditions in the previous chapter. In that case, the contrast is probably due to the long-range electrostatic force of carboxylate group to the negatively charged AFM probe. A silicon nitride ( $\text{Si}_3\text{N}_4$ ) AFM tip has terminal silanol groups on its surface, which can be deprotonated and produce negative charge in a high dielectric solvent. If the thiocholine does not adsorb to the AFM tip, then the thiocholine and the tip are oppositely charged. The attractive electrostatic interaction between the two should make the contrast negative. It is possible that the thiocholine (or acetylthiocholine) does adsorb to the tip to change the charge, but this is unlikely to still occur after rinsing with salt.

A possible explanation on this contrast mechanism is that the counter ions in the solution electrostatically adsorb on the quaternary ammonium of thiocholine and produce the high contrast. The substrate (ATCh) used for the surface trapping experiment contains an iodide as a counter ion.

As a check for our hypothesis, we produced a quaternary ammonium group-terminated patch in a hydroxyl group-terminated SAM and imaged the surface in solution of different counter ions using tapping mode AFM phase imaging.<sup>17,18</sup> We first coated a smooth gold sphere with a monolayer of  $\text{HS}(\text{CH}_2)_{11}\text{OH}$  (OHthiol) by deposition from ethanol solution for 24 h. We then used nanografting to create a 500 nm-long line patch of quaternary ammonium groups in the monolayer by deposition of  $\text{HS}(\text{CH}_2)_{11}\text{N}^+(\text{CH}_3)_3$  (Quat-thiol) and thoroughly washed the surface with pure water. Note that both of  $\omega\text{-OH}$  and  $\omega\text{-N}^+(\text{CH}_3)_3$  have similar chain length. However, the quaternary ammonium pattern shows negative contrast as we expected probably due to its opposite charge to the AFM tip surface (Figure 9A and C). Two samples with quaternary ammonium pattern were prepared (A and C). The sample A was exposed to 0.1 M KCl and the sample C to 0.1 M KI solutions, and they were observed using a tapping mode phase imaging method. The  $\text{Cl}^-$  sample is shown in B and the  $\text{I}^-$  sample is shown in D.

There is no significant change of contrast within the patch on the chloride sample whereas the iodide patch has many white lumps. These lumps are similar to those

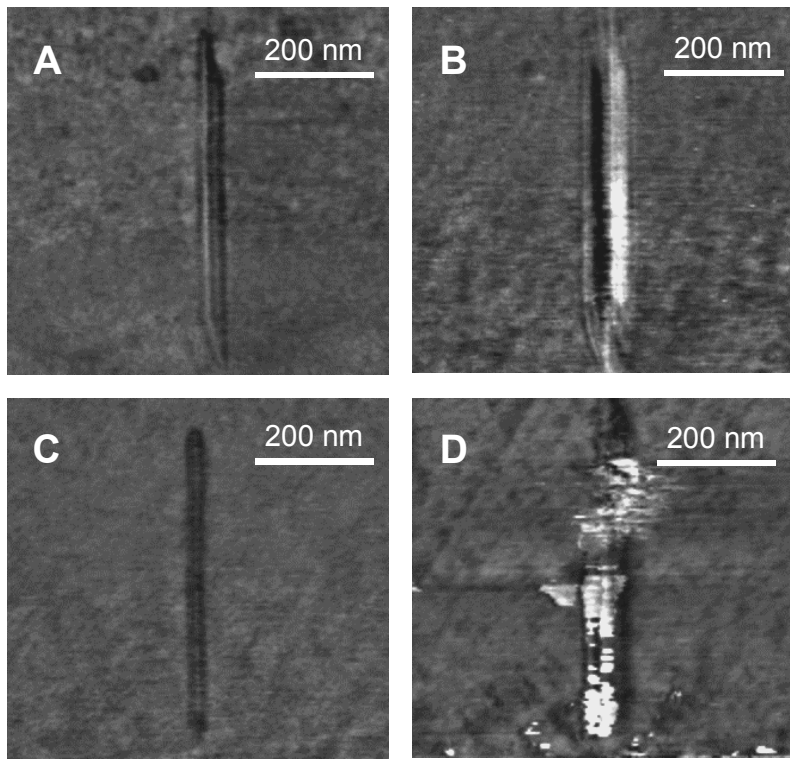


**Figure 5.9** The counterion effect on the contrast change of a quaternary ammonium pattern. (A) and (C) 500 nm-long line patch was nanografted in a hydroxyl ( $\text{HS}(\text{CH}_2)_{11}\text{OH}$ ) SAM by deposition of  $\text{HS}(\text{CH}_2)_{11}\text{N}^+(\text{CH}_3)_3$ . (B) The surface (A) was immersed in a 0.1 M aqueous solution of KCl. (D) 0.1 M of aqueous KI solution was introduced on the surface (C). All images were taken by tapping mode AFM phase imaging method.

observed in the AChE experiments. Thus we hypothesize that the high contrast in the AChE experiments is due to the adsorption of  $\Gamma^-$  ions to quaternary ammonium. It is well known that  $\Gamma^-$  binds more strongly than  $\text{Cl}^-$  to  $-\text{N}^+(\text{CH}_3)_3$ .<sup>19</sup> Although we have discovered the chemical source of the high contrast ( $\Gamma^-$ ), it is still not clear why  $\Gamma^-$  produces such a high contrast. In order to understand the contrast mechanism clearly, more experiments are required using more counter ions with varying electron densities and polarizabilities, such as  $\text{SCN}^-$ ,  $\text{NO}_3^-$ ,  $\text{Br}^-$ ,  $\text{SO}_4^{2-}$ ,  $\text{HCOO}^-$ ,  $\text{F}^-$ .

## **5.5 Conclusions**

We have produced a nanometer-scale patch of enzyme and demonstrated that it is catalytically active through a surface-trapping experiment. Iodide ion bound to the surface-trapped thiocholine produced high contrast in a tapping mode AFM image, which contributes to the verification of catalyzed product. The localization of active biological material enables the fabrication of high-density biological assays. In addition, the localization of an active catalyst is a step in the evolution of nanostructures that can be used as an aid in the fabrication of additional or more complex nanostructures.

## References

- (1) Shipway, A. N.; Katz, E.; Willner, I. *Chemphyschem* **2000**, *1*, 18.
- (2) Quake, S. R.; Scherer, A. *Science* **2000**, *290*, 1536.
- (3) Moriarty, P. *Rep. Prog. Phys.* **2001**, *64*, 297.
- (4) Greig, L. M.; Philip, D. *Chem. Soc. Rev.* **2001**, *30*, 287.
- (5) Ellman, G. L.; Courtney, K. D.; Andres, V. J.; Featherstone, R. M. *Biochemical Pharmacology* **1961**, *7*, 88.
- (6) Doctor, B. P.; Taylor, P.; Quinn, D. M.; Rotundo, R. L.; Gentry, M. K. *Structure and Function of Cholinesterases and Related Proteins*; Plenum Press: New York, 1998.
- (7) Liu, G.-Y.; Xu, S.; Qian, Y. L. *Accounts Chem. Res.* **2000**, *33*, 457.
- (8) Lahiri, J.; Isaacs, L.; Tien, J.; Whitesides, G. M. *Anal. Chem.* **1999**, *71*, 777.
- (9) Froede, H. C. *J. Biol. Chem.* **1984**, *259*, 11010.
- (10) Puu, G. *Biochem. Pharmacol.* **1990**, *40*, 2209.
- (11) Ostuni, E.; Yan, L.; Whitesides, G. M. *Colloids and Surfaces B* **1999**, *15*, 3.
- (12) Rosenberry, T. L. *Adv. Enzymol. Relat. Areas Mol. Biol.* **1975**, *43*, 103.
- (13) Bourne Y.; Grassi J.; Bourgis, P. E.; Marchot, P. *J. Biol. Chem.* **1999**, *274*, 30370.
- (14) Xu, S.; Miller, S.; Laibinis, P. E.; Liu, G.-Y. *Langmuir* **1999**, *15*, 7244.
- (15) Green, T. W.; Wuts, G. M. *Protective Groups in Organic Synthesis*; 3rd ed.; Wiley: New York, 1999, pp 482.
- (16) Bar, G.; Thomann, Y.; Brandsch, R.; Cantow, H. J.; Whangbo, M. H. *Langmuir* **1997**, *13*, 3807.
- (17) Sanders, G. H. W.; Davies, M. C.; Roberts, C. J.; Tendler, S. J. B.; Williams, P. M. *Langmuir* **1999**, *15*(17), 5433.
- (18) Knoll, A.; Magerle, R.; Krausch, G. *Macromolecules* **2001**, *34*(12), 4159.
- (19) Ninham, B. W.; Yaminsky, V. *Langmuir* **1997**, *13*, 2097.

"This chapter was reproduced in part with permission from [Jang, C.-H.; Stevens, B. D.; Carlier, P. R.; Calter, M. A.; Ducker, W. A. **Immobilized Enzymes as Catalytically-Active Tools for Nanofabrication** *J. Am. Chem. Soc. (Communication)*, **2002**, *124*(41), 12114-12115.] Copyright [2002] American Chemical Society."

## **Chapter 6. A Strategy for the Sequential Patterning of Proteins: Catalytically-Active Multiprotein Nanofabrication**

### **6.1 Introduction**

The preparation of arrays of immobilized proteins is important for the preparation of assays and sensors and is useful for the study of protein activity.<sup>1,2</sup> Recently, there has been some interest in the preparation of nanoscale protein arrays using the nanografting technique of atomic force microscopy (AFM).<sup>3,4</sup> This technique may allow the fabrication of small and high-density sensors. For most applications, an array of proteins finds use when the array contains a number of different proteins, but to the best of my knowledge there is no established technique for the preparation of an array of different active proteins on the nanoscale. In a serial approach to producing heterogeneous arrays, difficulty can arise because the immobilization steps for the subsequent proteins can adversely affect the activity of the previously immobilized enzymes. For example, it is simple to immobilize proteins by reaction with aldehyde groups,<sup>5</sup> but aldehyde introduced into a solution that bathes an immobilized enzyme will react with amine groups on the immobilized enzyme and could inactivate the enzyme (see Figure 6.1A).

This chapter describes a strategy for the serial immobilization of nanoscale protein patches while maintaining enzyme activity. This method is demonstrated by first immobilizing acetylcholinesterase (AChE), then immobilizing insulin, and then showing that the AChE remains catalytically active. Insulin is not a catalyst. It is simply an inexpensive protein that was immobilized after the AChE. The strategy is to create an aldehyde on a SAM surface without exposing the immobilized enzyme to the aldehyde. This strategy relies on the oxidative selectivity of periodate for the diol group.<sup>6</sup> 1,2- or vicinal diols are known to be cleaved by periodate into two carbonyl compounds. The oxidation reaction proceeds via formation of a cyclic periodate ester. 1,2-diols reacts to form a cyclic periodate ester and then the periodate ester undergoes a rearrangement of the electrons, which results in the cleavage of the carbon-carbon bond and the formation of two carbonyl compounds (Scheme 6.1).

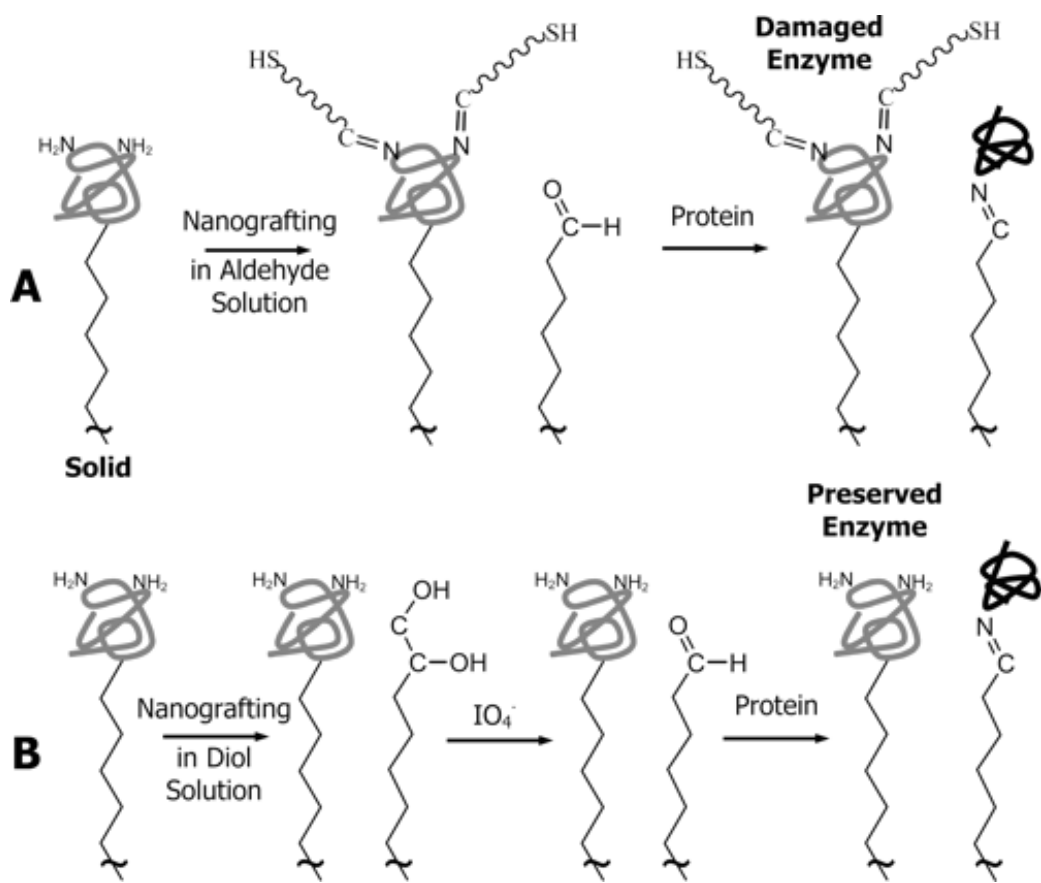
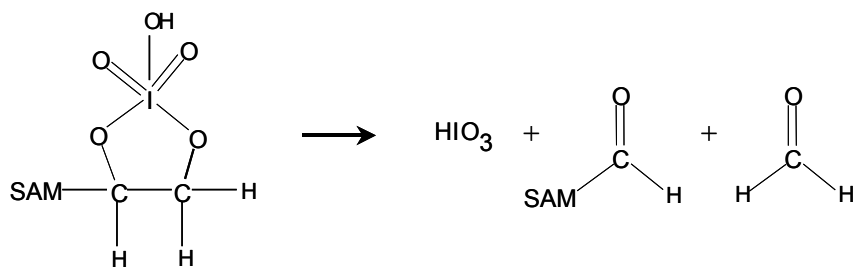


**Figure 6.1** Schematic of immobilization of a series of enzymes: (A) Reagents that can immobilize an enzyme can also modify enzymes that are already in the film. (B) Strategy showing the enzyme being exposed to two reagents, neither of which react with the enzyme, but which reacts together to form an immobilization site.

None of the 20 or so common amino acids contains a diol group, so proteins are relatively immune to oxidation by periodate. The diol group does not react with proteins, but oxidation of the diol with periodate proceeds only as far as the aldehyde, which can then undergo reaction with the amine groups in proteins (see Figure 1B). In addition, it is facile to incorporate diols into a self-assembled monolayer (SAM). Therefore, the diol can be introduced into a SAM as a "latent aldehyde" ready to be switched into an immobilizing site. The switch does not inactivate enzymes that are already immobilized on the surface.



**Scheme 6.1**

## 6.2 Experimental Section

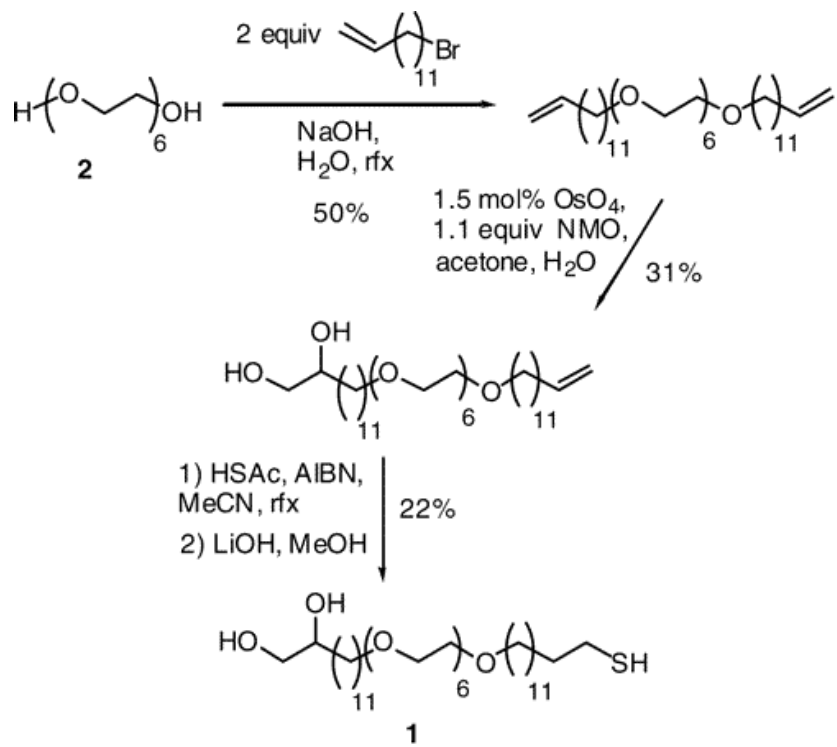
### 6.2.1 Materials

The tri(ethylene glycol)-terminated thiol ( $\text{HS}(\text{CH}_2)_{11}(\text{OCH}_2\text{CH}_2)_3\text{OH}$ ) and the diol-terminated thiol ( $\text{HS}(\text{CH}_2)_{11}(\text{OCH}_2\text{CH}_2)_6\text{O}(\text{CH}_2)_{11}\text{CH}(\text{OH})\text{CH}_2\text{OH}$ ) were synthesized. Other materials and chemicals were used as received. AChE (*Electrophorus electricus* Type V-S), insulin (human, recombinant, expressed in *E. coli*), and acetylthiocholine (ATCh) were purchased from Sigma. Sodium periodate ( $\text{NaIO}_4$ ) was purchased from Aldrich. Au wire (1.0 mm diameter, 99.9985 %) was obtained from Alfa Aesar. Phosphate-buffer saline (PBS: 10 mM phosphate, 138 mM NaCl, and 2.7 mM KCl – pH 7.4) was obtained from RICCA Chemical.

### 6.2.2 Synthesis of $\omega$ -Diol Thiol

$\omega$ -diol thiol was synthesized by B. D. Stevens in Professor Michael Calter's group at the University of Rochester. The synthesis of the diol thiol **1** began with the alkylation of polyethylene(ethyleneglycol) diol **2** with  $\omega$ -bromoundecene (Scheme 6.2). Dihydroxylation of this compound using catalytic osmium tetroxide and stoichiometric *N*-methyl morpholine-*N*-oxide (NMO) afforded a mixture of the singly and doubly

dihydroxylated compounds. After separation, the singly dihydroxylated compound was converted into **1** by addition of thioacetic acid followed by thioester hydrolysis.



**Scheme 6.2**

### 6.2.3 Sample Preparation

#### Au(111) Substrates

Flat gold substrates were prepared by annealing a gold wire in a  $\text{H}_2/\text{O}_2$  flame as described in section 4.2.2.

## **Monolayers**

Self-assembled monolayers were prepared with tri(ethylene glycol)-terminated thiol using the standard self-assembly procedure as described in section 4.2.2.

### **6.2.4 Atomic Force Microscopy**

All imaging and patterning were carried out in a desired solution with a NanoScope IIIa AFM (Digital Instruments, Santa Barbara, CA) as described in section 4.2.3.

### **6.2.5 Patterning of the Diol and the Trap**

The trap sites and diol pattern were created using the nanoshaving and nanografting procedures described in section 5.2.4.<sup>3</sup>

### **6.2.6 Oxidation of the Diol**

After producing diol patterns on an ethylene glycol surface (See Figure 6.4B), nonspecifically adsorbed diol molecules were carefully rinsed with ethanol and water. The patterned 1,2-diols were then cleaved with sodium periodate ( $\text{NaIO}_4$ : 0.1 mM, 20 min) to produce aldehyde groups. The surface was then rigorously rinsed with pure water and phosphate-buffer saline was introduced over the surface for the next immobilization step.

### **6.2.7 Immobilization of the Protein**

Acetylcholinesterase and insulin were covalently attached to the aldehyde via imine bonds simply by introducing the protein into solution. After producing aldehyde from the patterned diol by oxidative cleavage with periodate, the surface was rigorously washed with pure water. Aqueous protein (1mg/10ml) was then introduced into the AFM liquid cell for 10 min for the immobilization of the protein. The surface was carefully washed with water to remove nonspecifically adsorbed proteins. The resulting pattern was observed using tapping mode AFM imaging.

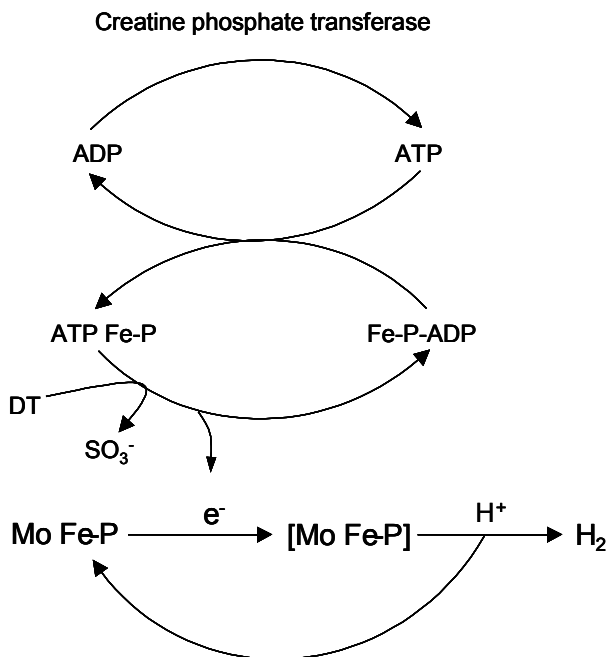
### 6.2.8 Trapping Hydrolyzed Product

A trap for the reaction product, thiocholine, was created by using nanoshaving to expose a region of gold. The enzyme reaction with the substrate was investigated by trapping a product directly into the exposed gold surface as described in section 5.2.6.

## 6.3 Results and Discussion

### 6.3.1 Possible Reaction of NaIO<sub>4</sub> with Enzymes

Our strategy for serial immobilization relies on the lack of reaction of NaIO<sub>4</sub> with enzymes. Our first step was to check whether this was true. We tested the effect of NaIO<sub>4</sub> on enzyme activity using the two-component nitrogenase system because assays for



Scheme 6.3

activity of nitrogenase (Scheme 6.3)<sup>7</sup> are routinely performed in the Biochemistry Department at Virginia Tech.

The following tests were performed in collaboration with J. H. Han in the Department of Biochemistry. An aqueous mixture of ATP Fe-P, MoFe-P, and creatinephosphate kinase in 0.1 mM NaIO<sub>4</sub> was prepared. At the same time, a control experiment was performed with the same enzyme assay solution, but without periodate. After 20 min, the enzyme activities of the two mixtures were measured by analyzing the amount of gas (H<sub>2</sub>) produced using gas chromatography (Figure 6.2). There was only a slight reduction in activity (13%) in the presence of periodate, thereby supporting the

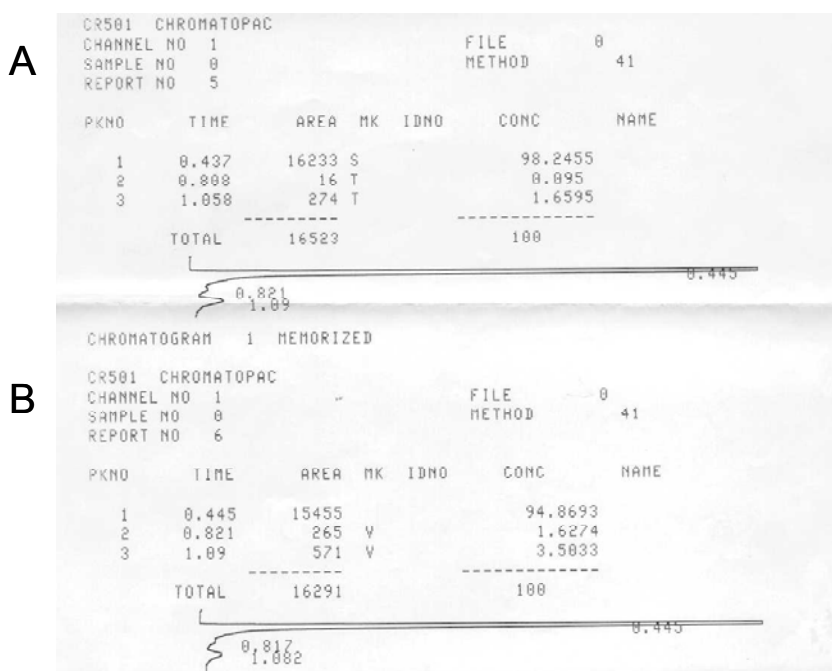


**Figure 6.2** Gas chromatography data of the activity of the two-component nitrogenase system in buffer solution in the absence (A) and then in the presence (B) of periodate solution. The enzyme activities of each were measured by analyzing the amount of product gas (H<sub>2</sub>).

hypothesis that periodate does not cause extensive inactivation of the enzyme. Note that this test is more harsh than the conditions for the immobilization strategy. The periodate is actually present during the catalysis, whereas in our strategy the periodate is a wash prior to any step requiring catalysis. In the latter case, any reversible reaction of the enzyme with periodate could potentially be undone by reacting with water after the periodate solution is rinsed away.

### 6.3.2 Preparation of Films Containing Two Different Protein Patches

For the immobilization experiments, a monolayer of  $\text{HS}(\text{CH}_2)_{11}(\text{OCH}_2\text{CH}_2)_3\text{OH}$  (EOthiol)<sup>8,9</sup> was prepared on a very smooth gold sphere<sup>10</sup> and a small patch of 1,2-diol groups was then nanografted on the monolayer by deposition of  $\text{HS}(\text{CH}_2)_{11}(\text{OCH}_2\text{CH}_2)_6\text{O}(\text{CH}_2)_{11}\text{CH}(\text{OH})\text{CH}_2\text{OH}$  (diol).

After rinsing out the unadsorbed diol molecules with ethanol and water, the patterned 1,2-diols were cleaved with sodium periodate ( $\text{NaIO}_4$ : 0.1 mM, 20 min) to produce aldehyde groups. It was found that higher concentrations of periodate caused modification of the EOthiol background (Figure 6.3). Our results do not allow us to determine whether this is physisorption or chemisorption by reaction with two  $\omega$ -alcohols from neighboring EOthiols. AChE (This product contains 7-15% active AChE.) was then covalently attached to the aldehyde via imine bonds<sup>11</sup> simply by introducing the protein into solution. Nanografting was then used a second time to create a second small patch of 1,2-diol on the same surface. The second patch was oxidized using periodate and then insulin was covalently attached to the second patch by introducing the protein into solution. The AFM image of the two protein patches is shown in Figure 6.4D. Note that the height of the second patch increased after the attachment of insulin but that the insulin patch is still 1 nm lower than the AChE patch. The molar mass of AChE is about 75 kDa per catalytic site<sup>12</sup> and the molar mass of insulin is 5.8 kDa.<sup>13</sup> The diameters of monomeric AChE and insulin are ~4-5 nm and ~3 nm, respectively. Both proteins are known to have oligomeric molecular forms in a solution at neutral pH. Insulin forms a

hexamer at pH 7. AChE presents many different molecular forms, ranging from monomers to the large collagen-tailed forms, which include up to twelve catalytic subunits. Our data shows that both proteins formed the monomeric layers on the surface.

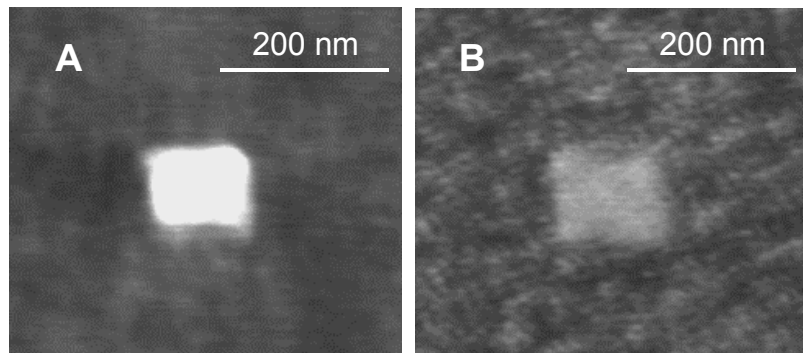


**Figure 6.3** AFM images in water of an aldehyde pattern from the oxidation of a patterned diol. (A) A 1,2-diol pattern was nanografted in an EO SAM and exposed to 0.1mM solution of NaIO<sub>4</sub> for 20 min. The EO surface was not damaged. (B) The patterned surface was exposed to 1.0-mM NaIO<sub>4</sub> for 20 min. The EO surface was modified by periodate. Both images have 2 nm Z-range.

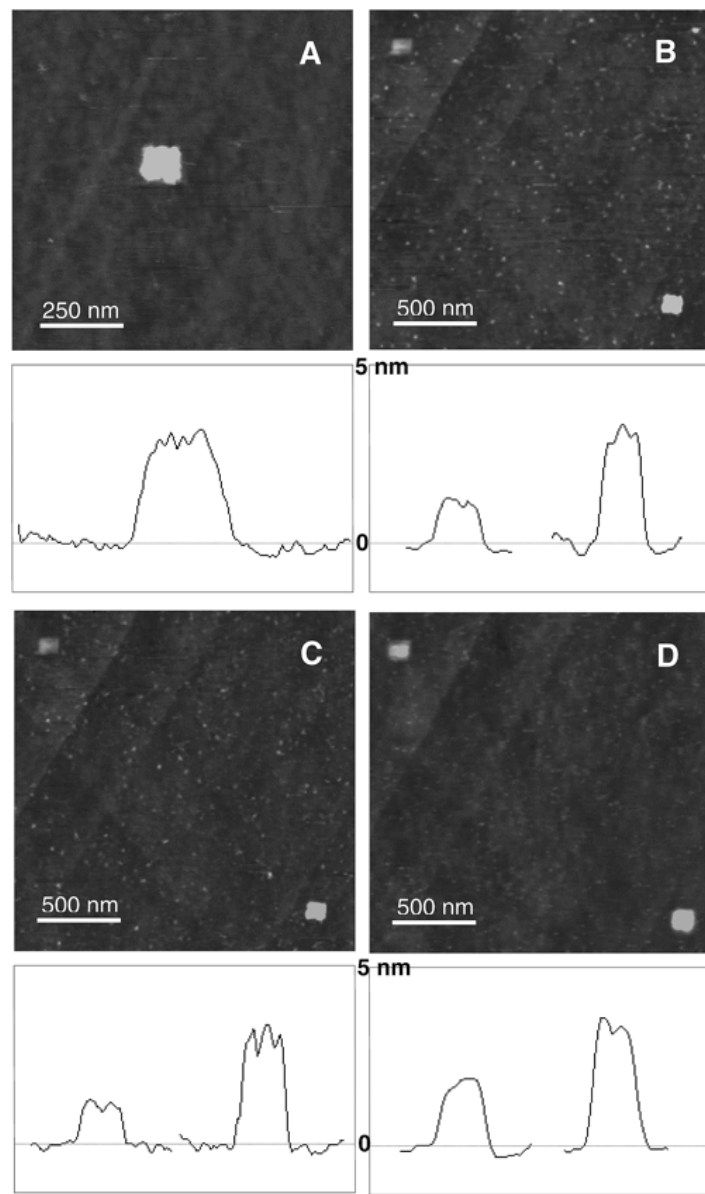


**Figure 6.4** Tapping-mode AFM images in water showing the formation of two-protein nanopatterns on a smooth gold ball using the diol immobilization strategy. (A) The white square is an AChE patch immobilized via imine bonds. (B) A diol pattern was produced on the top left using nanografting. The bright square on the bottom right is the AChE patch shown in (A). (C) An aldehyde patch (top left) was produced from the diol pattern using oxidative cleavage with periodate. (D) The same area imaged after 10 min of immersion in an insulin solution. Insulin was immobilized on the aldehyde patch. Corresponding cross-sectional lines show the height of each patch. All images have a 10-nm Z-range.

### 6.3.3 Test of AChE Activity

We tested the catalytic activity of the immobilized AChE (which was the first protein to be attached). Because of the very small number of AChE molecules in the nanopatch, it is not possible to discern activity through a conventional assay. Therefore we monitored catalytic activity, using the procedure described in Chapter 5, by first trapping some of the catalyzed-reaction product at the surface in a second reaction before it can diffuse away, and then imaging the trapped product as described previously (Figure 6.5).<sup>14</sup>

We produced an AChE patch and then an insulin patch in an ethylene oxide SAM using a 1,2-diol protocol. The surface was rigorously washed with phosphate buffer (pH 7), with water, and then with ethanol to remove both unwanted reactants and nonspecifically bound enzyme. Two thin rectangular patches of bare gold were created above the proteins. This exposed gold is the trap for thiocholine, the product of acetylthiocholoine (ATCh) hydrolysis by AChE. A 9 mM aqueous solution of ATCh in phosphate buffer (pH 7) at 33 °C was introduced for 1 h, and then the reaction vessel was rinsed with buffer and water. The white dots in the trap show the adsorption of the thiocholine (Figure 6.5B). The presence of thiocholine demonstrates the activity of the AChE that was exposed to periodate. The density of white spots is greater in the trap near the AChE than it is in the trap near the insulin, which is consistent with catalysis by the AChE. A series of control experiments described in Chapter 5 show that neither the substrate, buffer, acetic acid, enzyme, nor the surrounding ethylene oxide material are responsible for filling the trap. Because AChE enzyme is still active after exposure to periodate, the diol/periodate method can be used to create nanopatterns of more than one active enzyme.

Consistent with the decrease in bulk catalytic activity observed after exposure of nitrogenase to periodate, we also found a reduction in success of trapping experiments using enzyme exposed to periodate (trap filled in 2 of 3 experiments) compared to enzyme that was not exposed to periodate (trap filled in 4 of 5 experiments). The possible reduction in activity could be due to (1) the fact that in the serial nanolithogrphy with

enzymes, the AChE was exposed to ethanol and imaged many times, and (2) the partial deactivation by  $\text{IO}_4^-$  as observed for nitrogenase.

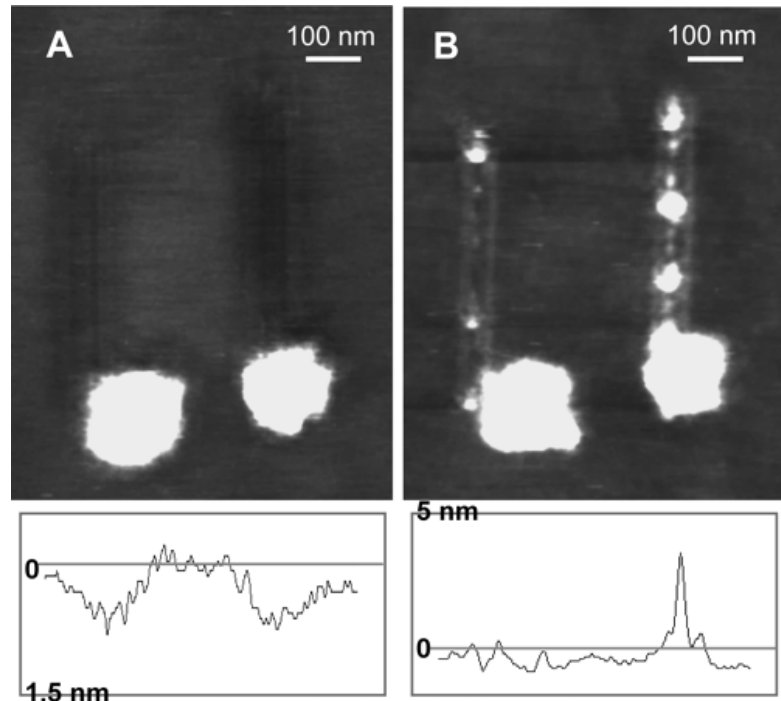


**Figure 6.5** Tapping mode AFM images in water of the proteins and the product trap: (A) before addition of ATCh and (B) after addition of ATCh. In both figures, the large white patch on the right is AChE and the large white patch on the left is insulin. Above the protein patches are two traps (bare gold) that have been created by scraping away EOthiol. The bioresistive EOthiol covers the remainder of the gold surface. After addition of ATCh, bright spots appear in the traps, which, using the controls of chapter 5. I attribute to adsorption of thiocoline. The line traces below the images show cross-sections through the trap (1.5 nm vertical scale for A and 5 nm vertical scale for B.) Both images have 3-nm Z-range.

#### **6.4 Conclusions**

We have demonstrated a new and convenient method of immobilizing enzymes to SAMs through the creation of adsorbed aldehyde molecules from adsorbed diols. This immobilization method is simple and convenient, and may offer a useful alternative to existing techniques (such as the EDC protocol)<sup>8</sup> for producing homogeneous films of immobilized compounds. The diol/periodate strategy also enables the serial immobilization of different enzymes while preserving their catalytic activities. This approach is possible because neither the diol nor the periodate react with enzymes, only the product of their reaction (the aldehyde) reacts with enzymes. In principle, this strategy could be used to build up complex films with many different enzymes immobilized to a surface. We have demonstrated the technique by producing a film with two proteins, while maintaining catalytic activity for the first protein that was immobilized.

## References

- (1) Ekins, R. P.; Berger, H.; Chu, F. W.; Finckh, P.; Krause, F. *Nanobiology* **1998**, *4*, 197-220.
- (2) Rowe, C. A.; Tender, L. M.; Feldstein, M. J.; Golden, J. P.; Scruggs, S. B.; MacCraith, B. D.; Cras, J. J.; Ligler, F. S. *Anal. Chem.* **1999**, *71*(17), 3846-3852.
- (3) Liu, G.-Y.; Xu, S.; Qian, Y. L. *Acc. Chem. Res.* **2000**, *33*, 457-466.
- (4) Kenseth, J. R. H.; Jones, V. W.; Porter, M. D. *Langmuir* **2001**, *17*, 4105-4112.
- (5) Wadu-Mesthrige, K.; Xu, S.; Amro, N. A.; Liu, G. *Langmuir* **1999**, *15*, 8580-8583.
- (6) March, J. *Advanced Organic Chemistry*; McGraw-Hill: New York, 1977; p 1087.
- (7) Fisher, K.; Dilworth, M. J.; Kim, C.-H.; Newton, W. E. *Biochemistry* **2000**, *39*, 10855-10865.
- (8) Lahiri, J.; Isaacs, L.; Tien, J.; Whitesides, G. M. *Anal. Chem.* **1999**, *71*, 777-790.
- (9) Ostuni, E.; Yan, L.; Whitesides, G. M. *Colloids Surf. B* **1999**, *15*, 3-30.
- (10) Hayes, W. A.; Shannon, C. *Langmuir* **1998**, *14*, 1099-1102.
- (11) Jones, M. *Organic Chemistry*; W. W. Norton & Company, Inc.: New York, 1997; p 1092.
- (12) Rosenberry, T. L. *Adv. Enzymol. Relat. Areas Mol. Biol.* **1975**, *43*, 103.
- (13) Smith, L. F. *Am. J. Med.* **1966**, *40*, 662.
- (14) Jang, C.-H.; Stevens, B. D.; Carlier, P. R.; Calter, M. A.; Ducker, W. A. *J. Am. Chem. Soc.* **2002**, *124*, 12114-12115.

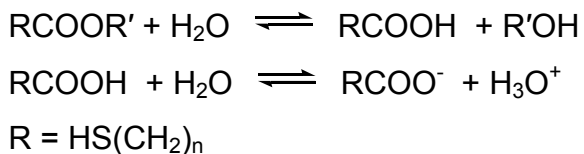
"This chapter was reproduced in part with permission from [Jang, C.-H.; Stevens, B. D.; Phillips, R.; Calter, M. A.; Ducker, W. A. **A Strategy for the Sequential Patterning of Proteins: Catalytically Active Multiprotein Nanofabrication** *Nano Lett.* (Communication), **2003**, *3*(6), 691-694.] Copyright [2002] American Chemical Society."

# Chapter 7. Chemically Specific Nanolithography using an Enzyme-Immobilized AFM Tip

## 7.1 Introduction

The strength of AFM nanografting is the ability to engineer and image complex molecular architectures with high spatial precision. However, this technique has a disadvantage that even a very tough AFM tip will lose resolution through wear. A better approach is to avoid wear on the tip by maintaining a gap between the tip and surface, and to use the tip as a reaction catalyst. For example, Muller et al. coated an AFM tip with platinum to create a scanable catalyst for hydrogenation.<sup>1</sup>

In this chapter, I repeat my efforts to use both immobilized enzymes and immobilized organic catalysts to produce patterns on SAMs. A strategy to chemically specific nanolithography is that enzymes are attached to AFM tips to use their specific catalytic activity on particular functional groups. An example of enzyme catalytic activity is the hydrolysis of an ester to a carboxylic acid by lipase.<sup>2</sup> The hydrolysis reaction proceeds very slowly at room temperature and neutral pH, but tip-bound lipase can accelerate the reaction.



A lipase is the natural enzyme that causes ester cleavage in living organisms. According to the nucleotide sequences of *Candida cylindracea* lipase gene, there are twenty-two lysine residues in one molecule of the lipase. The known three-dimensional structure predicts most of them are located on the outer surface of the molecules (Figure 7.1).<sup>3</sup> These characteristics lead to the immobilization of lipase by the  $\epsilon$ -amino group of lysine on inorganic supports such as silica, alumina, and AFM tips.

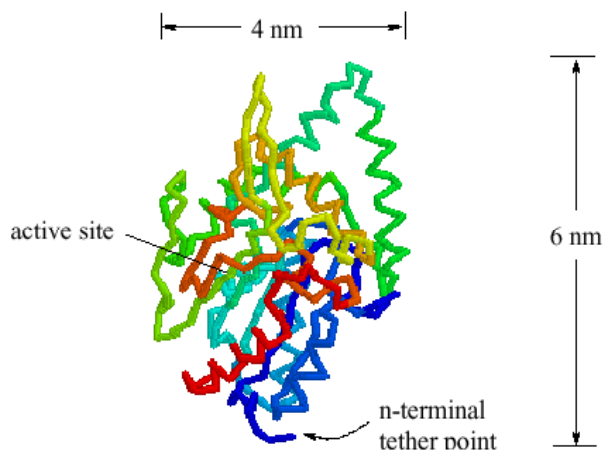


**Figure 7.1** *Candida cylindracea* lipase

When the immobilization of the enzyme is carried out at 25 °C, the amount of immobilized enzyme is greater than in the case of the immobilization at 4 °C because the nucleophilic substitution is favored by the higher temperature.<sup>3-6</sup> However, the high temperature reduces the catalytic efficiency due to the thermal deactivation of the enzyme during the immobilization process. *Candida* lipases are known to deactivate above 42 °C.<sup>4</sup> The immobilized derivatives can be stored at 4 °C for one month without appreciable loss of the catalytic activity.<sup>3</sup>

If tip-bound lipase produces a pattern in a SAM by hydrolyzing the ester to produce a carboxylic acid, one will need a tool for identifying the product pattern. The  $pK_a$  of the surface-confined carboxylic acid is around  $5.5 \pm 0.5$ ,<sup>7</sup> so most of the carboxylic acid groups exist as charged carboxylates at neutral pH. Even if there is not much difference in chain length, the reactant ester and the product carboxylate are still distinguishable by the different forces exerted on an AFM tip. An alkyl ester is hydrophobic and uncharged, and carboxylic acid is hydrophilic and charged. A regular AFM tip is negatively charged so it is repelled by the negatively charged carboxylate surface (Figure 7.2).

## Force on Tip

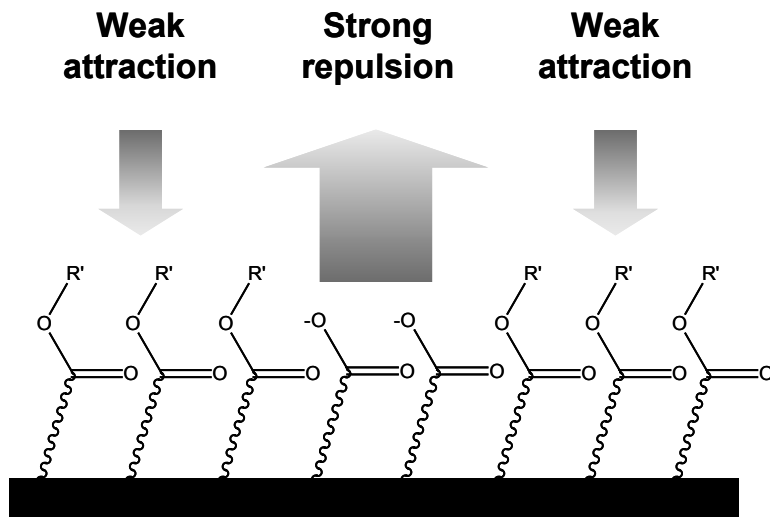


**Figure 7.2** Interaction forces between the AFM tip and the different surface functional groups

There are several different imaging methods in an AFM such as topographic, deflection, and frictional images in contact mode, and topographic, amplitude, and phase images in tapping mode. By selecting an appropriate method, the compositional mapping ability of AFM can be increased. A normal AFM tip has more than one cantilever on each side. Therefore, one of them can be used as the writing tip by chemically attached lipase on a tip and the other one can be used as the reading tip. By switching the sample stage back and forth under the probes, different tips alternately sit above the same part of the sample and perform the write-read process (Figure 7.3).

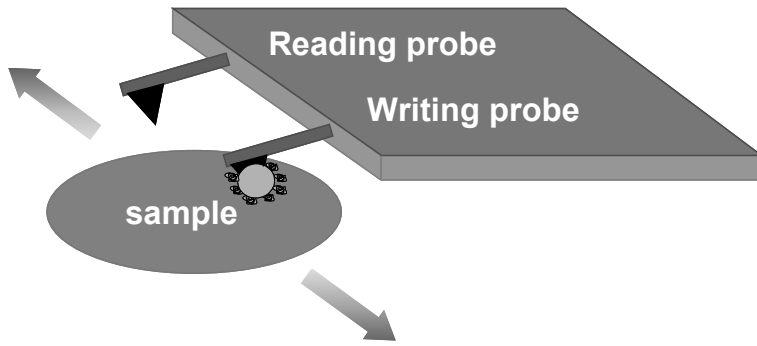


**Figure 7.3** Two-probe AFM for write-read

## 7.2 Experimental Section

### 7.2.1 Materials

16-mercaptopentadecanoic acid methyl ester were synthesized in Professor Michael Calter's lab in the Department of Chemistry at Virginia Tech. 16-mercaptopentadecanoic acid, 11-mercaptopentadecanoic acid, octanethiol, 4-(dimethylamino)pyridine (>99 %), succinic anhydride (>99 %), diethyl ether (>99.5 %, H<sub>2</sub>O <0.005 %), pyridine (>99.9 %, H<sub>2</sub>O <0.005 %), acetyl chloride (>99 %), and 1,2-dichloroethane (anhydrous, 99.8%) were purchased from Aldrich. Lipase (type VI-S, from porcine pancreas) was purchased from Sigma. Gold substrates (5 nm titanium followed by 100 gold coating on flat glass slide) were purchased from EMF. These gold samples were not as good as the flame annealed gold balls. But the better procedure was not developed when these experiments were performed. Glass spheres (2-10 μm diameter) were purchased from Polysciences Inc.

### 7.2.2 Surface Force Measurements

Surface forces measurements were carried out between a silica sphere (or lipase-modified bead) and an ester-terminated SAM using a Digital Instruments Nanoscope III

AFM at room temperature. A silica sphere (or a lipase-modified bead) was secured to the end of a triangular silicon nitride cantilever using Epon 1004 resin (Shell Chemical Co.). The cantilever attached silica sphere was cleaned immediately prior to force measurement by UV irradiation for 20 min. The cantilever and the monolayer were then installed in the AFM fluid cell. The cell was flushed with pure water several times and equilibrated for 2-3 min. Force-separation curves were measured during *approach* of the sphere on the tip toward the monolayer surface and also during *separation* from the surface.

### 7.2.3 Infrared Spectroscopy Experiments

To characterize the formed and modified monolayer, FTIR reflection-adsorption (IRAS) measurements were performed using a Nicolet Model 710 Infrared Spectrometer in Professor Mark Anderson's lab in the Department of Chemistry at Virginia Tech. The infrared light source was p-polarized using a ZnSe wire-grid polarizing filter (Cambridge Physical Sciences, IGP228) and the incident angle of light was fixed at 80°. The sample chamber was purged with H<sub>2</sub>O- and CO<sub>2</sub>- free air for at least 20 min before each measurement. The spectra were typically collected with 512 scans using an MCT/A detector. The acquisition and the processing of spectral data were performed using Nicolet's Omnic data acquisition software. All spectra were referenced to a bare gold slide treated with the same cleaning procedure as the monolayer coated gold slide.

## 7.3 Results and Discussion

### 7.3.1 Enzyme Catalysts for Lithography

#### Catalytic Activity of Free Lipase on SAM

As a preliminary experiment, the catalytic activity of lipase on an ester-terminated SAM was investigated by exposing a SAM to a solution of lipase. Changes in the monolayer chemistry were determined by measuring the force between the AFM tip and the monolayer before and after exposure to lipase.

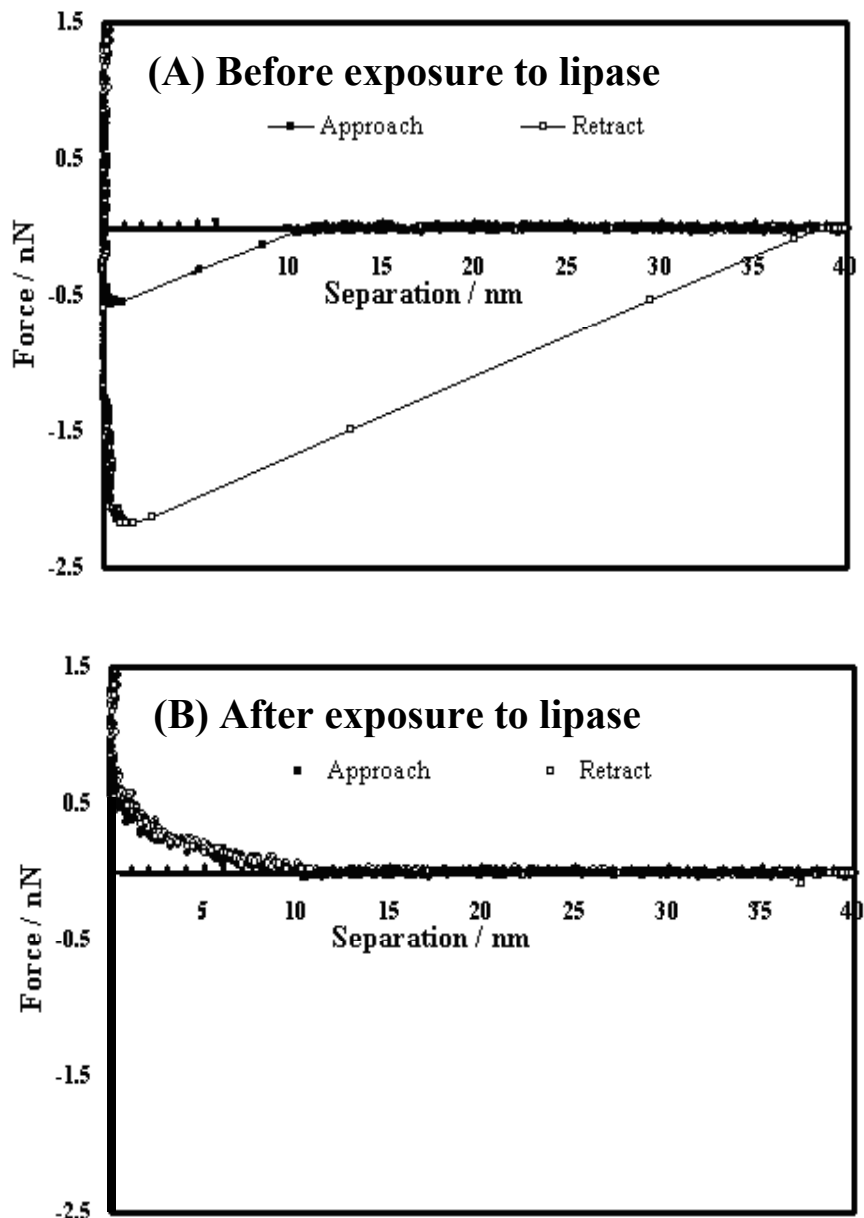


**Figure 7.4** Force curve obtained before and after the hydrolysis of an ester SAM by a lipase solution.

A SAM was prepared with 16-mercaptophexadecanoic acid methyl ester on a gold substrate using the standard self-assembly procedure. The gold substrates were immersed

in a 2 mM ethanolic solution of selected thiol molecules for 24 hours. The substrates were then placed into a pure ethanol for several hours to remove the physisorbed layer and dried in a N<sub>2</sub> stream. The ester-SAM was set in an AFM fluid cell followed by the injection of pure water into the cell. A surface force measurement was performed between the monolayer and the AFM tip.

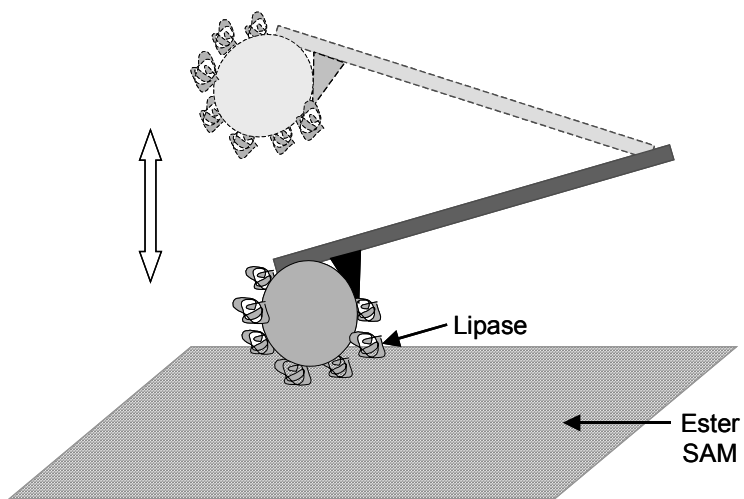
Figure 7.4A shows the force curve before the lipase was injected. The forces on approach and separation are attractive. This observation is consistent with a van der Waals force or a hydrophobic force between the surfaces. A 0.24 mg/ml lipase solution with phosphate buffer (pH 8) was then injected into the cell for 15 min. The surface was thoroughly cleaned with buffer and pure water to remove the physisorbed proteins. A surface force was measured again in water. Figure 7.4B shows the force after the lipase was injected. The force on approach and separation is now repulsive, which shows that the SAM surface has been altered. Hydrolysis of the surface to yield a carboxylic acid would give a charged surface resulting in a repulsive force. Very recently, Humphrey et al. reported the lipase-catalyzed reaction on a solid phase substrate.<sup>8</sup>

### Catalytic Activity of Immobilized Enzyme

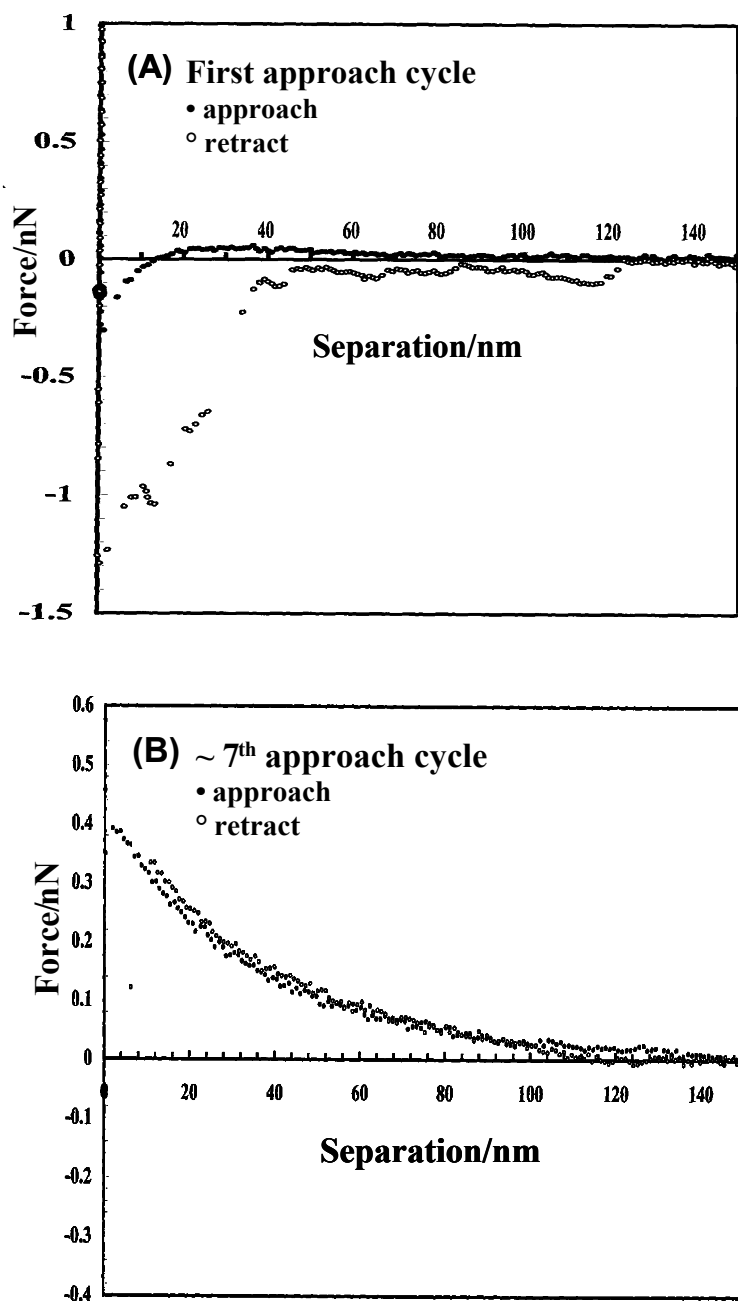
If one could demonstrate catalytic activity for lipase immobilized on an AFM probe, then one could use the scanning capability of the AFM to produce pattern of catalyzed thiol molecules on a surface. To give the best chance of success, we immobilized the lipase enzyme on a silica sphere,  $r = 10 \mu\text{m}$ . The silica sphere was then glued onto an AFM cantilever. This provides a large contact area than an AFM tip and therefore increases the probability of active enzyme contacting the SAM. The silica sphere was brought to the ester-SAM surfaces and then retracted, and the surface force was measured for each cycle. This cycle was repeated several times. A schematic of this experiment is shown in figure 7.5.

Figure 7.6 shows the force versus relative separation profiles for the lipase-tip catalyzing the ester groups in a SAM interface. An attractive force was measured on the first few approaches. Then a repulsive force was observed between 5 and 10 cycles. There are two possible explanations for this result: (1) The enzyme hydrolyzes the surface ester groups to produce carboxylates, which then causes the repulsive force. (2) A small

amount of lipase is transferred from the tip to the surface during the intermittent contacts. Because the enzyme is charged, one would expect the physisorbed enzyme on the SAM and the sphere to produce a repulsive force. Using this data alone it is not possible to determine whether or not catalysis has occurred.



**Figure 7.5** Single spot hydrolysis using a lipase tip. The lipase is about 3 nm in size, compared to the sphere diameter of 10  $\mu\text{m}$ , and is not drawn to scale.



**Figure 7.6** Force-separation curve for lipase immobilized on a silica sphere as it approaches an ester SAM. Lipase tip repeatedly approaches and retracts on a single spot in an ester-SAM and the force curve was observed for each movement. (A) At the first approach, an attractive force curve was measured. (B) After 5-10 approach cycles, the force is now repulsive

## Lithography Using Scanning Silica Spheres

Despite the failure to unambiguously assign a mechanism to the change in force produced by the contact of the silica-immobilized lipase to the ester SAM, we tried to use the silica sphere to write a pattern on the SAM. It was hoped that a patterned surface could still be made, and that it might help to distinguish between the mechanisms. Presumably, if lipase were being deposited, then this would be a limited supply, which would eventually become exhausted.

For the lithography experiment, it is desirable to obtain immediate feedback on the success or failure of each patterning trial. If the pattern is drawn by the tip-bound lipase, the size of pattern will be very small and there will not be much difference in chain length between the reactant ester and the product carboxylic acid. Therefore, the best tool to test the fidelity of AFM lithography would also be the AFM. Because the commercial AFM probes are in chips of more than one probe, one can use the second one as the reading probe by switching the sample back and forth under the probes so that different tips alternately sit above the same part of the sample (see Figure 7.3).

Lithography was performed on an ester-SAM. The AFM probe with a lipase bead attached is brought gently to the writing surface (ester-SAM). The enzyme tip then repeatedly scans over a single line by deactivating y-scan direction of the scanner with scan speed of 50-500 nm/sec. The position of the tip is monitored with a video microscope ( $\sim 1 \mu\text{m}$  resolution). An overhead transparency is placed in the video screen and the site of the lithography is marked on it to find the patterned area after switching to the reading tip. After the writing, the sample stage moves to align the patterned site to the reading tip. The success of lithography is examined by observing the patterned surface with contact and frictional mode imaging techniques. Many experiments have been done with changing conditions such as scan speed, applied force on the tip, pH, and temperature, however, the pattern has never been observed.

The possible reasons for this failure are: (1) The enzyme was deactivated while immobilizing it on the bead and attaching the bead to the AFM probe. (2) All enzymes have their specific active site in their tertiary structure. Because the lipase was randomly immobilized on the bead surface, most of them may not be properly oriented to the substrate molecules. (3) The rate of a lipase-catalyzed hydrolysis reaction is not fast

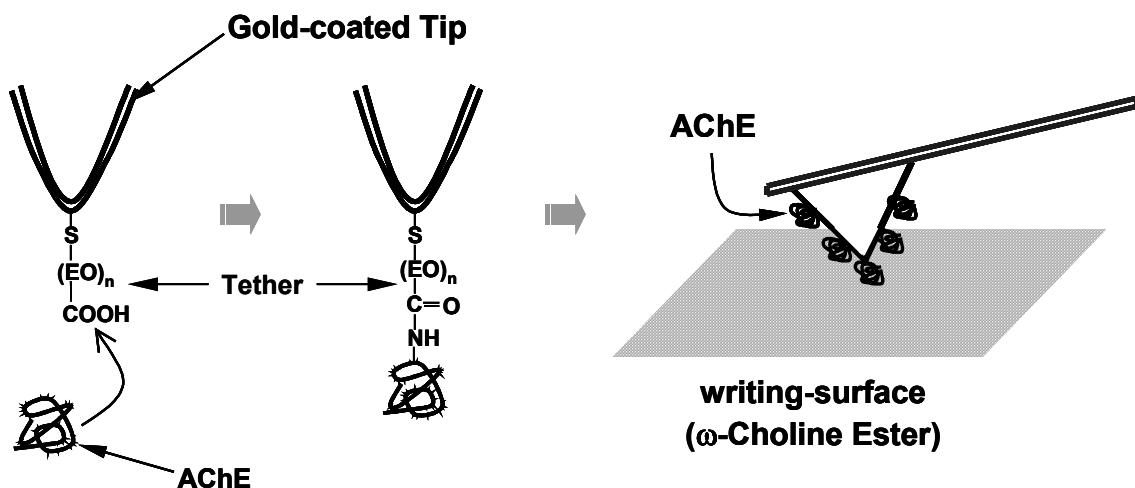


**Figure 7.7** Attachment of AChE to an AFM tip to use its specific catalytic actions on a writing-surface.

enough for the production of pattern by scanning the tip over the surface. The lateral spacing of the substrate molecules in a SAM is about 0.5 nm. The enzyme must be able to make at least 100 reactions/second to produce a pattern with the scan speed of 50 nm/second. However, each free lipase can only make 1.56 reactions/second with monomeric ester in a solution.<sup>6</sup> In addition, the catalytic activity of enzyme is known to decrease when it is immobilized on a solid support. (4) Lipase has a unique additional structure that is not observed in most of the enzymes. It has a flap covering the active site of the enzyme. Therefore, a large conformational change of the flap domain to open at the interface is required to allow substrate molecules to approach the active site. Because of this translocation procedure, lipase-catalyzed hydrolysis shows an initial induction period before the reaction takes place, which negatively affects the proposed lithographic method.

In order to make progress on this project, higher reaction rates and more precise spatial control of the enzyme and the substrate were required as follows: (1) Because the lipase-catalyzed hydrolysis is not fast enough for this purpose, an enzyme with higher catalytic activity, such as acetylcholinesterase (AChE), must be used. As described in

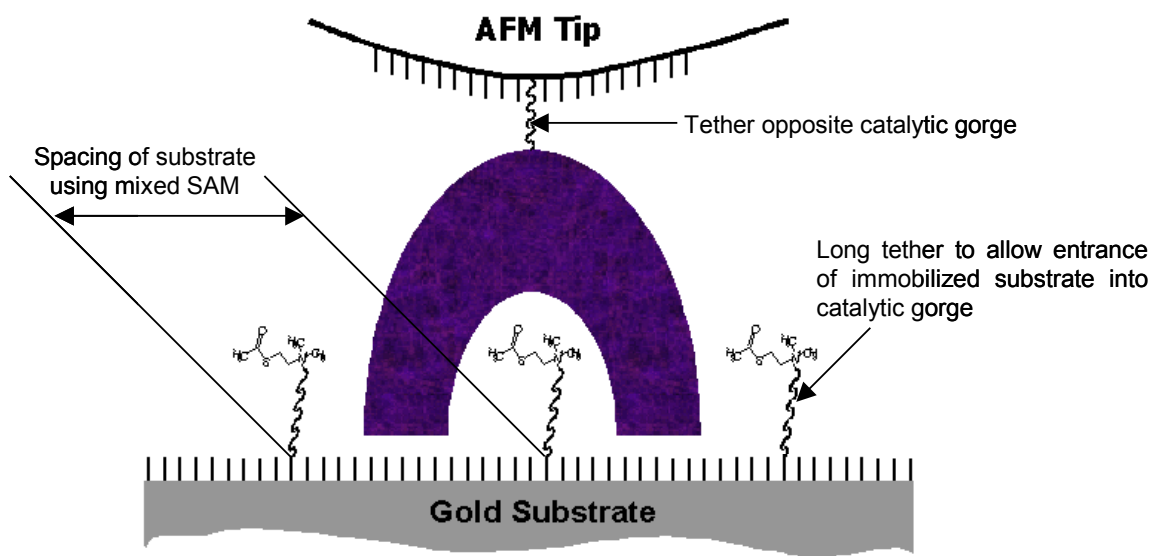


**Figure 7.8** Tethering of an AChE and choline substrate for the enzyme-tip lithography

chapter 5, AChE is one of the fastest enzymes known to hydrolyze the substrate. The catalytic turnover rate for acetylcholine (ACh) is about  $1.6 \times 10^4$  reactions/second. The introduction of ACh functional group into a monolayer is also required to use this enzyme for the lithography. (2) When enzymes are attached directly to an AFM tip, it is difficult for the enzyme to obtain a proper binding with the solid-phase ester. The introduction of an organic tether between the enzyme and the tip should be beneficial. It allows extra flexibility for the enzyme to adopt a favorable orientation for binding (Figure 7.7). Hinterdorfer et al. reported that improved antibody-antigen binding was obtained when the antibody was connected to the tip via a polyethylene glycol (PEG) spacer molecule.<sup>9</sup> The flexibility of a tether has the additional advantage of allowing the enzyme to move away from the zone of highest force at the very end of the tip. It is possible that the force exerted by the AFM tip and the solid substrate on the enzyme may affect enzyme activity. (3) If AChE is used, the serine active site of AChE is located in a deep (about 2 nm from the surface) and narrow catalytic gorge. Introducing a spacer between the substrate molecule and the background surface is required to allow the

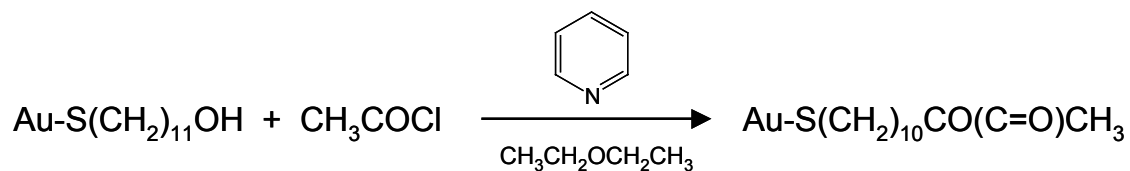
substrate to reach the active site in the gorge. The dimension of AChE is about  $4 \times 5 \times 6$  nm, therefore the substrate molecules should be laterally spaced by around 2.5 nm. Finally, tethering enzymes on a specific site (the opposite side of the active site) is desirable to make the enzyme-substrate binding more favorable (Figure 7.8).

### 7.3.2 Organic Catalysts for Lithography

Given the problems with enzyme catalysis, it was decided to examine the possibility of using an organic catalyst for the lithography. This strategy has the disadvantage of slower rates, but the advantage of simple and perhaps more robust chemistry. This project was in collaboration with Professor Carlier in the Chemistry Department at Virginia Tech.

#### Reaction with Free Catalyst

The first reaction investigated was the esterification of hydroxyl groups with a pyridine catalyst<sup>10</sup> (Scheme 7.1). Before applying this reaction to lithography, the catalytic activity of free pyridine for the surface hydroxyl group was examined. Mixed SAMs with 11-mercaptoundecanoic acid and octanethiol (1:4 molar ratio) were prepared on a gold substrate using a standard self-assembly procedure. The reason for making the mixed monolayer is that the shorter octanethiol leaves lateral space between the hydroxyl functional groups. This spacing provides room for the reactant and the catalyst to bind in a favorable conformation. The monolayer was immersed in 50 ml of diethyl ether and then 0.1 ml of pyridine was added followed by 0.06 ml of acetyl chloride. The solution was sealed and left to equilibrate for



Scheme 7.1

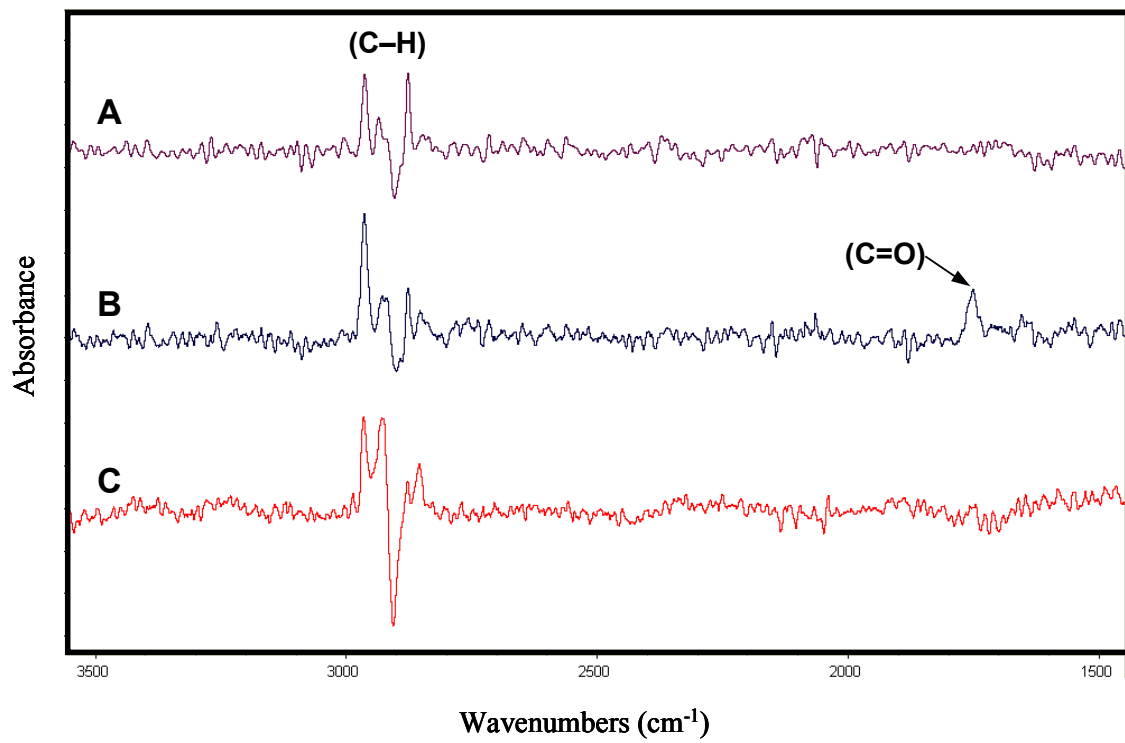
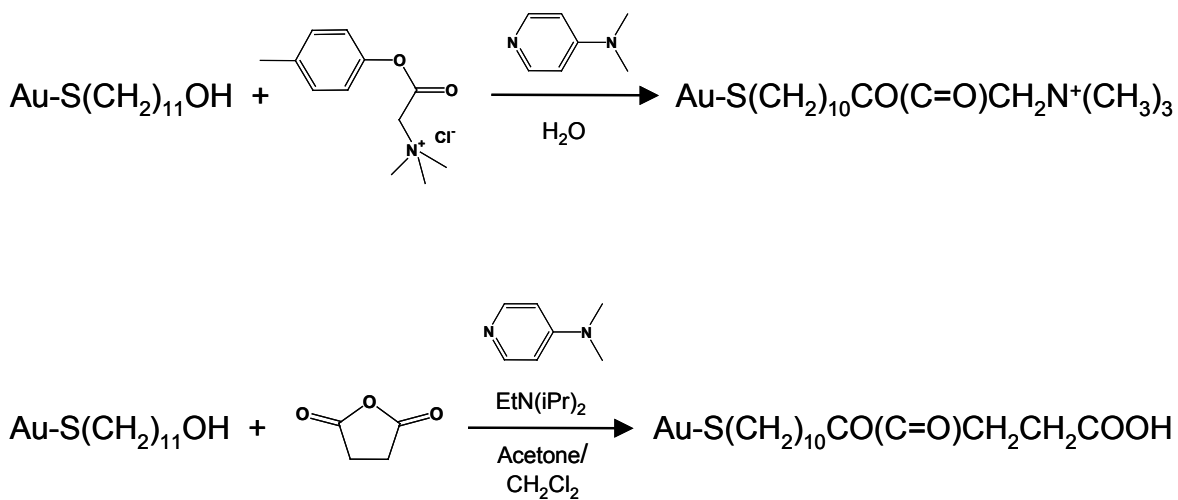


**Figure 7.9** IRAS spectra of monolayers: (A) hydroxy-terminated SAM, (B) hydroxy-terminated SAM exposed to acetylchloride in the presence of pyridine catalyst, and (C) hydroxy-terminated SAM exposed to acetylchloride in the absence of pyridine catalyst. All spectra were collected with 512 scans at room temperature.

20 min. The surface was then thoroughly rinsed with ether and with ethanol. When this reaction is used for lithography using a pyridine-modified tip, the background hydroxyl groups must not react with acetyl chloride to produce a pattern. Therefore, the same reaction without the pyridine catalyst was also performed. The monolayers before and after the reaction were investigated with FTIR reflection-absorption spectroscopy (IRAS) to ascertain their chemical identities.

Figure 7.9 shows the spectra for (A) a hydroxyl surface, (B) a hydroxyl surface exposed to acetylchloride in the presence of pyridine catalyst, and (C) a hydroxyl surface exposed to acetylchloride in the absence of pyridine catalyst. All monolayers show a C-H stretch between 2800-3000  $\text{cm}^{-1}$ . The functionalized surface with the pyridine catalyst



**Scheme 7.2**

clearly shows a C=O stretching peak at 1750 cm<sup>-1</sup>, which indicates that the surface has been esterified by acetyl chloride and pyridine catalyst. A C=O stretching peak is not observed for the surface reacting without the catalyst. This result is promising because the surface is modified only when the catalyst is added to the reaction medium. However, the low boiling point of the diethyl ether solution presents a serious problem in the application of this reaction for the tip-catalyzed lithography. When we image a surface with AFM, fluctuations in temperature cause differential expansion of various parts of the AFM. This produces a drift of the tip, which is not known or controlled. Because the boiling temperature of diethyl ether is only 34.6 °C and the AFM cell is not completely sealed, evaporation will cause a lot of drift in the tip-sample position.

Therefore, we examined the reaction with another solvent (1,2-dichloroethane) that has a higher boiling point (83.0 °C) than diethyl ether (34.6 °C) but a similar dielectric constant (10.3 for 1,2-dichloroethane, 4.3 for diethyl ether). Unfortunately, the surface reaction rate was much slower in 1,2-dichloroethane. After 20 min, the IR

spectrum showed no evidence of reaction (no C=O stretch). It took 24 h to produce a spectrum similar to that observed in Figure 7.9B.

Other surface reactions were also investigated for this project (Scheme 7.2). We tested the use of better catalysts, various solvents, and various reacting groups. However, none of these reactions showed a high enough reaction rate (at least 100 reactions/second) for the proposed lithography.

#### 7.4 Conclusions

The aim of this study was the development of a new AFM lithographic method that avoids the tip wear by using an enzyme or other catalyst attached to an AFM tip. To this end several interfacial hydrolysis reactions on monolayer surfaces have been examined using lipase and pyridine-based catalysts. AFM force measurements after exposure of a SAM to free lipase and after contact of immobilized enzyme with the surface were consistent with a catalytically active enzyme. However, they were also consistent with deposition of the enzyme. AFM imaging using a lipase-coated sphere did not produce a pattern that could be recognized by AFM imaging. Thus the lithography procedure was not successful. We then turned to organic catalysts as an alternative. An IRAS study showed that the esterification of hydroxyl-terminated monolayer by acetyl chloride is accelerated by the pyridine catalyst. However, we could not find a combination of catalyst and solvent that produced a high reaction rate that was suitable for AFM lithography. Our research on AChE suggests that this would be a suitable catalyst.

## References

- (1) Muller, W. T.; Klein, D. L.; Lee, T.; Clarke, J.; McEuen, P. L.; Schultz, P. G. *Science* **1995**, *268*, 272.
- (2) Xu, X.; Fomuso, L. B.; Akoh, C. C. *J. Agric. Food Chem.* **2000**, *48*(1), 3.
- (3) Moreno, J. M.; Sinisterra, J. V. *J. of Molecular Catalysis* **1994**, *93*, 357.
- (4) Brady, C.; Metcalfe, L.; Slaboszewski, D.; Frank, D. *JAOCs* **1998**, *65*, 6.
- (5) Moreno, J. M.; Arroyo M.; Hernaiz, M. J.; Sinisterra, J. V. *Enzyme Microb. Technol.*, **1997**, *21*, 552.
- (6) Sanchez E. M.; Bello J. F.; Roig M. G.; Burguillo, F. J.; Moreno, J. M.; Sinisterra, J. V. *Enzyme Microb. Technol.*, **1996**, *18*, 468.
- (7) Vezenov, D. V.; Noy, A.; Rozsnyai, L. F.; Lieber, C. M. *J. Am. Chem. Soc.* **1997**, *119*, 2006.
- (8) Humphrey, C. E.; Turner, N. J.; Easson, M. A. M.; Flitsch, S. L.; Ulijn, R. V. *J. Am. Chem. Soc.* **2003**, *125*(46), 13952.
- (9) Hinterdorfer, P.; Baumgartner, W.; Gruber, J.; Schindler, K. *Proc. Natl. Acad. Sci.* **1996**, *93*, 3477.
- (10) Engquist I.; Lestelius, M.; Liedberg, B. *Langmuir* **1997**, *13*, 4003.

## **Chapter 8. Summary and Future Work**

The studies carried out in this thesis were aimed at developing AFM-based procedures to construct chemically specific nanostructures in a self-assembled monolayer using a variety of materials such as polymers, particles, and proteins. This thesis is especially focused on the nanometer scale fabrication of catalytically-active enzyme patches.

Chapter 4 demonstrated the covalent attachment of simple organic molecules, functionalized gold particles, and proteins to a specifically patterned site on a 20-40 nm length scale. These studies allowed us to formulate a solid technical basis to explore nanometer scale manipulation of enzymes in the following chapters. This section also demonstrates the nanopatterning of polyelectrolyte multilayers by first producing a carboxylate patch in a SAM and then sequentially adsorbing alternating charged polymer layers. This method provides a good alternative route to modify surface properties on the nanometer scale.

Chapter 5 verifies the catalytic activity of immobilized acetylcholinesterase by developing an *in situ* nanoscale detection method: the surface trapping of enzyme catalysis product. The trap site was produced by exposing a gold substrate near the enzyme patch, and therefore the reaction product, thiocholine, was captured by the trap via S-Au bond formation before diffusing away. The trapped thiocholine was successfully identified using AFM tapping mode imaging. This observation was the first reported result of detecting the chemical activity of localized enzyme on the nanometer scale, which is a useful step in the evolution of miniaturized biosensors.

Chapter 6 describes a new strategy for immobilizing enzymes on the surface that will allow the preparation of thin films containing several different catalytically active enzymes. This method uses the oxidative selectivity of periodate for vicinal diol groups to produce an aldehyde within a SAM, without inactivating protein molecules. The retention of catalytic activity of the first immobilized enzyme after immobilization of a second protein was demonstrated by the surface trapping experiment. This work is the

first reported method for producing an “array” of different proteins with retention of catalytic activity.

Chapter 7 proposes a new method for chemically specific nanolithography that uses an enzyme’s extraordinarily specific catalytic action. In this method, enzymes are immobilized on an AFM tip and the lithography is performed by scanning the tip-bound enzyme on the surface covered by the substrate molecules. Hypothetically, the enzyme then catalyzes the reaction on the surface following the intended path, which results in the production of a pattern. This technique was not successfully implemented. Preliminary experiments suggested that free lipase was active on SAM surfaces. The solid-solid interaction between the tip-bound enzyme and the monolayer substrate was also examined, but lithography was not successful. The catalytic action of pyridine on the esterification reaction of hydroxy-terminated SAM by acetyl chloride was observed using FTIR reflection-absorption spectroscopy. In summary, organic catalysts were found to be too slow for nanolithography and lipase catalyst was found to be either too slow or inactive. AChE would be a good future target because of its high turnover rate and its demonstrated activity at surfaces.

This thesis has presented new strategies for AFM-assisted nanometer-scale modification of SAMs using a broad range of materials. AFM is particularly beneficial in the fabrication of biomaterials because of its capability to observe the patterned proteins, without damaging them, immediately after the fabrication procedure. We hope that the methods developed in this study will allow us to make advances in many fields, with particular focus on the integration of biological systems and electronic devices.

One possible application is the study of the interaction of insulin with specific receptors on the surface of a membrane. In contrast to insulin, the mechanism of biological response by the insulin receptor is not well known. The insulin receptor is partially buried in the membrane bilayer and recognizes the very low concentration of insulin present in the blood. Then it generates the intercellular signal that initiates a biological response. However, how the insulin binding triggers a biological response is not known.

Our nanofabrication technique could be used to create membrane-based devices (Figure 8.1). A nanoelectrode could be patterned on the SAM surface as described in

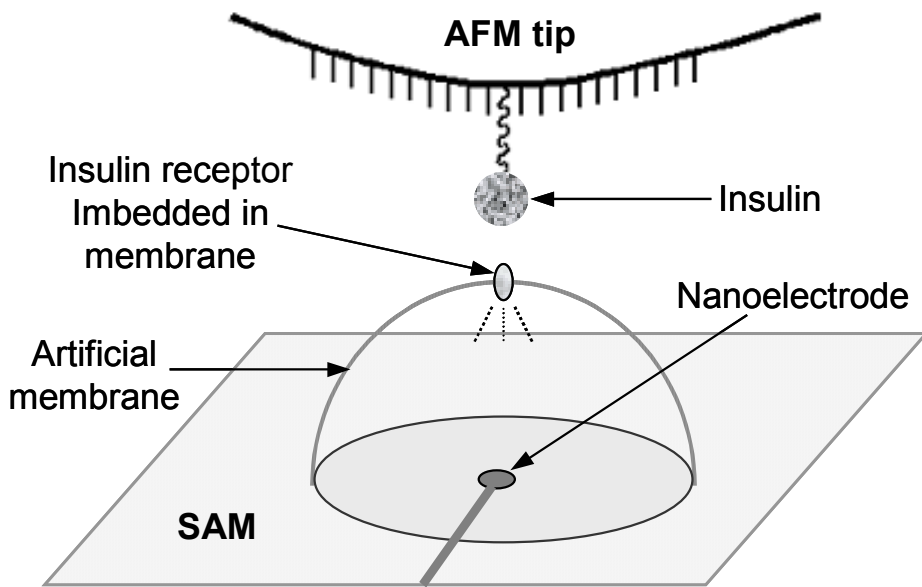


**Figure 8.1** Membrane-enclosed electrode

Chapter 4, which is then covered by an artificial cell membrane with insulin receptors imbedded into

the membrane. A strategy for the construction of artificial cell membrane composed of a phospholipid bilayer surrounding embedded membrane proteins was proposed by Professor Ducker and Professor Calter in the Department of Chemistry at Virginia Tech. For this construction, our protein patterning techniques described in Chapter 5 and 6 will be applied. Insulin could be tethered to a gold-coated AFM tip using a polyethylene glycol spacer as proposed in Chapter 7. This elaborate system will allow us to observe two phenomena at the same time: (1) The interactions between the insulin and the insulin receptor can be investigated by the AFM force measurement using an insulin-modified tip. (2) The cellular response of the insulin receptor to an insulin binding can be studied by monitoring potential changes inside the membrane using the nanoelectrode constructed in our system.

Our multi-protein patterning technique will also allow us to produce biochemical assays in which we can perform many different assays in a single chip faster and with less sample than was previously possible.

## Appendix:

### Nanoscript Program for Producing 9-dot Pattern in Figure 4.5A

```
#include<litho.h>

//Lithosq9
//Draws nine squares
//Chang

void DrawSquare(float sqsize, int traverses, float fast, float slow) {

    //square start and finish point: bottom, left corner
    //sqsize in um
    //traverses is the number of times the square is drawn
    //fast is the fast-axis scan-velocity um/s
    //slow is the slow-axis scan-velocity um/s

    int i, count;

    for (count = 1; count <= traverses; ++count) {
        for (i = 1; i <= sqsize*1000; ++i) {
            LithoTranslate(sqsize, 0, fast);
            LithoTranslate(-sqsize, 0, fast);
            LithoTranslate(0, 0.001, slow);
        }
        LithoTranslate(0, -sqsize - 0.001, fast);
    }
}
```

```

    }

}

void DrawRect(float xdim, float ydim, int traverses, float fast, float slow) {

    //rectangle start and finish point: bottom, left corner
    //xdim and ydim are the rectangle dimensions in um in x and y
    //traverses is the number of times the rectangle is drawn
    //fast is the fast-axis scan-velocity um/s
    //slow is the slow-axis scan-velocity um/s

    int i, count;

    if (xdim >= ydim) {
        for (count = 1; count <= traverses; ++count) {
            for (i = 1; i <= ydim * 1000; ++i) {
                LithoTranslate(xdim, 0, fast);
                LithoTranslate(-xdim, 0, fast);
                LithoTranslate(0, 0.001, slow);
            }
            LithoTranslate(0, -ydim - 0.001, slow);
        }
    }
    else {
        for (count = 1; count<= traverses; ++count) {
            for (i = 1; i <= xdim*1000; ++i) {
                LithoTranslate(0, ydim, fast);
                LithoTranslate(0, -ydim, fast);
                LithoTranslate(0.001, 0, slow);
            }
            LithoTranslate(-xdim - 0.001, 0, slow);
        }
    }
}

```

```

    }
}

}

void main() {

LITHO_BEGIN

LithoDisplayStatusBox(); // display litho status box
LithoScan(FALSE); // turn off scanning
LithoCenterXY(); // move tip to center of field

float fastrate = 5.0; //for large increment movements 4 um/s
float slowrate = 0.01; //for small increment movements 0.01 um/s

LithoTranslate(-0.2, -0.2, fastrate); //move to corner of square 1
LithoSet(lsSetpoint, 5.0); //increase set point to 5.5 volts
DrawSquare(0.005, 1, fastrate, slowrate); //draw square 1
LithoSet(lsSetpoint, -1); //decrease set point to -1 volts

LithoTranslate(0.2, 0, fastrate); //move to corner of square 2
LithoSet(lsSetpoint, 5.0); //increase set point to 5.5 volts
DrawSquare(0.005, 1, fastrate, slowrate); //draw square 2
LithoSet(lsSetpoint, -1); //decrease set point to -1 volts

LithoTranslate(0.2, 0, fastrate); //move to corner of square 3
LithoSet(lsSetpoint, 5.0); //increase set point to 5.5 volts
DrawSquare(0.005, 1, fastrate, slowrate); //draw square 3
LithoSet(lsSetpoint, -1); //decrease set point to -1 volts
}

```

```
LithoTranslate(-0.4, 0.2, fastrate); //move to corner of square 4  
LithoSet(lsSetpoint, 5.0); //increase set point to 5.5 volts  
DrawSquare(0.005, 1, fastrate, slowrate); //draw square 4  
LithoSet(lsSetpoint, -1); //decrease set point to -1 volts
```

```
LithoTranslate(0.2, 0, fastrate); //move to corner of square 5  
LithoSet(lsSetpoint, 5.0); //increase set point to 5.5 volts  
DrawSquare(0.005, 1, fastrate, slowrate); //draw square 5  
LithoSet(lsSetpoint, -1); //decrease set point to -1 volts
```

```
LithoTranslate(0.2, 0, fastrate); //move to corner of square 6  
LithoSet(lsSetpoint, 5.0); //increase set point to 5.5 volts  
DrawSquare(0.005, 1, fastrate, slowrate); //draw square 6  
LithoSet(lsSetpoint, -1); //decrease set point to -1 volts
```

```
LithoTranslate(-0.4, 0.2, fastrate); //move to corner of square 7  
LithoSet(lsSetpoint, 5.0); //increase set point to 5.5 volts  
DrawSquare(0.01, 1, fastrate, slowrate); //draw square 7  
LithoSet(lsSetpoint, -1); //decrease set point to -1 volts
```

```
LithoTranslate(0.2, 0, fastrate); //move to corner of square 8  
LithoSet(lsSetpoint, 5.0); //increase set point to 5.5 volts  
DrawSquare(0.01, 1, fastrate, slowrate); //draw square 8  
LithoSet(lsSetpoint, -1); //decrease set point to -1 volts
```

```
LithoTranslate(0.2, 0, fastrate); //move to corner of square 9  
LithoSet(lsSetpoint, 5.0); //increase set point to 5.5 volts  
DrawSquare(0.01, 1, fastrate, slowrate); //draw square 9  
LithoSet(lsSetpoint, -1); //decrease set point to -1 volts  
LithoTranslate(-0.2, -0.2, fastrate); //return to starting position
```

```
LITHO_END  
}
```

## **Vita**

Chang-Hyun Jang was born on April 22, 1965 in Seoul, Korea. He obtained his Bachelors of Science and Masters of Science in Chemistry from Hanyang University in 1988 and 1991, respectively under the direction of Dr. Hong. He then worked in industry for 6 years with LG Chemical Ltd. as a research scientist, where he investigated microencapsulation and surfactant systems. He enrolled in Virginia Tech in the spring of 1999 in pursuit of a Ph.D. Degree under the direction of Dr. Ducker. Upon completion of his Doctor of Philosophy Degree in Chemistry in the spring of 2004, he will join the Department of Chemical and Biological Engineering at University of Wisconsin-Madison as a research associate.